Università Campus Bio-Medico di Roma

School of Engineering

PHD COURSE IN BIOMEDICAL ENGINEERING
(XXVI - 2011/2013)

PhD Thesis

Multimodal Interfaces for Upper-Limb Rehabilitation Robotic Machines

Author:
Eugenia Papaleo

Supervisor:
Prof. Eugenio Guglielmelli
Co-supervisor:
Ing. Loredana Zollo

A thesis submitted in fulfilment of the requirements
for the degree of Doctor of Philosophyin Biomedical Engineering

Università Campus Bio-Medico di Roma
School of Engineering

March 2014

Declaration of Authorship

I, Eugenia PAPALEO, declare that this thesis titled, 'Mutlimodal Interfaces for Upper-Limb Rehabilitation Robotic Machines' and the work presented in it are my own. I confirm that:

- This work was done wholly or mainly while in candidature for a research degree at this University.
- Where I have consulted the published work of others, this is always clearly attributed.
- Where I have quoted from the work of others, the source is always given. With the exception of such quotations, this thesis is entirely my own work.

Signed: 

Date:
March 25th, 2014

"Out of clutter, find simplicity.
From discord, find harmony.
In the middle of difficulty lies opportunity."

Albert Einstein

Eugenia Papaleo

Abstract

Mutlimodal Interfaces for Upper-Limb Rehabilitation Robotic Machines

by Eugenia Papaleo

Stroke is one of the leading cause of permanent disability. Numerous rehabilitation methodologies can be adopted to deal with stroke motor impairment, but the optimal training approach remains unclear. Robotic technologies are recognized as powerful tools to promote neuroplasticity and stimulate motor re-learning. They allow delivering high-intensity, repetitive, active and task-oriented training; in addition, they provide objective measurements for patient evaluation. However, typical stroke robot-aided rehabilitation is very task specific and conceived for applying a sort of "if-then" algorithm: if the patient performs an incorrect motion, then the robot applies a predefined unidirectional action.
Nowadays, the increasing employment of bio-cooperative systems for the administration of robot-aided therapy to stroke patients represents a real breakthrough. Such systems place the patient in the control loop, by feeding back his/her biomechanical and physiological state, and automatically adapt the control system on the basis of the monitored patient states, with the aim of motivating in an engaging and challenging way the patient.

This work presents the design and the development of a bio-cooperative system for upper-limb robot-aided therapy consisting of two main modules: (i) a multimodal interface, able to evaluate patient performance and realtime display a virtual reality environment relative to the performed task, (ii) an adaptive robotic controller, able to modulate the complexity of the assigned motor task, allowing the administration of a patient-tailored therapy. A special attention has been paid to the development of an unobtrusive multimodal interface for monitoring patient state without altering user natural motion.

Furthermore, a reliable method for reconstructing the 7-DoF upper-limb kinematics during robot-aided tasks with end-effector machines is presented and experimentally validated.

Finally, two applications of the developed bio-cooperative system are presented: (i) a robotic system for 3D upper-limb rehabilitation, (ii) the quantitative evaluation of the outcomes of a clinical study involving chronic stroke patients. Preliminary experimental results of both the applications are reported.

Eugenia Papaleo

Acknowledgements

Foremost, I would like to express my gratitude to my co-supervisor, Loredana Zollo, for the support during my Ph.D course, for her knowledge and for her patience. Her guidance helped me in the time of research and writing this thesis.

I would like to thank my supervisor, Prof. Eugenio Guglielmelli, for his encouragement, insightful comments, and "hard" questions.

My sincere thank also to all the friends of my Laboratory and to the timeless ones for giving my true laughters, also in worst days.

Eugenia Papaleo

Contents

Eugenia Papaleo

Eugenia Papaleo

Eugenia Papaleo

List of Figures

Eugenia Papaleo

Eugenia Papaleo

Eugenia Papaleo

Eugenia Papaleo

List of Tables

Eugenia Papaleo

A mamma, per la forza inesauribile che sa trasmettermi

A papà, per la fiducia con cui mi ha da sempre "lasciato fare"

A Mody e Enza, per essere sempre stati i miei 2/3

A Fabio ...

Eugenia Papaleo

Chapter 1

Introduction

Stroke affects thousands of people worldwide often causing severe disabilities that affect people daily living. Motor impairment is the most common consequence of stroke and is managed through rehabilitation treatments.
In recent years, new rehabilitation techniques are emerging to deal with motor impairment in the upper-limb; in particular, robots are valuable tools for motor rehabilitation since they allow the repetitive application of controlled forces to the affected limb and the precise recording of movements. However, typical stroke robot-aided rehabilitation is very task specific and conceived for applying only predefined unidirectional actions that are not tailored on patient state; in this way, the patient has mainly a passive role and his/her needs and/or intentions are ignored. An interesting alternative for obtaining a more efficient patient-robot interaction is represented by the administration of therapies tailored on patient biomechanical and physiological states; multiple evidences show that such therapies allow obtaining a faster learning and recovery time [9].
Nowadays, an emerging trend in rehabilitation robotics is the development of bio-cooperative control systems that, placing the patient in the control loop, by feeding back his/her biomechanical and physiological state, automatically adapt the control system on the basis of the monitored states, with the aim of motivating in an engaging and challenging way the patient [5].

In this work a bio-cooperative system for upper-limb robot-aided rehabilitation is proposed. The presented bio-cooperative system is grounded on two main modules:

- A multimodal interface that monitors patient motor performance and real-time displays a virtual reality environment on task execution;

Eugenia Papaleo

- An adaptive control system that adjusts the assigned motor task, allowing the administration of a patient-tailored therapy.

This dissertation thesis is structured as follows:

- In Chapter 2, the neurophysiological assumptions of post-stroke physical rehabilitation and the traditional methodologies for stroke rehabilitation and stroke evaluation are discussed. The state of the art on rehabilitation robotics is analysed and the main technologies and techniques for robot-aided therapy and robot-based evaluation, respectively, are presented. The key features of bio-cooperative control systems for stroke robot-aided rehabilitation are presented.

- In Chapter 3, the proposed bio-cooperative system for upper-limb robot-aided rehabilitation is presented. The functional architecture of the multimodal interface is illustrated and the methods for patient data acquisition and processing as well as for the extraction of performance indicators are described. The modulation functions for updating control parameters and the developed virtual reality software are discussed. The adaptive robot control system is illustrated.

- In Chapter 4, a reliable method for reconstructing the upper-limb kinematics of stroke patients during robot-aided exercises with end-effector machines is presented. The kinematic model of the upper-limb and the algorithm for inverse kinematics are presented. The experimental tests carried out for assessing method accuracy and evaluating its applicability during robot-aided rehabilitation are illustrated; the experimental results of a two-stage experimental evaluation are reported.

- In Chapter 5, the application of the proposed bio-cooperative system to a robotic system for 3D upper-limb rehabilitation is presented. It is composed of a 7-DoF robot arm, the adaptive interaction control system and the multimodal interface. The proposed bio-cooperative robotic system is presented and its experimental validation, carried out on healthy subjects, is reported. Both the experimental protocol and the experimental results in 2D and 3D space are provided.

- In Chapter 6, a further application of the system proposed in Chapter 3 is presented. In particular, the developed multimodal interface is used for

Eugenia Papaleo

the quantitative evaluation of the outcomes of a novel rehabilitation treatment that joins together transcranial Direct Current Stimulation (tDCS) and upper-limb robotic therapy. Study background and methodology are presented. The tools for measuring the outcomes of the treatment are illustrated and the preliminary results on chronic stroke patients are reported.

- In Chapter 7, conclusions are reported.

Eugenia Papaleo

Chapter 2

Robot-aided rehabilitation and bio-cooperative controllers for stroke patients: State of the Art

Stroke is one of the major causes of mortality or permanent disability. The most widely recognised impairment caused by stroke is motor impairment and rehabilitation treatments are the most effective interventions to address it.

A variety of rehabilitation approaches have been proposed to deal with motor impairment in the upper-limb; however, the type of therapy leading to optimal results remains controversial and elusive. Moreover, the traditional evaluation of motor and functional impairment is managed by clinical scales that, being based on therapist observations, suffer from a series of drawbacks.

Robots can be successfully exploited to augment therapists' skills in promoting neuroplasticity and stimulating motor re-learning since they allow administering high-intensity, repetitive, active and task-oriented training; in addition, they provide objective metrics for patient evaluation. However, traditional stroke robot-aided rehabilitation is very task specific and conceived for applying unidirectional actions to the patient.
Currently, a powerful alternative is represented by the development of bio-cooperative control systems that, feeding back patient biomechanical and physiological states, allow administering therapies tailored on patient needs, thus obtaining increased patient involvement and faster learning and recovery times.

Eugenia Papaleo

This Chapter is structured as follows. The aspects relative to traditional stroke rehabilitation and evaluation are discussed in Sections 2.1 and 2.2, respectively, while the main diffused technologies and methodologies for upper-limb robot-aided rehabilitation and evaluation are treated in Sections 2.3. Finally, the key features of bio-cooperative control systems for stroke robot-aided rehabilitation are presented in Section 2.4.

2.1 Stroke rehabilitation

In Italy about 200.000 persons are affected by stroke each year, and in United States approximately 795.000 old Americans experience each year a new or recurrent stroke [10] [1]; moreover, the percentage of people affected by stroke grows dramatically with age [11] (Figure 2.1). It can be estimated that the 14% of patients suffering from stroke will have another one within a year, while around 25% of stroke survivors will have another stroke within five years [12].
Stroke consists of a loss of brain functions due to an insufficient supply of blood to a brain area; stroke can be either ischemic or hemorrhagic. The mainly diffused type is the ischemic stroke; it is caused by the obstruction of a brain blood vessel and account for approximately 87% of all stroke cases. The remaining 13% of cases are relative to the hemorrhagic stroke that consists in the breakage of a brain vessel.

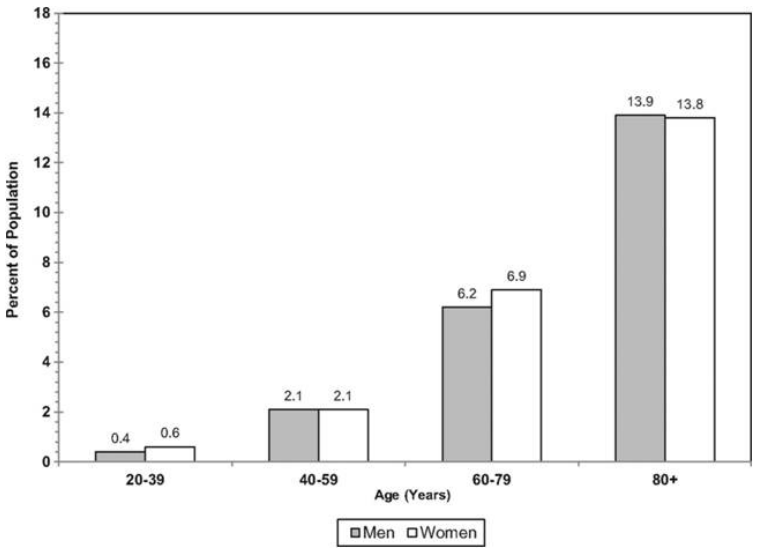

FIGURE 2.1: Prevalence of stroke by age and sex [1]

Although most people survive stroke, the damage to brain tissues can produce a variety of deficits at different levels (i.e. motor, sensory, cognitive and psychological). The severity of the stroke determines the gravity of subsequent deficits that are grouped as follows [1]:

- Physical deficits - The paralysis of one side of the body due to a damage on the opposite side of the brain is called hemiplegia. The paralysis, or weakness, may affect only one side of the face, one arm, or one leg, or may affect an entire side of body and face.
  For example, as regards upper-limb motor deficits, the decreased arm and hand functions as well as the consistent upper extremity weakness may cause serious difficulties in the execution of the simplest Activities of Daily Living (ADLs).
- Balance and co-ordination deficits - A stroke patient may have problems performing ADLs, such as walking or dressing due to difficulties with balance and coordination.
- Cognitive deficits - Stroke may cause problems with thinking, awareness, attention, learning, judgment, and memory.
- Language deficits - Stroke victims may find it hard to understand or form speech; this deficit is called aphasia and may also cause problems in reading or writing.
- Emotional deficits - Stroke patients may find it difficult to control their emotions or may express inappropriate emotions in certain situations. One common emotional problem is depression.
- Pain - Stroke patients may experience pain, uncomfortable numbness, or strange sensations after a stroke.

After stroke onset, a spontaneous neurological recovery can be observed. The extent of this recovery is very different between patients, since it depends on both the area of the lesion and the size of the damage; the timing of such a spontaneous recovery can take from some weeks to several months.
A hypothetical trend of recovery from the stroke onset to six months has been clinically described in [2] (Figure 2.2): after an initial phase of spontaneous motor recovery, a plateau is reached.

However, multiple scientific evidences show that rehabilitation must be preferred to spontaneous neurological recovery post stroke, regardless of the chosen therapy

Eugenia Papaleo

[13]; in fact, targeted therapies can facilitate the key factor of the neurological recovery process, i.e. neural plasticity, and help compensate for the functional loss [14]. Neuroplasticity is a brain physiological mechanism enabling the brain to reorganize itself by forming new neural connections and changing the cortical representations of motor actions, in order to compensate for its damaged area [15] [16]. This cortical reorganization can occur in sites close to and/or far from the lesioned area and allows the development of new neural pathways that bypass those damaged by stroke. These neuroplastic changes are favored by therapies based on repetitive movements, active movements and temporized sensorimotor stimuli [17].

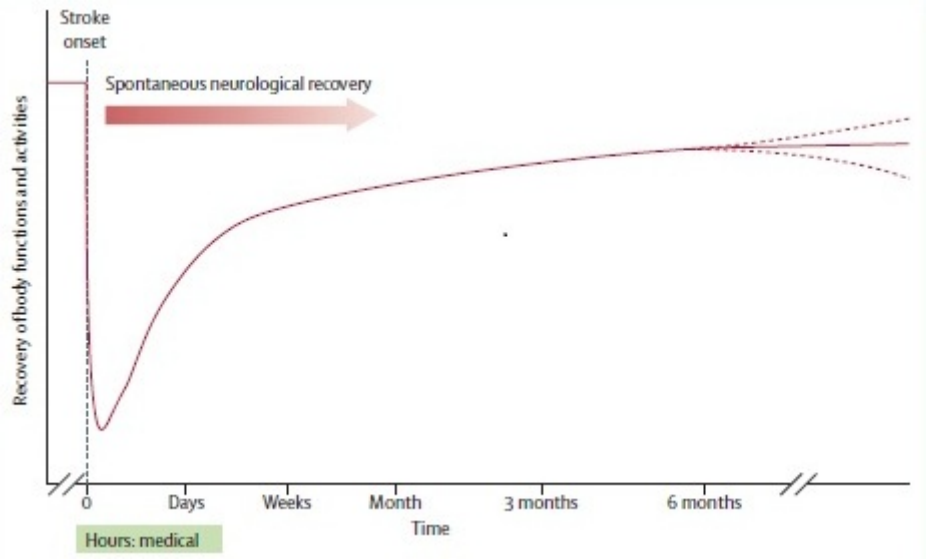

FIGURE 2.2: Hypothetical pattern of spontaneous neurological recovery after stroke (adapted from [2])

Motor deficit is the prominent residual impairment in stroke survivors [18]; the most common motor impairment is hemiplegia (or hemiparesis). It has been estimated that about 80% of stroke survivors are affected by motor control or sensory feedback deficits in the upper-limb of the paretic side [1]. Typical neurological impairments due to motor control deficits are:

- Muscle weakness - It depends on the decreased cortex activation and the subsequent minor muscular recruitment;
- Hyperactive reflexes - They are due to an increased muscle tone, joint resistance and spasticity;
- Abnormal muscle synergies - They are due to the loss of independent joint control and involuntary co-activaction of muscles, even if antagonist.

Eugenia Papaleo

Rehabilitation is the prominent intervention for dealing with upper-limb motor impairment [2].

Up to sixty years ago, rehabilitation of upper-limb impairments after stroke was considered an orthopedic problem, and thus managed by surgery, bracing and muscle re-education (i.e. training of individual muscles) [19]. Nowadays, stroke therapy generally includes aspects of the different approaches that have been developed in last decades, ranging from muscle re-education to neurofacilitation techniques and repetitive task practice [20].

In recent years, a variety of approaches have been proposed to deal with motor impairment in the upper-limb; these include the following:

- Modified constraint-induced therapy (mCIT) - It is an intensive motor practice that consists in restricting the use of the unimpaired limb and forcing the patient to use the affected limb. The therapy is applied varying intensity and duration over time, depending on patient motor residual capabilities [21].
- Electrical stimulation - It is used in the treatment of hemiparesis to enhance sensory awareness, strengthen a weakened body part (such as the arm) and improve range of motion. Therapy consists in placing small electrical pads on the weakened muscles of the affected limb and releasing electrical stimulation for helping muscles to contract, as the patient works to perform a movement [22].
- Cortical stimulation - It is the electrical stimulation of the brain cortex. It has a twofold approach:
  - TMS (transcranial magnetic stimulation), that uses magnetic fields coming from a coil to stimulate the nervous tissue [23],
  - tDCS (transcranial direct-current stimulation), that employs direct currents released through electrodes applied on the scalp [24].
- Motor imagery - It is the process of imagining the movement of the affected limb. This mental practice activates some motor areas of the brain and some muscles as if the patient is really doing an activity. However, since the cortical activation patterns of stroke patients are essentially unexplored, the underlying mechanism of motor imagery training need to be further investigated [25].

Traditional motor rehabilitation for stroke patients consists of individual sessions with a therapist that administers repetitive motor exercises and assists the patient

Eugenia Papaleo

in their execution. Although there are different treatment procedures and different recommendations (e.g. the exercises to administer, the type of movements to perform, etc.), the interaction between therapist and patient has been categorized into four main classes [26]:

- Passive movement - The patient remains relaxed, while the therapist moves his/her joints. This approach mainly aims at maintaining range of motion at joints and flexibility in muscles and connective tissues.
- Active-assisted movement - The patient attempts to move a joint or the affected limb, and the therapist assists the patient as needed. This approach is used when the patient cannot complete a desired movement independently.
- Active-resisted movement - The patient has to perform a movement against some degree of resistance (gravity, additional weights, elastic band, or the therapist). This approach is used with mild-moderate patients.
- Bilateral movement - The patient moves the impaired limb imitating the simultaneous movement of the unimpaired limb.

Although the increasing effort made in the development of new methodologies to enhance motor recovery of patients following a stroke, the type of therapy leading to optimal results remains controversial and elusive [27] (due to several factors, e.g. discrepancies in therapy sessions, quantification of dosage and rehabilitation type) and patients are often left with considerable movement dysfunctions [4].

2.2 Stroke evaluation

As regards the evaluation of motor and functional impairment as well as motor and functional recovery, several clinical scales, that must be administered by qualified health care professionals, exist. Some of the scales that are most commonly employed in the clinical practice are reported in Figure 2.3 together with a brief description.
The use of standardized measures of the outcomes of rehabilitation treatments is an integral part of the stroke rehabilitation process and is widely recommended as good practice [28]. However, clinical scales have a series of drawbacks that cannot be neglected, e.g.: scales are subjective (operator-dependent), descriptive and limited to specific movement features; moreover, they have low sensitivity,

Eugenia Papaleo

discrete scores and require time-spending administration procedures.
In a recent survey [29] on 84 health care professionals and 12 service managers and commissioners working in stroke services, 81 different tools for therapy outcomes' evaluation were identified, 16 of which were unpublished and unvalidated. Furthermore, the barriers perceived by clinicians in the daily use of clinical scales included lack of time and training and lack of knowledge of the appropriate measures to perform. However, the same clinicians stated the importance of demonstrating the efficacy of rehabilitation interventions and monitoring patients' progress.

Scale	Descripted features
Fugl-Meyer (FM)	Motor and joint function and sensation
Motor Power (MP)	Shoulder and elbow force
Wolf Motor Function Test (WMFT)	Joint-specific and total limb performance
Modified Ashworth Scale (MAS)	Muscle tone
Barthel Index (BI)	Indipendent functioning and mobility in daily life
Functional Indipendence Measure (FIM)	Sensitivity and comprehensiveness in daily life
Motor Activity Log (MAL)	Arm usage

FIGURE 2.3: Examples of clinical scales employed for the evaluation of motor and functional impairment in the upper-limb [3]

2.3 Rehabilitation robotics

As mentioned above, an important feature of traditional therapy is that high-intensity, repetitive, active and task-oriented training is a key factor for promoting neuroplasticity and stimulating motor re-learning [30]. In this line, the use of technological tools can provide the opportunity to design interventions that take this type of training into account; in particular, a promising key-factor is the employment of rehabilitation robotics to complement conventional therapy.

2.3.1 Robot-aided therapy

In 2010, the American Heart Association (AHA) published a comprehensive overview on nursing and interdisciplinary rehabilitation care of stroke patients [31]; here, the best available evidences for screening tests and medical treatments, including

Eugenia Papaleo

traditional rehabilitation therapies and robot-assisted therapies, were reported. In short, upper-extremity robot-aided therapy is considered as Class I-Level of Evidence A for stroke outpatients care and chronic care settings, while it is considered as Class IIa-Level of Evidence A for stroke inpatients care.

The use of robots offers several potential advantages in stroke rehabilitation, since it enables:

- high-intensity, repetitive, active and task-oriented training [32];
- movement constraints' application [33];
- repeatability and precisely controllable assistance or resistance [14];
- labour-intensive and patient independent training [4];
- the acquisition of objective kinematic and dynamic metrics that can be exploited for i) the evaluation of patient residual motor capabilities and therapy outcomes, ii) the administration of patient-tailored therapies that adapt the assistance to subject motor outcomes, iii) the investigation on pathology-related planning and motor strategies [34] [35];
- the use of game scenarios for augmenting patient involvement [9].

The open question that researchers have tried to address for several years is if the administration of robot-aided motor therapy can lead to higher motor and functional improvements than conventional therapy. Many randomized controlled trials have been performed on this topic [33] [36] [37]. The results show, in general, that when the duration and the intensity of conventional therapy are perfectly matched with those of the robot-aided therapy, no meaningful differences exist in terms of motor recovery, activities of daily living, strength, and motor control; instead, extra sessions of robot-aided therapy, in addition to regular conventional therapy, can lead to an improvement of motor recovery of the hemiparetic limb with respect to standard conventional therapy alone.
Therefore, robotic technologies can be exploited to augment therapist skills [38] and can be seen as advanced tools available to therapists; moreover, it must be considered that robotic systems cannot replace those abilities that are typical of a human operator.

In line with the types of patient-therapist interaction reported in Section 2.1, robotic devices can be programmed in different ways for applying forces that

Eugenia Papaleo

guide, stimulate or contrast patient movement [26]; therefore: (i) in passive mode, the robotic device moves the arm of the patient along a pre-planned trajectory, while the patient remains relaxed, (ii) in active-assisted mode, the robotic device provides assistance during patient motion if the patient is not able to complete the movement, (iii) in active-resisted mode, the robotic device opposes a pre-determined resistance to the movement executed by the patient.

According to the patient-robot mechanical interface, upper-limb rehabilitation machines can be classified into two main categories [39] (Figure 2.4):

1. *End-effector robots*, where the physical contact with the patient is limited to the end-effector;
2. *Exoskeleton robots*, conceived as machines to be worn by the patient, thus entailing a physical contact all along the arm or part of it.

Motor exercises for end-effector systems are defined in the Cartesian space (the space in which the hand and the end-effector move) and the robotic assistance is generally provided through impedance/admittance control schemes in the robot task space.
There are two main types of end-effector systems, all characterized by the lack of control on arm joint rotations: 2D systems (e.g. MIT-MANUS [40] Figure 2.5(a), Braccio di Ferro [41] Figure 2.5(b)) and 3D systems.
Referring to Figure 2.4, *multi-robot* are 3D systems that use a dual robot configuration (e.g. REHAROB [42] Figure 2.6(a), iPAM [43] Figure 2.6(b)) to coordinate the movement of upper arm and forearm segments. *Bilateral* end-effector systems are conceived for delivering bilateral therapies (MIME [44] Figure 2.7(a), Bi-Manu-Track [45] Figure 2.7(b)) being equipped with a second robot (or a passive arm) which end-point is attached to the hand of the unimpaired arm. *Wire-based* systems, such as the Gentle/S system [46] (Figure 2.8), represent a particular case since, combining orthosis for the arm segments and passive sling suspension mechanisms for gravity support, this robots can be considered at the halfway point between end-effector and exoskeleton robots (Figure 2.4 - unilateral+wire-based).
On the other and, exoskeleton robots allow controlling arm joint motion where the Degrees of Freedom (DoF) of the robot are active (e.g. ARMin [47] Figure 2.9(a), L-EXOS [48] Figure 2.9(b)). While this means that the arm joint angles are known and monitored, the misalignments between the exoskeleton robot axes and the patient arm joint axes are always possible.

Eugenia Papaleo

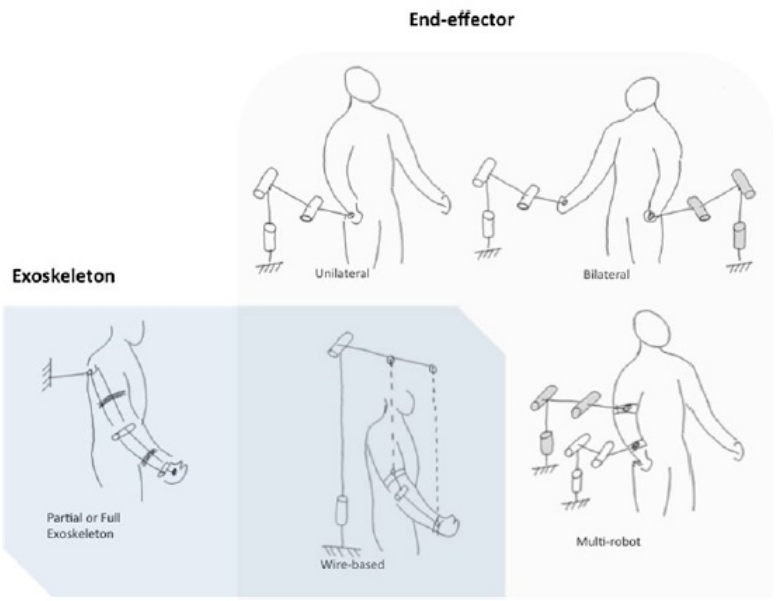

FIGURE 2.4: Upper limb rehabilitation robot generalized categories [4]

(a) MIT-MANUS system

(b) Braccio di ferro system

FIGURE 2.5: Examples of 2D end-effector robots

(a) REHAROB system

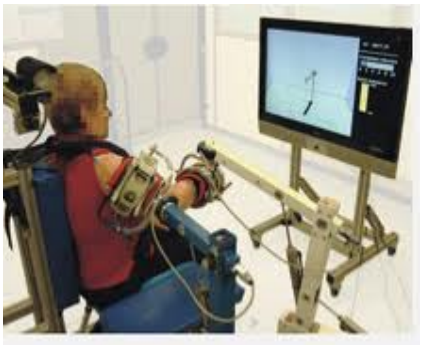

(b) iPAM system

FIGURE 2.6: Examples of multi-robots

Eugenia Papaleo

(a) MIME system

(b) Bi-Manu-Track system

FIGURE 2.7: Examples of bilateral end-effector robots

FIGURE 2.8: Gentle/S system

(a) ARMin system

(b) L-EXOS system

FIGURE 2.9: Examples of exoskeleton robots

Eugenia Papaleo

System	Developer	UL segment	DOF assisted	Description
Act 3D	Northwester University, USA	Shoulder + elbow	3 active DOF, 3D space	Gravity compensated or enhanced. Passive, active assistive, resistive modes. Based on the Haptic Master robot.
ADLER	Medical College of Wisconsin, USA	Shoulder + elbow + forearm + wrist	3 active, 3 passive DOF, 3D space	Based on the Gentle/S system. Reaching in any direction with real target objects. Used in combination with a FES glove for grasping of real objects.
ARM-Guide	Northwester University, USA	Shoulder + elbow	1 active DOF, 2D space	Gravity mitigated, reaching in any plane, address learn non-use. Passive, active assistive, resistive modes. Based on slide mechanism allowing straight line movement.
Bi-Manu-Track	Klinik-Berlin/Charite Hospital Germany	Forearm + wrist	1 active DOF at one time	Gravity mitigated, address learn non-use and uses mirror image movement. Passive, active assistive, resistive modes.
Braccio di Ferro	University of Genova, Italy	Shoulder + elbow	2 active DOF, 2D space	Planar reaching. Passive, active assistive, resistive modes. Based on MIT-MANUS system.
Gentle/S	University of Reading, UK	Shoulder + elbow + forearm + wrist	3 + 1 active, 2 passive DOF, 3D space	Gravity compensated, reaching in any direction, visual, haptic and audio feedback. Passive, active assistive, resistive, trajectory decision making. Based on Haptic Master robot.
iPAM	University of Leeds, UK	Shoulder + elbow + forearm	5 active DOF, 3D space	Similarly to REHAROB system it uses two robots. Passive, active assistive modes.
MEMOS	Fondazione Salvatore Maugeri/SSSA, Italy	Shoulder + elbow	2 active DOF, 2D space	Planar reaching. Passive, active assistive, resistive modes. Visual and audio feedback.
MIT-MANUS (InMotion2)	Massachusetts Institute of Technology/ Interactive Motion Technologies, USA	Shoulder + elbow	2 active DOF, 2D space	Gravity mitigated, planar reaching, address learn non-use. Passive, active assistive, resistive modes. Based on SCARA type manipulator.
MIT-MANUS (InMotion3)		Forearm + wrist	3 active DOF	Similar to above, but motion is for pro-supination of forearm and Ab-adduction, Flex-extension of wrist)
Java Therapy	University of California, Irvine, USA	Wrist	2 active DOF, 2D space	Limited planar motion and active assistive modes. Game-like visual and audio feedback, telerehabilitation function.
MIME	Rehab Research Development Center at VA, Palo Alto, USA	Shoulder + elbow	3 active DOF, 3D space	Mirror image passive, active assistive and resistive movement therapy. Address learn non-use, can perform also unilateral exercises.
NeReBot	University of Padova, Italy	Shoulder + elbow	3 active DOF, 3D space	Gravity compensated. Passive and active assistive. Visual and audio feedback. Splint, 3 wires and linkages provide arm orientation/position.
REHAROB	Budapest University of Technology and Economics, Hungary	Shoulder + elbow + forearm	5 active DOF, 3D space	Passive, single or multijoint coordination, range of motion training to address spasticity. Visual feedback. Based on two 6DOF industrial robots.

FIGURE 2.10: Main end-effector robotic rehabilitation systems used in upper-limb clinical practice or research [4]; the developer, the upper-limb (UL) segment trained by the robot, the number of robot DoF and a brief system description are reported

A summary of the main end-effector and exoskeleton robotic rehabilitation systems used in upper-limb clinical practice or research is reported in Figures 2.10 and 2.11.

Eugenia Papaleo

System	Developer	UL segment	DOF assisted	Description
ARMin	ETH, Zurich, Switzerland	Shoulder + elbow	4 active, 2 passive DOF	Gravity compensated, massed practice with target, visual and audio feedback, passive, active assistive.
Hand Mentor	Kinectic Muscles, Inc. USA	Wrist + hand	2 active (wrist and fingers flex-extension)	Portable system, EMG and force feedback. Passive, active assisted modes. Based on McKibben pneumatic actuators.
HWARD	University of California, Irvine, USA	Wrist + hand	3 active (1 wrist, 1 fingers MCP, 1 thumb)	Active assistive motion combining wrist extension with hand grasping and wrist flexion with hand release. Visual and audio feedback.
KIST	Korea Institute of Science and Technology, Korea	Shoulder + elbow + wrist	7 active, 6 passive DOF	Portable system, Passive, active assisted modes. Based on pneumatic and electric brake actuators.
L-EXOS (PERCRO)	Scuola Superiore Sant'Anna, Italy	Shoulder + elbow	4 active, 1 passive DOF	Gravity compensated, massed practice with target, visual and audio feedback, passive, active assistive.
MGA	Georgetwon and Maryland Univ., USA	Shoulder + elbow	4 active, 1 passive DOF	Gravity compensated, visual and audio feedback, passive, active assistive modes.
Myomo e100	Myomo, Inc., USA	Elbow	1 active DOF	Active assistive motion using EMG biofeedback.
Pneu-WREX	University of California, Irvine, USA	Shoulder + elbow	4 active, 1 passive DOF	Gravity mitigated, passive, active assistive. Visual and audio feedback. Based on the T-WREX system.
RUPERT	Arizona State University, Phoenix, USA	Shoulder + elbow + wrist	4 active DOF (1 shoulder, 1 elbow, 1 forearm, 1 wrist)	Passive, active assisted. Graphical display of arm moving to goal. Based on McKibben pneumatic actuators.
Rutgers Master II	Rutgers, State University New Jersey, USA	Hand	4 active DOF (1 thumb, 3 fingers)	Active assisted, resistive modes. Visual, haptic and audio feedback. Used custom pneumatic actuators.

FIGURE 2.11: Main exoskeleton robotic rehabilitation systems used in upper-limb clinical practice or research [4]; the developer, the upper-limb (UL) segment trained by the robot, the number of robot DoF and a brief system description are reported

2.3.2 Robot-based evaluation

As stated in Section 2.2, the traditional evaluation of stroke motor and functional impairment performed through clinical scales suffers from a serious of drawbacks that can be unlikely overcome. However, rehabilitation robots are equipped with sensors that can allow accurate measurements of movement kinematics (e.g. limb trajectories) and kinetics (interaction forces). These measures can be fruitfully exploited for quantitatively assessing patient motion performance through opportune indicators that can be combined with clinical scores for a more exhaustive evaluation of the patient.

Robot-based performance indicators can be classified into three broad categories [35]:

- Kinematic indicators - they quantify spatial and temporal features of patient movement and are defined either in the Cartesian space or in the arm joint space, depending on the feature, the task and/or the type of robot used;

- Kinetic indicators - they quantify force, work, energy consumption and power related to patient movement;
- Neuromechanical indicators - they quantify, for example, the viscoelastic properties or the mechanical impedance of the upper limb at rest.

The meaning of a performance indicator depends on two factors: (i) the motor task for which it is conceived and (ii) the method used for its calculation. Although there are indicators that can be associated with all motor tasks (e.g. the time employed to perform the task), others are specifically conceived for particular motor task.

For clarity of presentation, it must be pointed out that this dissertation is essentially focused on two main types of motor task which are of particular interest in upper-limb robot-aided rehabilitation: (i) point point-to-point tasks, in which the patient hand has to move along a straight line between known start and end points [49] [50], (ii) tracking tasks, in which the patient is required to draw a specific spatial trajectory, such as a square or a circle [50] [51].

Several indicators currently used in rehabilitation robotics for quantifying motor performance exist; each of them is relative to a specific feature of patient motor ability. In the following, the main motor performance indicators are reported (note that, even if the names used here may differ from those used in the cited papers, from the theoretical point of view indicators are equivalent).

- *Accuracy* [52] [53] [54] is a measure of the difference between the trajectory performed by the patient and the desired path. This kinematic measure can be calculated for any movement for which a desired movement path can be defined.

- *Target error* [52] [55] [56] is a quantification of patient capability to move in the direction of the target. This kinematic measure is primarily suited for point-to-point tasks.

- *Duration* [52] [57] [58] measures the time employed by patient to perform the task. This is a general indicators that can be used with most tasks.

Eugenia Papaleo

- *Path length* [52] [55] is the measure of the trajectory traveled by the patient to reach the target and is considered a measure of movement efficiency. This metric can be applied to both the point-to-point and the tracking tasks.

- *Smoothness* [52] [59] [57] [55] is a measure of how gradually a movement is changing. Smoothness is a typical features of healthy motion; it often lacks in stroke subjects' motion that is characterized by a velocity profile with multiple peaks and deep valleys (arrest phases). Smoothness is quantified through different indicators based on the velocity profile or the jerk magnitude. This metric can be applied to both the point-to-point and the tracking tasks.

- *Movement coordination* [60] [61] [62] is the quantification of the spatial and/or temporal coordination between different upper limb joints during multijoint tasks. The upper-limb motion of healthy people is characterized by some synergies between two or more arm joints. Traditionally, this metric is used for quantifying the correlation between shoulder and elbow joint angles and torques and is applied to both the point-to-point and the tracking tasks.

- *Amount of assistance* [53] [55] [56] is a measure that quantifies the patient ability to execute the motor task without the robot assistance. This is a general indicators that can be used with most tasks.

- *Force direction error* [63] [52] [64] quantifies the patient ability to exert force in a desired direction (target direction). This kinetic measure is primarily suited for point-to-point tasks.

Despite the advantages that can be obtained combining traditional clinical evaluation and quantitative robot-based evaluation of motor performance, this latter is still a research topic rather than a clinical tool. The analysis of the State of the Art on this field suggests three possible reasons:

- The clinical use of the quantitative robot-based evaluation of motor performance is not defined. Different types of robotic metrics for quantifying movement behavior have been developed, but there are no evidences on how they can be used for clinical decision making. A meaningful consideration about this lack of evidences is stated in [35]: *How can the smoothness of*

Eugenia Papaleo

supported planar reaching movements be used for tailoring therapeutic intervention that aims to improve a subject's use of his/her arm in activities of daily living?

- The lack of a standard, in terms of tasks, specific indicators and methodologies for their computation.
- The results obtained with robot-aided evaluations are not yet totally convincing. Moreover, these results cannot be compared since studies are often performed considering different methods and tools (e.g. type of patient, robot, performance indicators, methodology for indicators computation).

2.4 Bio-cooperative controllers for rehabilitation machines

Typical stroke robot-aided rehabilitation is very task specific. It uses a sort of "if-then" algorithm: if the patient performs an incorrect motion, then the robot applies a predefined unidirectional action. In this way, the patient has mainly a passive role and his/her needs and/or intentions are ignored.
An interesting alternative for obtaining a more efficient patient-robot interaction is represented by the administration of therapies tailored on patient biomechanical and physiological states [5].

In this perspective, an emerging trend in rehabilitation robotics is the development of systems that place the patient in the control loop (human-in-the-loop) by feeding back his/her biomechanical and physiological state. This systems are called *bio-cooperative* systems. The basic idea of bio-cooperative robotic systems has been defined in [5] [65] and consists of automatically adapting the control system on the basis of the monitored biomechanical and physiological states, with the aim of motivating in an engaging and challenging way the patient.

The idea of monitoring stroke patient performance for updating therapy task difficulty is not new [66]; but, currently, is becoming an emerging theme since multiple evidences show that protocols based on monitoring patient performance and emotional states allow obtaining faster learning and recovery time [9].
In [67], a bio-cooperative system for stroke upper-limb rehabilitation is presented. It adapts the difficulty of a virtual task on the basis of the data provided by a multimodal interface using biomechanical performance metrics (movements and forces) and four physiological signals. In the same work, the question about what are

Eugenia Papaleo

the measurements needed for a bio-cooperative feedback loop (i.e. either task performance or physiological signals or their combination) is addressed. The results of the experimental trials performed on sixteen subjects show that physiological measurements can provide just supplementary information with respect to the performance analysis, but the accuracy of the bio-cooperative controller in matching subjects' preferences is increased when both the measures are considered.
In [68], a bio-cooperative system for stroke robot-assisted gait therapy is proposed. It provides a virtual task which cognitive workload is varied through the modulation of the task difficulty level; the modulation is obtained through a multimodal interface that acquires physiological and performance measurements. The experimental trials conducted on four stroke subjects show that the physiological signals employed are well suited for estimating the task cognitive workload during the robot-aided gait therapy (even if in the presence of the physical effort induced by walking). However, the performed trials suggest that the performance metrics are more practical to obtain in clinical settings and the addition of the physiological measurements to the performance metrics gives few improvements in recognizing patient needs.
In [69], a bio-cooperative robotic platform for stroke upper-limb training is proposed. The system updates the difficulty of the assigned task on the basis of the data provided by three physiological channels, with the aim of maintaining the therapy as intensive as possible. Reports from the questionnaires administered to eight healthy subjects enrolled in the experimental trials show that all subjects experienced a better challenging/satisfying relation in task execution, thus suggesting that the use of a bio-cooperative control system for modulating motor effort leads to an increased engagement of the user.

The functional scheme of a bio-cooperative rehabilitation robotic system is shown in Figure 2.12.

The main components of the system are:

- The patient - He/she interacts with the robot arm; simultaneously, his/her state is realtime monitored through the acquisition of physiological and biomechanical signals.
- The *multimodal interface* - It is the hardware/software complex system able to acquire data from multiple sensory channels and interpret patient biomechanical, physiological and psychological condition. Its output is the realtime quantification of patient global state and the online display of a visual feedback about the ongoing task.

Eugenia Papaleo

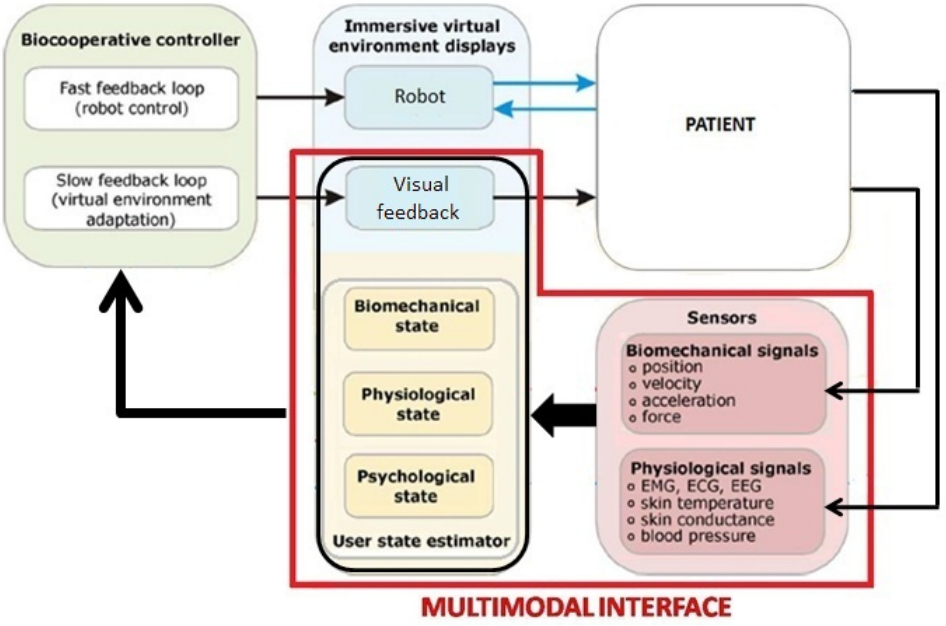

FIGURE 2.12: Functional scheme of a bio-cooperative rehabilitation robotic system (adapted from [5])

- The bio-cooperative controller - It integrates two types of control: the robotic control, characterized by a fast feedback loop, and the virtual environment adaptation, characterized by a slow feedback loop.
- The robot - It interacts with the patient by applying the corrective or resistive forces commanded by the robotic controller.

As regards the multimodal iterface, it is characterized by three unique features: (i) the real-time data processing, (ii) the fusion of different types of data and (iii) the display of a virtual reality environment relative to task execution.
The integration of virtual reality environments in robotic rehabilitation systems is an increasing trend since experimental evidences show that they represent a powerful tool for augmenting patient involvement and participation [9] [70]; moreover, they can provide different training scenarios and return enhanced feedback about patient movement [71].
While the estimation of patient biomechanical state (i.e. patient motor performance) is generally obtained exploiting robot-derived kinematic and dynamic measurements on task execution, additional sensory systems are employed for the acquisition of physiological signals, such as heart rate, respiration rate, skin conductance, skin temperature and electromyographic (EMG) activity. However, how to use these signals for extracting information on patient psycho-physiological state

Eugenia Papaleo

is still an open question. Researchers concur on the idea that psycho-physiological states, such as mood, motivation and engagement, are critical for rehabilitation success [72] and an increased patient participation during therapy can improve his/her recovery [73]. But, the interpretation of psycho-physiological states is very complicated for a twofold reason, i.e.: (i) physiological signals are influenced also by physical activity (i.e. there is an interplay between mental and physical activity on physiological responses) and (ii) the patient damage to the nervous system [74]. By now, physiological signals have been used for estimating the patient cognitive [68] and physical workload [69].

Electromyographic activity, instead, is not used for the interpretation of psycho-physiological states; but, since some signal features in temporal and frequency domain highly correlate with muscular force, power and fatigue [75] [76] [77], this signal is employed for the analysis of motor performance.

Eugenia Papaleo

Chapter 3

The proposed bio-cooperative system for upper-limb robot-aided rehabilitation

In this chapter the proposed bio-cooperative system for upper-limb robot-aided rehabilitation is presented. It is composed of two main modules (Figure 3.1), described in detail in the following:

- A multimodal interface (Section 3.1) - It evaluates patient performance and realtime displays a virtual reality environment relative to the execution of the assigned task;
- An adaptive robot control system (Section 3.2) - It modulates the complexity of the assigned motor task, allowing the administration of a patient-tailored therapy.

A special attention has been paid to the development of an unobtrusive system for delivering motor therapy without altering user natural motion.
Moreover, it is expected that the employment of such a system will allow adapting therapy to patient characteristics, maximizing patient motivation and involvement in the therapy by favoring his/her active role, continuously assessing the progress of the recovery and increasing the rate of motor re-learning.

Eugenia Papaleo

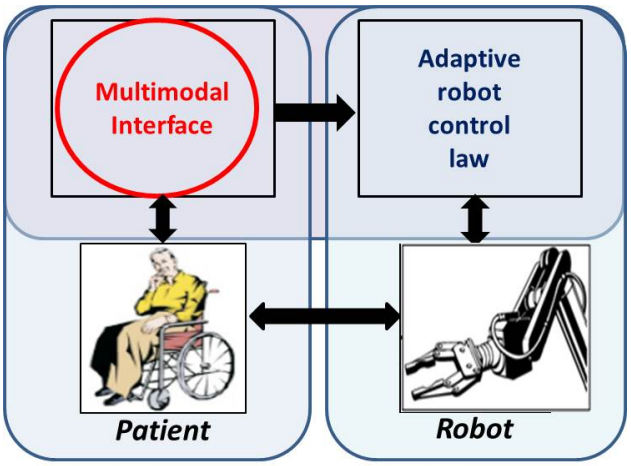

FIGURE 3.1: Functional scheme of the proposed bio-cooperative system for upper-limb robot-aided rehabilitation

3.1 The multimodal interface

The functional architecture of the proposed multimodal interface is shown in Figure 3.2. The interface receives as input motion, force and physiological data, and gives as output two types of data: one is sent to the video screen for displaying the virtual reality environment relative to task execution, one is sent to the adaptive robotic controller and consists in the quantification of the patient global performance.

The key issues pursued in the development of the multimodal interface are:

- Determining a complete picture of patient performance;
- Selecting measuring systems characterized by low obtrusiveness;
- Exploiting data from robot sensors, thus employing a minimum number of additional sensors;
- Requiring a low computational burden, thus enabling realtime applications.

Therefore, as explained in the following Sections, sensors for motion, force and physiological data have been selected and, where needed, a procedure for processing the acquired data has been defined. Then, kinematic, dynamic and physiological indicators able to quantify patient motor performance have been defined. Finally, the module for estimating patient global performance and the virtual reality software have been designed.

Eugenia Papaleo

The multimodal interface has been developed through the *Matlab/Simulink* software (Mathworks Inc.), *Real-time Windows Target* and *Virtual Reality* toolboxes.

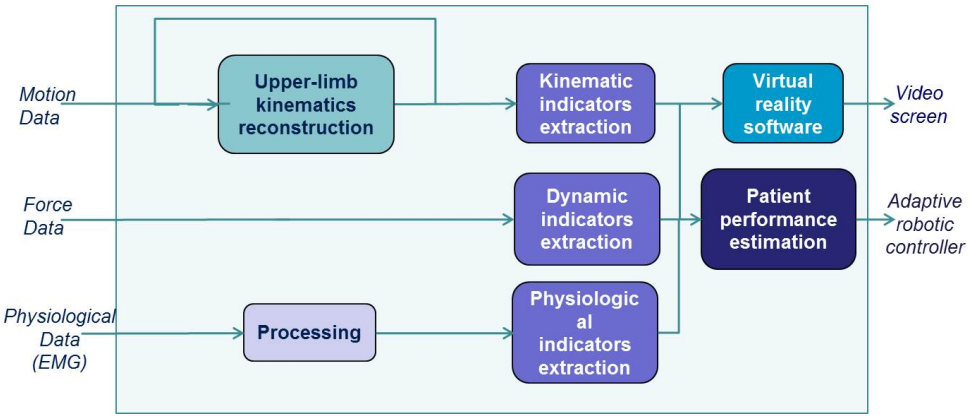

FIGURE 3.2: Functional architecture of the developed multimodal interface

3.1.1 Data acquisition

3.1.1.1 Motion data acquisition

Patient motion data are acquired by exploiting the sensory system embedded in the robotic machine. In particular, on the basis of the type of employed robotic machine:

- if an anthropomorphic exoskeleton robot is used, hand pose data and arm joint angles are easily provided by the robot;
- if an end-effector machine is employed, only hand motion data are available from the robotic device.

In this second case, a purposely developed method for reconstructing the entire upper-limb kinematics during robot-aided tasks with end-effector machines is applied; it is presented in Chapter 4.

3.1.1.2 Force data acquisition

As for motion data, the sensory system needed to the acquisition of the patient-robot interaction forces is either fully or partly embedded in the robotic machine. Therefore, depending on the type of robot used (exoskeleton versus end-effector

Eugenia Papaleo

robot) and/or the type of sensors embedded in the robotic machine, it has been chosen to exploit:

- the robot force sensors at the end-point level;
- the robot torque sensors at joint level.

In this second case, in order to obtain the interaction forces in the Cartesian space, the robot statics relation is applied, i.e.:

$$\bar{\tau} = J^T(\bar{q})\bar{\gamma}, \tag{3.1}$$

where $\bar{\tau}$ represents the joint torque vector and $\bar{\gamma}$ is the corresponding force/torque vector in the Cartesian space.

3.1.1.3 Physiological data acquisition and processing

As regards the analysis of patient physiological data, in order to evaluate the upper-limb muscular force, power and fatigue of patients undergoing robot-aided therapy, the surface electromyographic (EMG) activity of couples of agonist-antagonist muscles of the upper-limb has been considered.

The choice to limit the analysis of physiological data to the EMG signals is due to a series of considerations. On the one hand, there is still no a universally accepted set of rules for translating the commonly used physiological data (i.e. heart rate, respiration rate, skin temperature, skin conductance) into psychological states [74]; moreover, psychologists do not agree about the fact that psychological states can be classified into discrete, specific emotions [78]. On the other hand, the EMG activity, although is a physiological signal, is here used for assessing human muscular performance and, in this respect, is exploited for providing motor performance data.

For the acquisition of each EMG signal, a *bipolar* configuration of the electrodes has been used, since in bipolar recordings the differential amplification selectively amplifies the difference between the signals recorded by two electrodes and suppresses the common signal (i.e. the background noise).

The raw EMG recording contains very important information that only a targeted signal analysis can extract. Therefore, in order to extract those signal features that are related to muscular performance, a carefully processing procedure has been

Eugenia Papaleo

designed. In particular, it has been chosen to consider signal information related to both the time domain and the spectrum domain and, hence, two separated processing procedure have been applied.
In time domain, where features related to the amplitude of the signal are significant [6], the following steps have been considered:

1. Signal rectification,
2. Signal normalization,
3. Low pass filtering of the signal.

The rectification allows converting all negative signal values into positive values; the main effect is that standard amplitude parameters, such as mean, peak value and area, can be easily computed (the raw EMG has a mean value of zero).
The normalization is performed on the pre-recorded maximum voluntary contraction (MVC) [6]. One big drawback of any EMG analysis, in fact, is that the amplitude of the signal is strongly influenced by the detection conditions (i.e. electrode sites, subjects, electrode application, etc.), but the normalization procedure allows re-scaled it from microvolts to the percent of a reference value, i.e. the MVC (measured before starting the EMG acquisition).
Low pass filtering (cutoff frequency of $10Hz$ - Butterworth, 3rd order) allows obtaining the signal envelope. The pattern of any EMG signal, in fact, has a random nature depending on the number of motor units that are recruited. The non-reproducible part of the signal is minimized by applying a digital low pass filter that outlines the mean trend of signal [79].

In frequency domain, it is possible to extract EMG signal features related to muscular power and fatigue [6]. To this purpose, a two-step procedure has been designed:

1. In order to analyze the frequency contents of the EMG activity, the signal spectrum is computed through the Fast Fourier Transformation (FFT);
2. A band pass filter is applied.

The pass band of this latter filter has been chosen equal to $10-500Hz$. Except for the computation of the EMG signal envelope (for the amplitude analysis), in fact, scientific recommendations for research studies on surface EMG signals (SENIAM - surface EMG for non-invasive assessment of muscles, ISEK) [80] deny any narrow

Eugenia Papaleo

band setting and state that the aim is to measure the EMG activity in the full band length of 10 to $500Hz$.

Finally, the following couple of antagonist muscles have been selected:

1. biceps and triceps muscles,
2. pectoral and deltoid muscles;

The biceps muscle is a bi-articular muscle that acts on both the upper and forearm; besides stabilizing the scapulo-humeral complex (by contributing to hold the humerus head in the glenoid cavity of the scapula), it is the main responsible for forearm flexion. The triceps muscle is the principal extensor muscle of the forearm; moreover, through its longhead, it promotes shoulder adduction. The deltoid muscle belongs to the shoulder muscles; its contraction can abduct the arm up to 90°. In particular, the posterior deltoid acts on shoulder extension and, to a lesser extent, also on shoulder abduction and extra rotation. The pectoral muscle adducts and intra-rotates the upper arm and, with the humerus fixed, contributes to lift the trunk.

3.1.2 Extraction of indicators on patient performance

In this Section the performance indicators computed by the multimodal interface using the processed motion, force and EMG data are described.
In order to define the most suitable parameters for quantitatively describing patient motor performance, a careful analysis of the State of the Art on this theme has been carried out; then, indicators have been selected (if needed ad-hoc readapted) and defined. In particular, it has been chosen to consider movement features related to: kinematics (space and time features), dynamics (force and work features), electromyographyc activity (muscular force, muscular power and muscular fatigue).

The performance indicators extracted by the multimodal interface can be categorized into the following classes:

- Biomechanical performance indicators (Section 3.1.2.1),
  - Kinematic indicators in the Cartesian space,
  - Kinematic indicators in the joint space,

Eugenia Papaleo

– Dynamic indicators,

- Electromyographic indicators (Section 3.1.2.2).

As discussed in Section 3.1.3, the extracted performance indicators are used for quantitatively determining patient global performance. In Chapters 5 and 6, the employment of the selected indicators (i) in an experimental bio-cooperative robotic system for upper-limb rehabilitation and (ii) for the quantitative evaluation of the outcomes of a novel rehabilitation treatment, respectively, will be described.

3.1.2.1 Biomechanical performance indicators

The biomechanical performance indicators account for kinematic and dynamic features of the executed motion. They are specifically conceived for point-to-point movements, although some of them can be fruitfully employed with other tasks (e.g. circle-drawing task).

Kinematic indicators in the Cartesian space

The kinematic indicators in the Cartesian space are extracted from the sensory signals coming from the encoders embedded in the robot, after evaluating robot forward kinematics. They are conceived to assess the following movement features: direction, accuracy, smoothness, speed and efficiency.
They are listed and described in the following.

- *aiming angle* (ϕ) - It represents the angle between the target direction ($\vec{tg}_{dir}$) and the direction of travel ($\vec{h}_{dir}$) from the starting point up to peak speed point [52] (Figure 3.3); it accounts for movement direction and is defined as

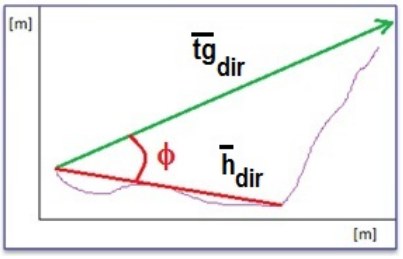

$$\phi = acos(\bar{tg}_{dir} * \bar{h}_{dir})/(||\bar{tg}_{dir}|| * ||\bar{h}_{dir}||).$$

FIGURE 3.3: Schematic representation of the *aiming angle* index

- *normalized Mean Deviation* - It is the mean absolute value of the distance between the desired path and the curve actually performed by the patient (Figure 3.4), normalized on the maximum deviation (or on the length of the theoretical path) [55]; it accounts for movement accuracy.

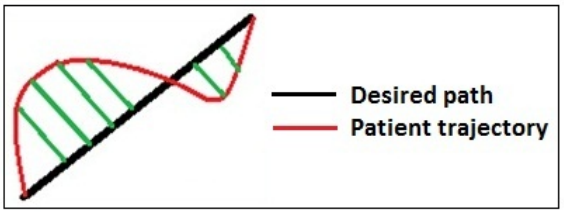

FIGURE 3.4: Schematic representation of the *normalized Mean Deviation* index

- *AREA* - It represents the area between the theoretical path and the trajectory performed by the patient [52] (Figure 3.5); as the previous, it accounts for movement accuracy.

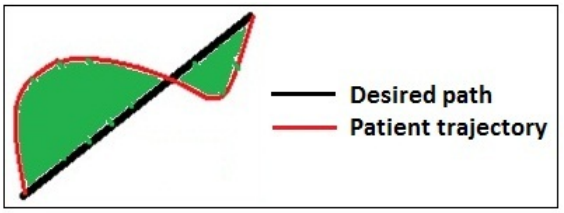

FIGURE 3.5: Schematic representation of the *AREA* index

- *Speed Metric* - It is the ratio between the mean speed and the peak speed and accounts for movement smoothness [59]. As known, unconstrained point-to-point movements of healthy subjects are characterized by high smoothness and modelled as *minimum jerk* trajectories [81] (Figure 3.6) with bell-shaped velocity profiles; conversely, stroke patients generally move in an "episodic" manner, stopping multiple times before reaching their objective (i.e. *jerky* motion). The speed profile of such a stroke motion is composed by multiple peaks or sub-movements (Figure 3.7), causing a decreased mean speed.

- *Mean Arrest Period Ratio* - It represents the proportion of time (i.e. the percentage of samples) that movement speed exceeds the 10% of the peak speed [59]; it accounts for movement smoothness.

- *Deviation from Ratio between Velocities* - It is the absolute deviation of the ratio between peak velocity and mean velocity from the constant value 1.875

Eugenia Papaleo

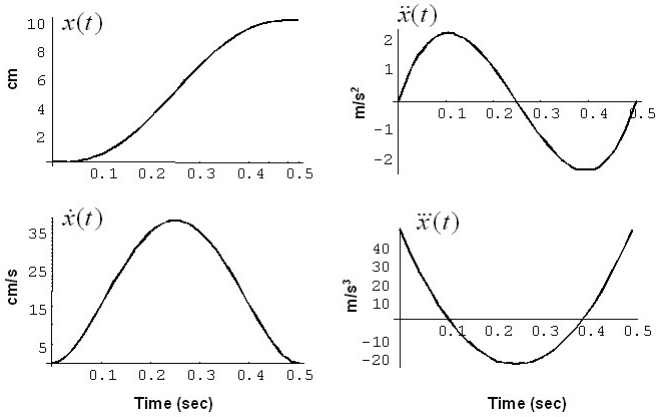

FIGURE 3.6: Representation of a *minimum jerk trajectoy*; the profiles of position, tangential velocity, acceleration and jerk are illustrated

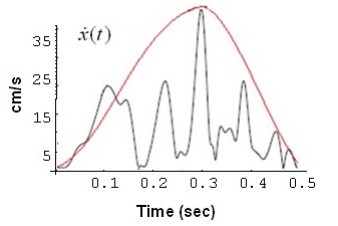

FIGURE 3.7: Representation of the tangential velocity profile of a *jerky* movement

(corresponding to the value of the same ratio in the minimum jerk trajectory [81]); it accounts for movement speed.

- *Success Rate* - It represents the percentage of times that the patient reaches the target during a therapy session [54]; it accounts for movement efficiency.
- *Movement Duration* - It is the time spent by the patient for executing the task and is computed from movement onset (i.e. when velocity exceeds the 10% of peak speed) and movement termination (i.e. when velocity goes below the 10% of peak speed) [52]; it accounts for movement efficiency.
- *Path Length* - It is the length of the path travelled by the patient and is computed as the line integral of the trajectory over the Movement Duration, normalized onto the desired path [55]; it accounts for movement efficiency.
- *Manipulability Indices* - They are computed from the 3D ellipsoid of manipulability (i.e. the velocity ellipsoid) in the Cartesian space [82]. Two indices are considered; the first one (w_1) is proportional to the volume of the ellipsoid and represents the global hand capacity of velocity generation, while the second index (w_2) is related to the isotropy of the ellipsoid and represents the distribution of the hand capacity of velocity generation along each direction of the Cartesian space (when its value tends toward zero, the ellipsoid approaches a spherical shape, meaning that the capability to generate a tangential velocity is the same in every direction). They account for movement efficiency and are computed as

$$w_1 = \sqrt{det\,(J(\bar{q})J(\bar{q})^T)}$$

Eugenia Papaleo

$$\text{and}$$

$$w_2 = \sqrt{1 - \frac{\sigma_n^2}{\sigma_1^2}},$$

being $J(\bar{q})$ the upper-limb Jacobian matrix and $J(\bar{q})^T$ its transpose, *det* the determinant of the product matrix, σ_n and σ_1 the highest and the lowest singular value of J, respectively, that are obtained by the singular value decomposition (SVD) of the matrix.

As can be noticed, there are indicators describing the same movement feature, thus allowing to choose the most appropriate in relation to the task and/or the application.

Kinematic indicators in the joint space

The kinematic indicators in the joint space are extracted from the signals coming from the robot sensors (and, if an end-effector robot is used, from a magneto-inertial sensor placed on the patient arm, after reconstructing patient joint angles - this is explained in Chapter 4). They are conceived to assess the following movement features: range of motion and coordination.
They are listed and described in the following.

- *Range of Motion* - It is the absolute value of the difference between the maximum and the minimum value of each joint angle, normalized on the anatomical range of motion.
- *Inter-joint coordination* - It is defined as the correlation index between two upper-limb joint angles q_i and q_j, and is computed as

  $$q_{corr_{i,j}} = R(q_i, q_j) / \sqrt{R_{q_i}(q_i) * R_{q_j}(q_j)},$$

  where $R(q_i, q_j)$ is the covariance matrix, $R_{q_i}(q_i)$ and $R_{q_j}(q_j)$ are the two auto-covariance matrices [61]. This index accounts for the coordination between two arm joint angles, which is normally affected after stroke.
- *Coefficient of Multiple Correlation of Continuous Relative Phases (CMC)* - It is the Coefficient of Multiple Correlation of the Continuous Relative Phases (CRPs) over repetitive tasks [83]. Since the CRP plot describes the coupling trend between two interacting joints, this indicator, conceived for cyclic movements, quantifies the repeatability of such a coupling. It is defined as

Eugenia Papaleo

$$CMC = \sqrt{1 - \frac{\frac{1}{T(N-1)} \sum_i^N \sum_t^T (CRP_{it} - C\bar{R}P_t)^2}{\frac{1}{TN-1} \sum_i^N \sum_t^T (CRP_{it} - C\bar{R}P)^2}},$$

being T the number of samples within the cyclic movement, N the number of cycles, CRP_{it} the $t-th$ point of the CRP of the $i-th$ cycle, $C\bar{R}P_t$ the mean CRP at point t over the N cycles and $C\bar{R}P$ the "grand mean".

Finally, as described in Chapters 5 and 6, performance indicators in the joint space are computed for the shoulder and the ebow DoFs, since the selected rehabilitation tasks, requiring hand positioning (rather than subtle hand orientation), mainly involve shoulder and elbow joints. In particular, the *Range of Motion* can be computed for all the shoulder and elbow DoF, while the *Inter-joint coordination* has been determined for i) shoulder abduction/adduction and elbow flexion/extension and ii) shoulder flexion/extension and elbow flexion/extension.

Dynamic indicators

The dynamic indicators are extracted from the sensory signals provided by the robot force/torque sensors. They are conceived to assess force exertion and work expenditure [52].
They are listed and described in the following.

- *Mean Force* - It is the mean value of the force exerted by the patient during task execution.
- *Useful Mean Force (UMF)* - It is the amount of mean force ($\bar{f}$) along target direction ($\bar{tg}_{dir}$) (Figure 3.8) and is defined as

$$UMF = (\bar{f} * \bar{tg}_{dir})/norm(\bar{tg}_{dir}).$$

- *Useful Peak Force* - It is the amount of peak force along target direction.
- *Useful Work* - It represents the portion of patient total work along target direction.

3.1.2.2 Electromyographic indicators

The electromyographic indicators are extracted from the signals provided through the acquisition of the EMG activity of couples of agonist-antagonist muscles of the

Eugenia Papaleo

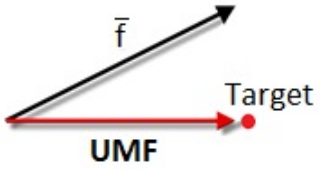

FIGURE 3.8: Schematic representation of the *Useful Mean Force* index

upper-limb, after signal processing (both in the time and the spectrum domain). The EMG indicators are conceived to assess muscular force, muscular power and muscular fatigue.
They are listed and described in the following.

- *Root Mean Square value* - It is the quadratic mean of the signal amplitude over the entire task execution. This indicator provides a measure of the muscular force [77] and the muscular power [6] [84].
- *Power Spectrum* (Figure 3.9) - It is the total power spectral density of the electromyographic signal; it provides a measure of the energy content of the myoelectric signal and, hence, of the muscular power [6] [84].
- *Co-Contraction Index (CCI)* - It quantifies the simultaneous activation of antagonist muscles crossing a joint; it is computed in the signal time domain as [85]

$$CCI = 0.5\frac{LowerEMG}{HigherEMG}(LowerEMG + HigherEMG),$$

  where $LowerEMG$ and $HigherEMG$ is the amplitude of the less and more active muscle, respectively. Since, excessive co-contractions of antagonist muscles during dynamic activities impair functional performance and increase the metabolic cost of performing the task [86], a low value of the co-contraction index is desirable.
- *Median Frequency* (Figure 3.9) - It is the median of the frequency distribution of the electromyographic signal obtained after the Fast Fourier Transform computation. This indicator is widely employed in the quantitative assessment of the electromyographic activity [87] [88] [89] and its trend is characterized by an increase with muscle force and a decrease with muscle fatigue [77].
- *Fatigue index* - It is the slope of the regression line of the Median Frequency over multiple tasks and quantifies the variation of muscle fatigue [6] [90]; its schematic representation is reported in Figure 3.10.

Eugenia Papaleo

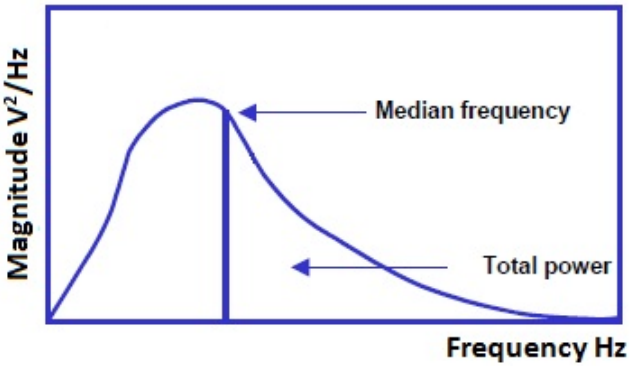

FIGURE 3.9: EMG frequency parameters, adapted from [6]

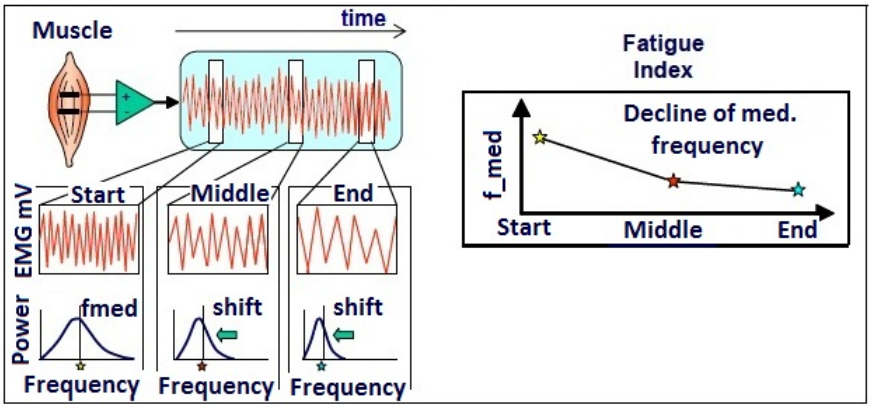

FIGURE 3.10: Schematic illustration of the median frequency shift towards lower frequencies in repetitive contractions and calculation of the muscle fatigue index. Adapted and redrawn from [7]

Before concluding this Section, it is worth reporting a few considerations about the functional meaning of the wide number of performance indicators that have been selected.

As regards the kinematic indicators in the Cartesian space, it is presumable that an improvement of direction, accuracy, smoothness, velocity, efficiency (enhancement of Movement Duration and Path Length), as well as a reduced percentage of pauses, during robot-assisted point-to-point movements can have positive effects in terms of capability also to carry out functional tasks typical of real life scenarios (e.g. feeding, drinking, dressing, bathing, reaching a bottle on a table or a book on a shelf, etc.). As regards the kinematic indicators in the joint space, an augmentation of the angular excursion of the upper-limb DoF could be easily reproducible also in real life movements as well as an increasing of the capability to independently move shoulder and elbow joints could be directly exploited also in ADL motions.

The same kind of considerations can be made for dynamic and electromyographic

Eugenia Papaleo

indicators; in fact, it can be expected that an increased ability in the generation of targeted forces and work or an augmentation of the muscular power and force during robot-aided exercises could be reflected by an improvement of kinetic performance also in functional tasks.
The expected transfer of the motion improvements from analytical to functional tasks is also supported by evidences in the literature, showing that robot-aided therapy benefits can be observed also in not trained motor tasks [61] [91] [92] (generalization of training outcomes). Therefore, it is reasonable to suppose that performance indicators can be employed also as predictive parameters of the overall (motor and functional) patient recovery.
However, since the relation between the improvement of performance indicators and the increasing of the capability to perform real life scenario tasks has a crucial importance, the idea to correlate the changes in performance indicators with the patient functional assessment (in addition to the motor assessment) has been considered, as reported in Chapter 6. This will allow identifying the most appropriate indicators, between the proposed ones, for quantitatively describing patient motor and functional recovery, and, moreover, returning to the bio-cooperative controller the most comprehensive feedback on patient performance status.

3.1.3 Patient global performance estimation

As explained in Section 3.2, performance indicators, extracted from motion, force and EMG data, are used to adjust robotic control parameters through properly defined modulation functions. The adjusted control parameters are: the robot stiffness, K, and the time allotted for the execution of a motor task, t.

The two modulation functions for K and t are described as follows.
First, all the extracted performance indicators are normalized with respect to their maximum and adjusted in order to increase with motor recovery.
Then, two weighted sums of the extracted indicators are computed. Through an opportune configuration of the weights, this step allows: (i) assigning more importance to those performance indicators that are relevant for the motor task under execution; (ii) discriminating between different quality levels of the executed movements. Obviously, greater weights are given to those indicators that are more indicative of a pathological behaviour versus a healthy behaviour.

Eugenia Papaleo

In detail, the two functions for modulating K and t are expressed as

$$C_K = \sum_{i=1}^{I} PI_i \tag{3.2}$$

$$C_t = \sum_{j=1}^{J} PI_j \tag{3.3}$$

where PI_i is the $i-th$ performance indicator ($i = 0, 1, 2, ..., I$) used for the adaptation of the robot stiffness, while PI_j is the $j-th$ performance indicator ($i = 0, 1, 2, ..., J$) used for the adaptation of the time allotted for task execution.

However, considering that C_K and C_t continuously vary in the interval $[0, 1]$, a threshold strategy is considered to define the discrete values needed for updating the control parameters through discrete scales. The discrete levels of patient performance for updating K and t are related to the output of functions (3.2) and (3.3) as

$$L_K = \begin{cases} 1 & 0 \leq C_K < 0.5 \\ 2 & 0.5 \leq C_K < 0.75 \\ 3 & 0.75 \leq C_K < 1 \end{cases} \tag{3.4}$$

and

$$L_t = \begin{cases} 1 & 0 \leq C_t < 0.5 \\ 2 & 0.5 \leq C_t < 0.75 \\ 3 & 0.75 \leq C_t < 1; \end{cases} \tag{3.5}$$

values of L_k and L_t are sent to the robotic control and are automatically associated to predetermined values of stiffness and task duration.

A different approach, that does not employ only discrete levels of stiffness and task duration, for the adaptation of control parameters has been considered. In this case, the two functions for modulating K and t are expressed as

$$K(n) = K(n-1) - \lambda_k(ws(n) - ws(n-1)), \tag{3.6}$$

$$t(n) = t(n-1) - \lambda_t(ws^*(n) - ws^*(n-1)); \tag{3.7}$$

here, $K(n)$ ($t(n)$) is the value of the robot stiffness (the time allotted for task fulfillment) during the task n ($n = 0, 1, 2, ..., N$), λ_k (λ_t) is a constant value equal to $1000N/m$ ($10s$), $ws(n)$ ($ws^*(n)$) is the value, during the $n-th$ task, of the

Eugenia Papaleo

weighted sum of the indicators extracted for the adaptation of the robot stiffness (the time allotted for task execution). Therefore, in order to obtain an updated value of the control parameters, their value during the previous task execution is adjusted considering how much the weighted sum is varied.

3.1.4 The virtual reality environment

The Matlab/Simulnik scheme of the developed virtual reality software receives as input (i) the reconstructed joint angles of the patient upper-limb, (ii) the calibration data of the reconstruction algorithm (i.e. shoulder position, upper arm and forearm lengths), (iii) the desired hand trajectory (provided by the robotic controller).
It real-time shows the patient motion and the correct trajectory for task fulfilment.

Two types of exercises have been designed:

- The clock game [93] - Point-to-point trajectories towards/backwards 8 targets placed around a central starting point and spaced 45° apart;
- ADL tasks (i.e. drinking task) - Execution of a drinking task consisting in grabbing a glass, taking it towards the mouth, placing again the glass on the table and returning to the initial position.

As anticipated, during the execution of the exercises the desired path is shown; in particular, the trajectory that the patient has to travel is colored red and becomes green when the patient completes the assigned task reaching the trajectory end-point.

Figures 3.11 and 3.12 show the virtual reality display during the execution of the clock game and the drinking task, respectively. As can be observed, different views of the clock game have been designed in way of choosing the most suitable on the basis of patient preferences.

3.2 The adaptive control system

The main goal of the designed adaptive controller is to assist the patient (who is connected to the end-effector of the robot) when he/she is not able to accomplish the task, with a level of assistance that is tuned on the patient global state. The

Eugenia Papaleo

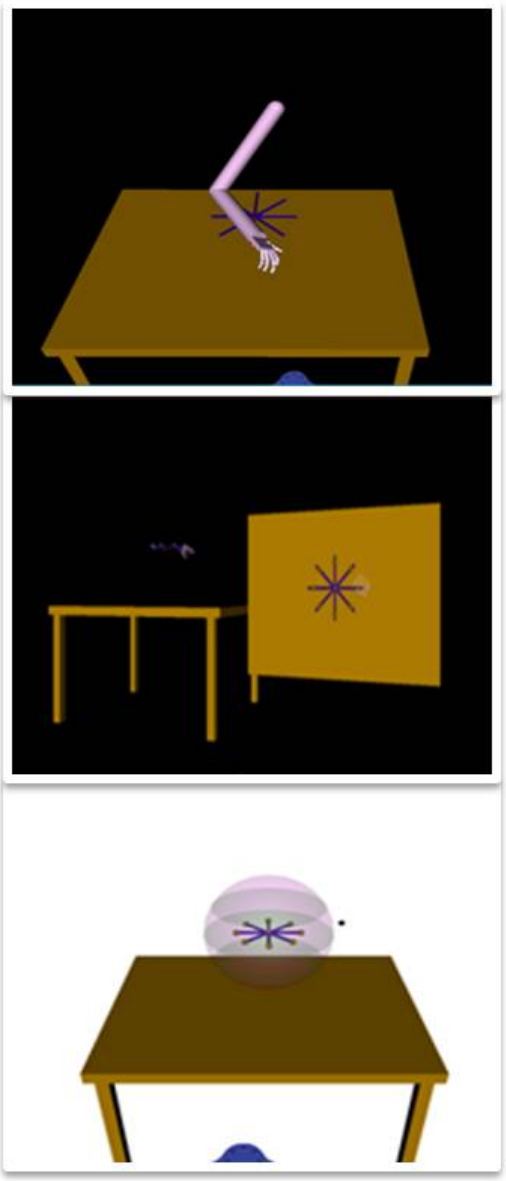

FIGURE 3.11: Virtual reality environment: different views of clock game execution

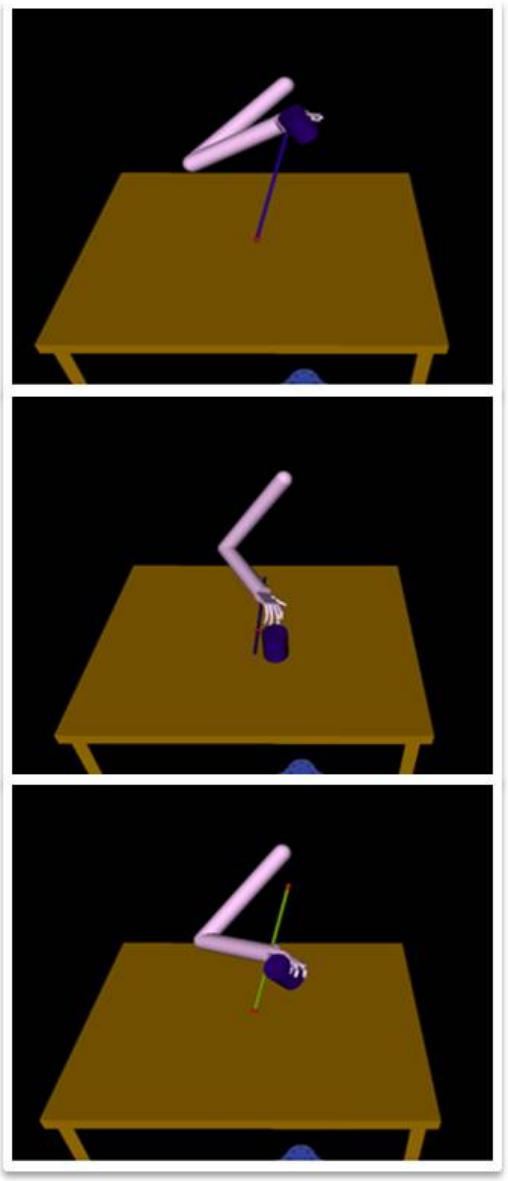

FIGURE 3.12: Virtual reality environment: ADL task (drinking task) execution

fundamental idea is to make the robot fully compliant when the patient is moving along the planned trajectory or, alternatively, stiffer and stiffer when the patient is moving away from it.

In order to achieve this, a strategy based on an impedance control in the Cartesian space has been implemented. In particular, control parameters are changed based on patient global performance, thus enabling various "degrees of assistance" as required by a specific subject.
Robot control law can be written as follows

Eugenia Papaleo

$$\vec{\tau}_{cmd} = J^T(\vec{\theta})\left[K\left(\vec{x}_p - \vec{x}\right) + \vec{FT}\right] + D\left(d\right) + \vec{f}_{dyn}\left(\vec{\theta}, \dot{\vec{\theta}}, \ddot{\vec{\theta}}\right), \tag{3.8}$$

where J^T is the transposed Jacobian matrix, K is the Cartesian Stiffness matrix, $\vec{x}_p$ is the vector of the desired Cartesian position, $\vec{x}$ is the vector of the actual Cartesian position, $D\left(d\right)$ is the damping term, $\vec{FT}$ is an eventual additional superposed Cartesian force, $\vec{\theta}$ is the vector of the actual joint positions and $\vec{f}_{dyn}$ is the dynamic model.

For encouraging patient effort, a sort of error variability around the desired path can be permitted, introducing a "dead band", namely an area around the trajectory in which no assistance is provided [66], [94].

Initially a 2D desired minimum-jerk trajectory has been used for $\vec{x}_p$, by analogy with [66]. Then, in order to enable 3D motion as well as ADL tasks, two different options have been analyzed for determining the desired trajectories:

- A 3D minimum-jerk trajectory, well suited for patients with limited movement ability [66] and typically used in robot-aided rehabilitation therapy;
- Pre-recorded trajectories from unimpaired volunteers or during therapist-guided assistance [94], for functional tasks.

For instance, for a 3D trajectory the command forces can be written as follows

$$F_{c,x}=\begin{cases} -k\left(x-x_{m,j}\right)-d\dot{x} & x < x_{m,j} \\ 0 & x_{m,j} \leq x \leq x_f \text{ and } x \geq x_{prev} \\ -k\left(x-x_{prev}\right)-d\dot{x} & x_{m,j} \leq x \leq x_f \text{ and } x < x_{prev} \\ -k\left(x-x_f\right)-d\dot{x} & x > x_f \end{cases}$$

$$F_{c,y}=\begin{cases} -k\left(y-y_{m,j}\right)-d\dot{y} & y < y_{m,j} \\ 0 & y_{m,j} \leq y \leq y_f \text{ and } y \geq y_{prev} \\ -k\left(y-y_{prev}\right)-d\dot{y} & y_{m,j} \leq y \leq y_f \text{ and } y < y_{prev} \\ -k\left(y-y_f\right)-d\dot{y} & y > y_f \end{cases}$$

$$F_{c,z}=\begin{cases} -k\left(z-z_{m,j}\right)-d\dot{z} & z < z_{m,j} \\ 0 & z_{m,j} \leq z \leq z_f \text{ and } z \geq z_{prev} \\ -k\left(z-z_{prev}\right)-d\dot{z} & z_{m,j} \leq z \leq z_f \text{ and } z < z_{prev} \\ -k\left(z-z_f\right)-d\dot{z} & z > z_f \end{cases}$$

$$T_{c,z} = -k_o\left(\varphi - \varphi_m\right) - d\dot{\varphi}$$
$$T_{c,y} = -k_o\left(\theta - \theta_m\right) - d\dot{\theta}$$

Eugenia Papaleo

$$T_{c,x} = -k_o\,(\psi - \psi_m) - d\dot{\psi}$$

where

- $F_{c,x}$, $F_{c,y}$, $F_{c,z}$ are the command forces along axes x, y and z;
- $T_{c,z}$, $T_{c,y}$, $T_{c,x}$ are the command torques about axes z, y and x;
- φ, θ, ψ are the RPY (Roll-Pitch-Yaw) angles representing the current orientation of the end-effector, while φ_m, θ_m, ψ_m represent the desired end-effector orientation (constant over time);
- $x_{m,j}{=}x_i{+}s/\|p_f{-}p_i\|\,(x_f{-}x_i)$ is the desired x-position at time t_j, described by the minimum-jerk trajectory; analogously for $y_{m,j}$ and $z_{m,j}$;
- $s{=}\,\|p_f{-}p_i\|\,[10(t_j/t_m)^3{-}15(t_j/t_m)^4{+}\,6(t_j/t_m)^5]$;
- p_i is the initial position;
- $p_f$is the final position;
- x, y, z are the Cartesian coordinates of the end-effector at time instant t_j, while x_{prev}, y_{prev}, z_{prev} are related to the time instant t_{j-1};
- d is the controller Cartesian damping (constant);
- k and k_o are the controller Cartesian stiffness values for the position and the orientation, respectively: k is tuned according to the estimated patient global performance, k_o is kept constant to a high value, in order to assure the same orientation during the task;
- t_m is the duration of the movement (which is tuned according to the estimated patient global performance).

Thus, robot control law (3.8) can be simplified as follows

$$\vec{\tau}_{cmd} = J^T\left(\vec{FT}_c\right) + \vec{f}_{dynamics}\left(\vec{\theta}, \dot{\vec{\theta}}, \ddot{\vec{\theta}}\right), \tag{3.9}$$

where $\vec{FT}_c = [F_{c,x}\ F_{c,y}\ F_{c,z}\ T_{c,z}\ T_{c,y}\ T_{c,x}]^T$.

Figure 3.13 shows robot behaviour under the proposed control. The black line represents the planned trajectory (from p_i to p_f), $p(t)$ is the desired position at time t and the blue parallelepiped represents the portion of space, at time t, where the robot end-effector is made compliant, thus providing no assistance.
In this way, the controller allows capable patients to complete the task unassisted. Moreover, the described control prevents that a patient who is moving ahead along the desired trajectory can go in the wrong direction.

Eugenia Papaleo

This approach can be easily generalized to a generic curve in 3D-Space, such as in the case of ADL tasks.

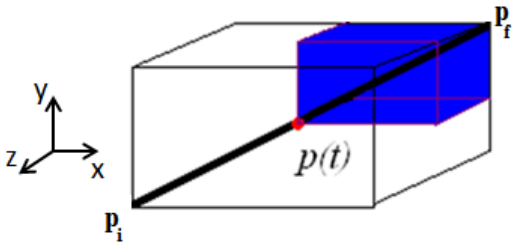

FIGURE 3.13: Robot behaviour at the end-effector level

As mentioned in Section 3.1.3, in order to guarantee adaptiveness to subject specific performance thus providing patient-tailored degrees of assistance, it has been chosen to make adjustable two control parameters: i) the value of Cartesian stiffness matrix K and ii) the task duration t.
In particular, they can assume three different pre-established levels, depending on the output of the multimodal interface; in particular low values of K and short task duration are associated to good global performance, while higher K values and longer task duration are associated to worse global performance.

Eugenia Papaleo

Chapter 4

Reconstruction of the upper-limb kinematics during robot-aided therapy with end-effector machines

This Chapter proposes a novel method for a reliable and unobtrusive reconstruction of the upper-limb kinematics of stroke patients during robot-aided rehabilitation tasks with end-effector machines. The method is based on a robust analytic procedure for kinematic inversion that simply uses, in addition to hand pose data provided by the robot, upper arm acceleration measurements for computing a constraint relative to the elbow position; this constraint is exploited for a task space augmentation.

The Chapter is structured as follows. The kinematic model of the upper-limb and the algorithm for inverse kinematics are presented in Sections 4.2 and 4.3; the experimental tests carried out for assessing the proposed method and measuring its performance are illustrated in Section 4.4. The experimental tests have been carried out with a two-stage procedure: first, a comparative analysis with data measured by an optoelectronic marker-based digital system (SMART-D, from BTS Bioengineering) has been performed; secondly, the method has been applied on healthy and stroke subjects during the execution of circle-drawing tasks with the InMotion2 rehabilitation robot. The experimental results of this two-stage experimental evaluation are reported in Section 4.5.

Eugenia Papaleo

4.1 Background

The analysis of arm joint trajectories of stroke patients undergoing robot-aided therapy can address a number of scientific and clinical issues, such as:

- Quantifying the residual motor capabilities of the patient, by investigating the behaviour of each degree of freedom involved in the motion;
- Assessing the outcomes of the therapy at Cartesian and joint level and, possibly, understanding the motor strategies possibly related to the pathology;
- Re-planning/re-configuring the treatment based on the recovery level and the motion capabilities of each specific patient;
- Improving patient safety keeping away arm motion from human joint limits.

Hence, the evaluation of patient motion also in the joint space can provide significant and useful information for a more thorough assessment of subject kinematic performance (e.g. AROM-Active Range of Motion [95], inter-joint coordination [61], etc.). The coupling of motion sensing systems with the robot is needed. However, while exoskeleton robots easily provide arm joint trajectories (i.e. trajectories of the human joints that are controlled by the robot), when end-effector robots are employed no data about upper-limb joint motion are available.

Typical systems for motion analysis (also used in clinics) are the following: i) electrogoniometers, ii) inertial or magneto-inertial sensors and iii) optoelectronic systems [35]. Electrogoniometers have been excluded for a series of drawbacks, i.e. it is difficult to eliminate the misalignment between the measuring system and the human joint axes of rotation; they are obtrusive systems and cannot measure rotations around the longitudinal axis of a limb segment (such as the shoulder intra-extra rotation). Inertial and magneto-inertial wearable sensors are cheap and small (due to the microfabrication procedures) and consume very low power [96]; however, they can be obtrusive and alter the natural motion of a subject if a net of sensors is used to reconstruct the entire arm kinematics. Optoelectronic devices are camera-based systems considered as the most accurate motion capturing systems as long as marker-based approaches are employed. However, they are very expensive and require a high structured acquisition environment and a time-consuming calibration procedure.

An alternative approach to the use of motion analysis systems relies on the use of computational methods to reconstruct upper-limb kinematics. In a recent review

Eugenia Papaleo

[97], it has been stated that the most appropriate way to solve the upper-limb inverse kinematics problem is to resort to methodologies derived from robotics. Unless one considers a simplified planar human arm model, as in [61], the inverse kinematics approach requires to face the redundancy of the human arm kinematic chain. In [97], two general approaches to solve arm redundancy are proposed, both based on intrinsic kinematic constraints. The former accounts for the minimization of the path covered from an initial to a final position, while the latter takes into account underlying relations between joint angles. However, while the first constraint has shown some inconsistencies with the experimental observations, methods based on the second constraint have been found valid only for particular movements, since the arm posture at a given hand position cannot be considered independent of previous configurations [98]. This is the case, for example, of the adaptation of the Donder's law to the human arm.
Other computational approaches for solving the upper-limb redundancy problem adopt simpler kinematic constraints or some geometrical simplifications [99]. The consequence is that just estimations (and not accurate measures) of the upper-limb angles can be provided.

Hence, the approach here presented aims at overcoming the shortcomings of the aforementioned systems and methods by enabling a reliable and unobtrusive reconstruction of the entire upper-limb kinematics in robot-aided rehabilitation with end-effector machines. The approach is based on a reliable algorithm of inverse kinematics, originally conceived for redundant anthropomorphic manipulators and here ad-hoc adapted to human motion reconstruction.
The kinematic redundancy of the arm is solved through a task space augmentation; this allows obtaining a closed-form solution for the inverse kinematics problem. Constrained solutions are found by simply performing an additional measurement with respect to the hand pose data provided by the robot, i.e. the radial acceleration of the upper arm segment. In this way, the so called *swivel angle* [100]-[101] (i.e. the angle that describes the internal motion of the upper-limb when shoulder and hand position are fixed) is computed, thus enabling parametrization of arm redundancy.

Eugenia Papaleo

4.2 Upper-limb kinematics

4.2.1 Kinematic model

The upper-limb kinematic chain consists of 7 DoF (Degrees of Freedom) and 2 links, namely l_u for the upper arm and l_f for the forearm, respectively. Three DoF belong to the shoulder spherical joint; they are: abduction-adduction (q_1), flexion-extension (q_2) and internal-external rotation (q_3). The elbow revolute joint has 1 DoF that accounts for forearm flexion-extension (q_4). Lastly, the wrist spherical joint is composed of pronation-supination (q_5), ulnar-radial deviation (q_6) and flexion-extension (q_7) of the hand. Although the pronation-supination degree of freedom anatomically belongs to the elbow joint, it has been considered as a wrist DoF, since it mainly affects hand orientation rather than its position.
In accordance with the Denavit-Hartenberg (D-H) convention [102], different frames have been placed all along the upper-limb kinematic chain, starting from the reference frame (indicated as frame 0), placed in the shoulder joint. The frame locations, the D-H parameters and the joint variables are shown on the left side of Figure 4.1.

Given the D-H parameters, the homogeneous transformation matrix from frame i to the frame $(i-1)$, $T_i^{i-1}(q_i)$, is computed. Hence, the forward kinematics is given by $T_7^0(\bar{q})$ and describes the hand pose as a function of the joint angles vector ($\bar{q}$). Matrix $T_7^0(\bar{q})$ can be calculated as

$$\mathrm{T}_7^0(\bar{q}) = \mathrm{T}_3^0(q_1, q_2, q_3) \quad \mathrm{T}_e(q_4) \quad \mathrm{T}_7^4(q_5, q_6, q_7), \tag{4.1}$$

where

i) $\mathrm{T}_3^0(q_1, q_2, q_3)$ accounts for translations and rotations of the elbow with respect to the reference frame;

ii)$\mathrm{T}_e(q_4) = [\mathrm{T}_4^3(q_4) \times \mathrm{Trans}(\hat{z}_4, l_f)]$, accounts for translations and rotations of the wrist with respect to the elbow frame;

iii) $\mathrm{T}_7^4(q_5, q_6, q_7)$, accounts for rotations of the hand with respect to to the wrist frame.

By regarding the human arm as a redundant 7-DoF manipulators [103], an additional variable can be introduced to describe the internal motion and exploit the kinematic redundancy. It is the *swivel angle* (α) shown on the right side of Figure

Eugenia Papaleo

4.1. It represents the angle between the reference plane, defined by vectors $\hat{V}$ and $s\bar{w}$ (Figure 4.1 - right side), and the plane containing $\bar{s} = O_1$, $\bar{e} = O_3$, $\bar{w} = O_7$, being O_i the origin of frame i. Therefore, the upper-limb internal motion can be described as a rotation of the plane containing arm joints around the vector $s\bar{w}$. Angle α is uniquely defined when shoulder and hand positions are fixed; in such a condition the elbow can move along a circular arc (indicated as *internal motion* on the right side of Figure 4.1) having a normal vector aligned with vector $s\bar{w}$ [104].

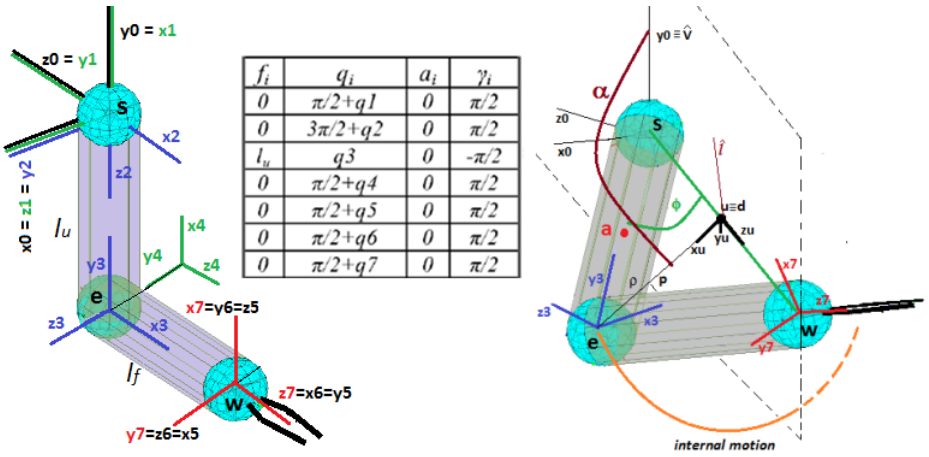

f_i	q_i	a_i	γ_i
0	$\pi/2+q1$	0	$\pi/2$
0	$3\pi/2+q2$	0	$\pi/2$
l_u	$q3$	0	$-\pi/2$
0	$\pi/2+q4$	0	$\pi/2$
0	$\pi/2+q5$	0	$\pi/2$
0	$\pi/2+q6$	0	$\pi/2$
0	$\pi/2+q7$	0	$\pi/2$

FIGURE 4.1: Left:Upper-limb frames and D-H parameters. Right: Internal motion representation: the swivel angle and the variables needed for its computation

4.2.2 Inverse kinematics algorithm with augmented Jacobian

The additional Cartesian variable expressed through swivel angle α allows solving the arm kinematic redundancy and, consequently, providing a closed-form solution for the inverse kinematics problem. In particular, the task space variables can be increased through the introduction of angle α in the hand pose vector as

$$\begin{bmatrix} \bar{x} \\ \alpha \end{bmatrix}, \tag{4.2}$$

being $\bar{x}$ the (6×1) vector describing hand position and orientation.

Hence, the (6×1) velocity vector in the task space ($\dot{\bar{x}}$) can be re-written as a (7×1) vector given by

$$\begin{bmatrix} \dot{\bar{x}} \\ \dot{\alpha} \end{bmatrix} \tag{4.3}$$

and the corresponding square (7×7) *Augmented* Jacobian matrix is computed as

Eugenia Papaleo

$$J_A(\bar{q}) = \begin{bmatrix} J_a(\bar{q}) \\ J_\alpha(\bar{q}) \end{bmatrix}. \tag{4.4}$$

The Augmented Jacobian is composed of two matrices; they are the analytic Jacobian matrix of the upper-limb ($J_a(\bar{q})$), accounting for the contribution of the joint speed vectors to the hand velocity, and the swivel angle Jacobian ($J_\alpha(\bar{q})$), i.e. a row vector that describes the contribution of the joint velocities to the rate of change of α. The computation of the swivel angle Jacobian is explained in detail in the following.

The inverse kinematics algorithm employing the Augmented Jacobian matrix is expressed as

$$\dot{\bar{q}} = J_A^{-1}(\bar{q}) \left(\begin{bmatrix} \dot{\bar{x}} \\ \dot{\alpha} \end{bmatrix} + K * \bar{er} \right). \tag{4.5}$$

Given hand velocity vector $\bar{v}$ and the rate of change of α, it allows computing joint speed vector $\dot{\bar{q}}$. The inversion error ($\bar{er}$), due to the time-discrete integration procedure for calculating joint trajectories ($\bar{q}$), can be reduced choosing a suitable value for gain matrix (K).

Finally, in order to extend the algorithm also to regions closed to kinematic singularities, a Damped Least-Squares Augmented Jacobian matrix can be used in equation (4.5) in place of J_A. It can be expressed as

$$J_A^\star = J_A^T \left(J_A J_A^T + k^2 I \right)^{-1}, \tag{4.6}$$

where J_A^T represents the transpose Augmented Jacobian matrix, k^2 is a damping factor useful for numerically conditioning the solution of the inversion procedure and I is the (7×7) identity matrix.

4.3 Joint reconstruction algorithm

The proposed method for upper-limb joint reconstruction has been specifically conceived for being used during robot-aided therapy with end-effector machines. In this context, patient hand pose (and velocity) is provided by robot position sensors. Joint motion can be computed through the inverse kinematics algorithm in equation (4.5), once the Augmented Jacobian matrix is calculated. Hence, the

Eugenia Papaleo

computation of the swivel angle and of the corresponding Jacobian vector $J_\alpha(\bar{q})$ is a key point. Both of them require measuring elbow trajectory, as explained below.

4.3.1 Computation of the swivel angle

As explained in Section 4.2.1, the swivel angle is the angle between the reference plane and the plane containing shoulder, elbow and wrist joints and is expressed as

$$\alpha = \text{atan2}\left(\hat{w}^T(\hat{V} \times \bar{p}), \hat{V}^T\bar{p}\right). \tag{4.7}$$

Note that the reference plane is not uniquely defined when vectors $\hat{V}$ and $s\bar{w}$ are co-linear. Choosing $\hat{V}$ as a vertical unit vector, the alignment with $s\bar{w}$ is avoided if fully outstretch of the arm along the vertical axis is not permitted. The swivel angle can be computed as a function of elbow ($\bar{e}$) and hand ($\bar{w}$) positions, once defined the following three parameters (Figure 4.1 - right side):

- projection of $\bar{e}$ onto $\bar{w}$, indicated as $\hat{d} = \hat{w}(\hat{w}^T\bar{e})$,
- minimum distance between vector $s\bar{w}$ and the elbow joint, denoted with $\bar{p} = \bar{e} - \bar{d}$,
- vector lying on the reference plane and orthogonal to vector $s\bar{w}$, i.e. $\bar{l} = (\bar{w} \times \hat{V}) \times \bar{w}$.

The swivel angle Jacobian in equation (4.4) can be computed as

$$J_\alpha(\bar{q}) = \frac{(\hat{w} \times \hat{p})^T}{\|\bar{p}\|}E + [\frac{\hat{V}^T\bar{w}}{\|\bar{l}\|}(\hat{w} \times \hat{l})^T - \frac{\hat{w}^T\bar{e}}{\|\bar{w}\|\|\bar{p}\|}(\hat{w} \times \hat{p})^T]W, \tag{4.8}$$

being

$$\dot{\alpha} = \frac{(\hat{w} \times \hat{p})^T}{\|\bar{p}\|}[E - \frac{\hat{w}^T\bar{e}}{\|\bar{w}\|}W]\dot{\bar{q}} + \frac{\hat{V}^T\bar{w}}{\|\bar{l}\|}(\hat{w} \times \hat{l})^T W\dot{\bar{q}} = J_\alpha(\bar{q})\dot{\bar{q}} \tag{4.9}$$

the time derivative of the swivel angle in equation (4.7) and E and W the Jacobian matrices that relate the joint speed vector to the translational velocities of elbow and wrist joints, respectively.

4.3.2 Computation of elbow joint trajectories

The method proposed in [105] has been applied to determine the position of the elbow in the space. To this purpose, an accelerometer placed on the upper arm has

Eugenia Papaleo

been used to provide upper arm static acceleration. Hand position data provided by the robot and static acceleration provided by the accelerometer have been used to estimate the vertical coordinate of the elbow joint e_y. The remaining two Cartesian coordinates of the elbow joint have been reconstructed by applying some geometrical considerations on arm internal motion.

The elbow joint Cartesian coordinates in the reference frame (shoulder frame) can be expressed as (Figure 4.1 - right side)

$$\bar{e} = \begin{bmatrix} l_u \sin q_1 \cos q_2 & -l_u \cos q_1 \cos q_2 & -l_u \sin q_2 \end{bmatrix}^T. \tag{4.10}$$

The accelerometer placed in $\bar{\mathbf{a}}$ in Figure 4.1 allows computing the elbow coordinate along y_0-axis as

$$e_y = \frac{-\ddot{a}_y l_u}{g} = -l_u \cos q_1 \cos q_2, \tag{4.11}$$

where $\ddot{a}_y$ is the radial acceleration of the upper arm in $\bar{\mathbf{a}} = \begin{bmatrix} a_x & a_y & a_z \end{bmatrix}^T$ (expressed in the elbow frame $O_3 - x_3, y_3, z_3$) and g represents the gravitational acceleration.
By analogy with the work in [105], it has been chosen to locate the accelerometer directly on the segment connecting the shoulder and elbow joints in order to neglect distances a_x and a_z. Therefore, the measured acceleration is given by

$$\ddot{a}_y \approx g \cos q_1 \cos q_2 + (l_u - a_y)\dot{q}_1^2 \cos q_2^2 + \dot{q}_2^2, \tag{4.12}$$

where $g \cos q_1 \cos q_2$ represents the radial static acceleration of the upper arm, while $(l_u - a_y)\dot{q}_1^2 \cos q_2^2 + \dot{q}_2^2$ is the corresponding dynamic acceleration. Because of the slow motion velocity of the addressed application, the static component dominates on the dynamic term; hence, dynamic acceleration can be neglected. Under this assumption, the radial acceleration measured on the upper arm is given by $\ddot{a}_y \approx g \cos q_1 \cos q_2$.

On the other hand, to compute x and z components of the elbow position, a number of parameters need to be calculated. They are (Figure 4.1):

- The normal vector to the internal motion arc, i.e. $\hat{z}_u = \hat{w}$.

Eugenia Papaleo

- The angle between vector $s\bar{w}$ and the upper arm segment; by invoking the cosine rule, it is expressed as

$$\phi = \text{acos}\frac{\|s\bar{w} - \bar{s}\|^2 + l_u^2 - l_f^2}{2l_u\|s\bar{w} - \bar{s}\|}.$$

- The radius and the center of the internal motion arc, given by $\rho = l_u \text{sin}\phi$ and $\bar{u} = l_u\hat{z}_u\text{cos}\phi$, respectively.

- The unit vectors $\hat{x}_u$ and $\hat{y}_u$ of the frame centered in $\bar{u}$. Unit vector $\hat{x}_u$ has been determined as follows:

  1. The vertical component of $\hat{x}_u$ is given by

$$\hat{x}_u^{(2)} = (e_y - u_y)/\rho;$$

  2. The other two components of $\hat{x}_u$ can be computed through the system of equations

$$\begin{cases} \|\hat{x}_u\|^2 = 1 \\ \hat{x}_u \cdot \hat{z}_u = 0. \end{cases}$$

  This yields

$$x_u^{(1)} = \frac{\sqrt{x_u^{(2)^2} z_u^{(1)^2} z_u^{(2)^2} - (z_u^{(1)^2} + z_u^{(3)^2})(x_u^{(2)^2}(z_u^{(2)^2} + z_u^{(3)^2}) - z_u^{(3)^2})} - x_u^{(2)} z_u^{(1)} z_u^{(2)})}{z_u^{(1)^2} + z_u^{(3)^2}}$$

  and

$$x_u^{(3)} = \frac{x_u^{(1)} z_u^{(1)} + x_u^{(2)} z_u^{(2)}}{z_u^{(3)}}.$$

  3. Once computed $\hat{x}_u$ and $\hat{z}_u$, unit vector $\hat{y}_u$ is given in a right-handed frame.

- Finally, elbow position in the frame centered in $\bar{u}$. It is given by

$$\bar{e}_u = \begin{bmatrix} \rho & 0 & 0 \end{bmatrix}^T.$$

Hence, elbow coordinates in the reference frame can be calculated as

$$\begin{bmatrix} \bar{e} & 1 \end{bmatrix}^T = \mathbf{U} \begin{bmatrix} \bar{e}_u & 1 \end{bmatrix}^T, \tag{4.13}$$

being

$$\mathbf{U} = \begin{bmatrix} \hat{x}_u & \hat{y}_u & \hat{z}_u & \bar{u} \\ 0 & 0 & 0 & 1 \end{bmatrix} \tag{4.14}$$

Eugenia Papaleo

the transformation matrix from the frame centered in $\bar{u}$ to the shoulder frame.

4.4 Experimental Validation

The experimental validation has the twofold purpose of assessing the method performance and evaluating method efficacy to discriminate pathological behaviour during robot-aided motor tasks. Therefore, the following experimental activities have been fulfilled

1. a comparative analysis with joint angles obtained from an 8-camera marker-based optoelectronic motion capturing system (SMART-D, from BTS Bioengineering);
2. the application to robot-aided rehabilitation, by reconstructing joint motion of healthy and stroke subjects performing circle-drawing tasks with a planar end-effector machine.

All subjects gave informed consent to take part in this study that was approved by the local scientific and ethical committees.

4.4.1 Validation of the reconstruction algorithm: subjects and protocol

This testing phase was aimed at assessing the validity of the proposed method and measuring its performance by means of a comparative analysis with a marker-based optoelectronic measurement system. It involved four healthy subjects (2 men and 2 women, mean age = 27.6 ± 1.9 years).

Each subject has been asked to seat on a chair, placing the hands on the thighs and the arms on the sides of the trunk; then, they have been required to reach a target placed in front of them and return to the starting position (i.e. *forward/backward movements*); the movement has been repeated 5 times with subject's self-paced velocity.

A wearable magneto-inertial sensor (MTx sensors, from Xsens - full scale: $\pm 5g$) has been positioned on the subject upper arm; in particular, since a triaxial accelerometer is embedded in the sensor, one of sensor axes has been aligned with the limb segment. Acceleration data have been sampled at 200 Hz, sent to a computer via serial connection (RS-232) and offline filtered with a 10th-order Butterworth

Eugenia Papaleo

low-pass filter. They are used to compute the swivel angle, once calculated the elbow trajectory (equations (4.7) and (4.13)). Thus, the reconstruction algorithm is used to reconstruct arm joint angles. The input signals for the reconstruction algorithm in equation (4.5) are the hand pose, the lengths of upper arm and forearm segments and the shoulder position; they are provided by the optoelectronic system used for validating the method. The output data of the algorithm are the arm joint velocities; they have been integrated through a numerical integration method (i.e. Euler's method), with a step-size of $0.005s$.

The optoelectronic system (Figure 4.2 - left side) is made of eight infrared digital cameras (sensors resolution 640×480 px, acquisition frequency $60 - 120$ Hz), passive and retro-reflective markers and one workstation for data processing and motion reconstruction; system accuracy is $<$ 0.2 mm on a volume $4 \times 3 \times 3$ m^3. The system has been used to measure the angle joints of the subject during the same movements described above and compare them with the angles computed through the reconstruction algorithm. To this purpose, a kinematic protocol has been developed in [106] and applied for the computation of the human arm angles. This protocol is a modified version of Rab protocol in [8]. Twelve infrared markers have been located on twelve arm anatomical landmarks, as shown in Figure 4.3, and the seven arm joint angles have been computed, starting from markers 3D coordinates (sampling frequency was 60 Hz). In particular, three right-handed frames have been placed on the arm kinematic chain with the x-axis directed laterally to the right, the y-axis directed forward, and the z-axis directed upward, as shown in Figure 4.3. Hence, the sequences of Euler rotations around the x,y,z axes have been computed and considered equal to flexion/extension, abduction/adduction and internal-external rotations.
Figure 4.2 (right side) illustrates the experimental setup for the validation of the proposed method; in particular, the placement of the infrared markers, the magneto-inertial sensor attached to the subject upper arm and the subject red stick figure plotted during recording are shown.

4.4.2 Experimental trials of robot-aided rehabilitation: subjects and protocol

Two chronic stroke patients (mean age 58.8 ± 1.2 years) have been recruited for these experimental trials. They had a single stroke event more than 6 months before the enrolment in this study. A 18-session robot-aided treatment has been delivered with a robotic machine for upper-limb training, i.e. the InMotion2 planar

Eugenia Papaleo

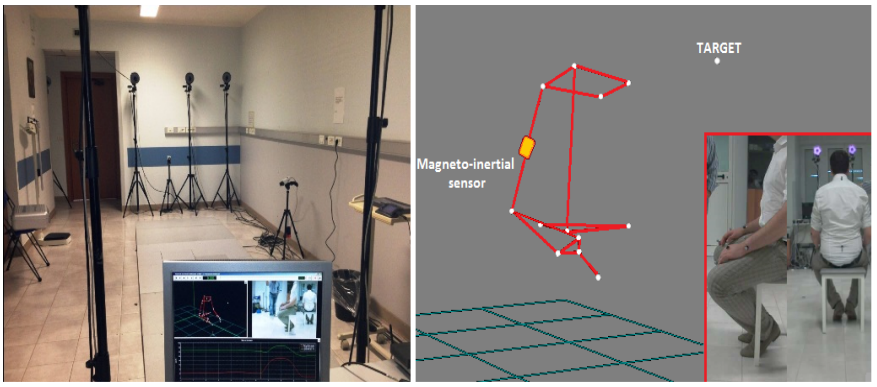

FIGURE 4.2: Left: SMART-D BTS optoelectronic motion capturing system: post-processing of the experimental trails. Right: Experimental trial for assessing method validity: the placement of infrared markers and magneto-inertial sensor is shown; the position of the subject corresponding to the red stick figure is shown in the bottom right corner

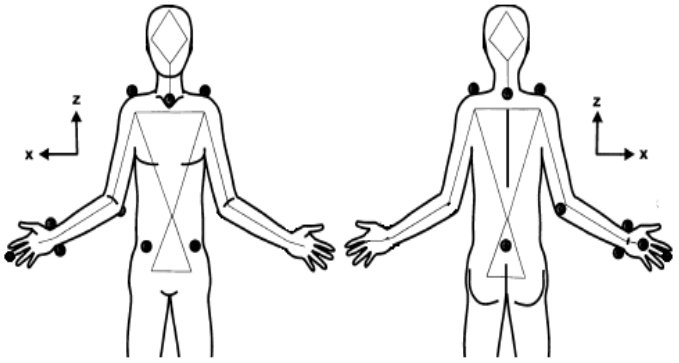

FIGURE 4.3: Placement of the infrared markers for the application of a modified version of the Rab protocol, adapted from [8]

robot (Interactive Motion Technologies Inc.). Each subject has been evaluated at admission to and discharge from this study through clinical scales (i.e. Fugl-Meyer and Motor Power) and quantitative measures provided by the joint motion reconstruction algorithm described in this paper. In particular, for the quantitative evaluation, patients have been required to perform a series of unassisted motion exercises with the InMotion2 Shoulder-Elbow robot. Cartesian motion have been monitored through position sensors embedded into the robot and joint motion has been reconstructed with the proposed algorithm in equations (4.4) and (4.5).

Tables 4.1 and 4.2 report data about the two enrolled patients. In Table 4.1 the lengths of upper arm and forearm segments, in addition to the paretic arm (right or left); in Table 4.2 the values of the shoulder-elbow Fugl-Meyer and Motor Power scales at admission (i.e. PRE) and discharge (i.e. POST) are shown.

Eugenia Papaleo

TABLE 4.1: Lengths of upper arm and forearm segments and paretic arm of enrolled patients.

Patient	**Upper arm length**	**Forearm length**	**Paretic arm**
1	0.35 m	0.32 m	*Right*
2	0.36 m	0.33 m	*Left*

TABLE 4.2: Values of upper extremity FM-SE and MP-SE for both patients before (PRE) and after (POST) the robotic treatment.

	Upper extremity FM-SE/42		**Upper extremity MP-SE/70**	
Patient	PRE	POST	PRE	POST
1	18	19	36	38
2	19	21	42	43

For comparative purpose, the same evaluation tests have been performed also on five healthy volunteers (age 26 ± 2.3 years) in order to define "healhty bands" for all the kinematic variables during the performed tasks.

The experimental trials have been performed as follows. Subjects have been seated on a chair and required to perform five repetitions of a task consisting in drawing a counterclockwise circle in the horizontal plane starting at 3 o'clock. They have been asked to move their hand along the desired circular trajectory (radius = 0.075 m) shown on a monitor in front of them, together with a visual feedback regarding the current hand position. The trunk of each subject has been tied through a seatbelt in order to avoid compensatory torso movements; the forearm has been placed and secured through velcro straps on a plastic support attached to the robot end-effector in order to minimize forearm pronation-supination and wrist movements. Robot motors have been turned off, thus no assistance has been provided to subjects during the exercise. The hand position of each subject is provided by the sensors embedded into the robot (sampling frequency of 200 Hz). Moreover, the MTx sensor has been placed on the subject upper arm for the acquisition of the radial acceleration data; lengths of limb segments have been manually measured.

In order to determine the shoulder position with respect to the robot base frame, an initial calibration phase has been carried out. Hence, after measuring upper-limb segment lengths, the subject hand has been positioned in the centre of the circle (coincident with the robot workspace center) with a flexion angle of 45° for the shoulder and the elbow and an abduction angle of 45° for the shoulder.
The circle-drawing task is a typical exercise for evaluating stroke patients after a robotic treatment [61]. In this study, it is particularly suitable to point out the

Eugenia Papaleo

joint activity, mainly in the simultaneous activation of shoulder and elbow angles that is typically compromised in stroke patients.

In Figure 4.4 (a) a sketch of the top view of subjects' position while performing the circle-drawing task and robot reference system are illustrated; on the other hand, Figure 4.4 (b) shows one of the tested healthy subjects performing the task.

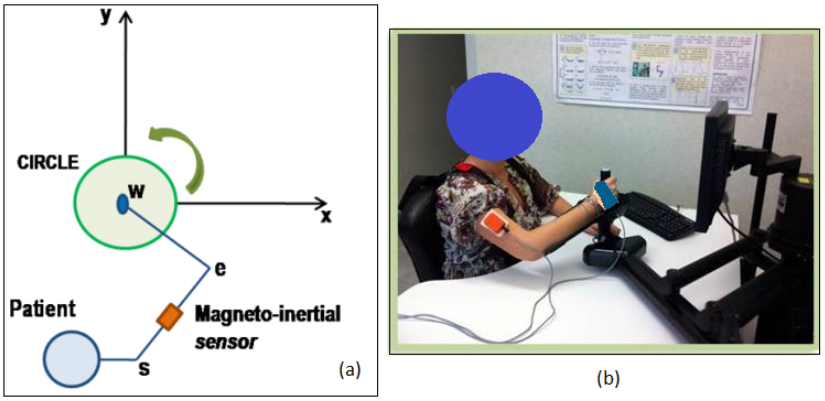

FIGURE 4.4: Experimental trial of robot-aided rehabilitation: (a) a sketch of the top view of subjects' position while performing the circle-drawing task and robot reference system; (b) a healthy subject performing the circle-drawing task.

4.5 Results

4.5.1 Performance of the joint reconstruction algorithm

Before providing the results on the joint reconstruction, the error evolution over time of the inverse kinematics algorithm in equation (4.5) has been analyzed. Figure 4.5 shows the norm of the error (i.e. variable $\bar{er}$ in equation (4.5)) during the inversion procedure with the augmented Jacobian. In particular, the norm of position error, orientation error and swivel angle error are reported with an initial condition of $\bar{q} = [0.43, -0.1, -0.7, -0.7, 0.68, -0.56, -0.14]^T$ rad, for the arm joint vector, and a gain matrix of $K = diag\{10 \dots 10\}$ N/m·s. As expected, although the error increases at the beginning, it rapidly converges to zero during movement reconstruction.

Figure 4.6 illustrates the upper-limb joint reconstruction of a *forward/backward movement* performed by one of the four tested subjects; in detail:

- the seven arm angles reconstructed through equation (4.5) are drawn with a dotted black line while arm angles measured through the optoelectronic system are shown in light blue;

Eugenia Papaleo

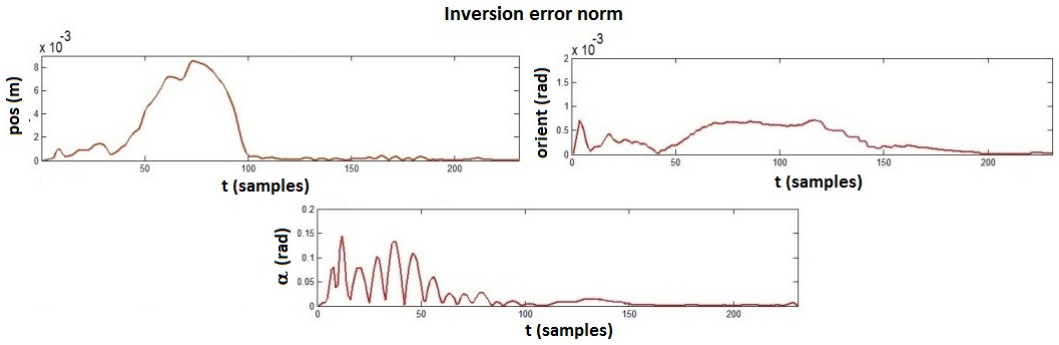

FIGURE 4.5: Norm of the error $\bar{er}$ due to the time-discrete integration; the error relative to position variables (upper left), orientation variables (upper right) and swivel angle (below) during the reconstruction of a *forward/backward movement* is represented

- the 3D hand trajectory obtained by applying the forward kinematics function to the seven reconstructed angles is shown with a dotted red line, while the hand position measured through the SMART-D optoelectronic system is drawn in blue.

In all the performed tests, the arm joint trajectories reconstructed with the proposed method are well overlapped with the angles computed through the optoelectronic motion capturing system. The *Root Mean Square Error* (RMSE) between the two trajectories in the joint space is $8.3 * 10^{-3} rad$ on average over all the performed experimental trials, with a variance of $1.8 * 10^{-3} rad$.
A graphical representation of the error committed with the proposed reconstruction algorithm is shown in Figure 4.7; it reports the RMSE (in grey) and the maximum error (in white) for each reconstructed upper-limb joint angle.

Although it is low, the error measured between the two methods can be due to a number of reasons: e.g. subtle and unavoidable trunk movements that entail small displacements of the reference frame, the neglected acceleration dynamic component that is presumably low but not null, markers movements on the skin during the task execution, which can produce a small error in the measure of the length of the upper-limb segments. Moreover, method accuracy can also be affected by i) the orientation of each joint functional axis (which can vary with respect to the modeled one), ii) possible relative movements between the accelerometer and the humerus, and iii) the identification of the initial conditions. Finally, it is also important to consider that in shoulder joint, modeled for simplicity as a single spherical joint, also translation movements correlated to rotations can occur.
Hence, the accuracy of the kinematic reconstruction method is strongly influenced by the measuring conditions and the calibration procedure.

Eugenia Papaleo

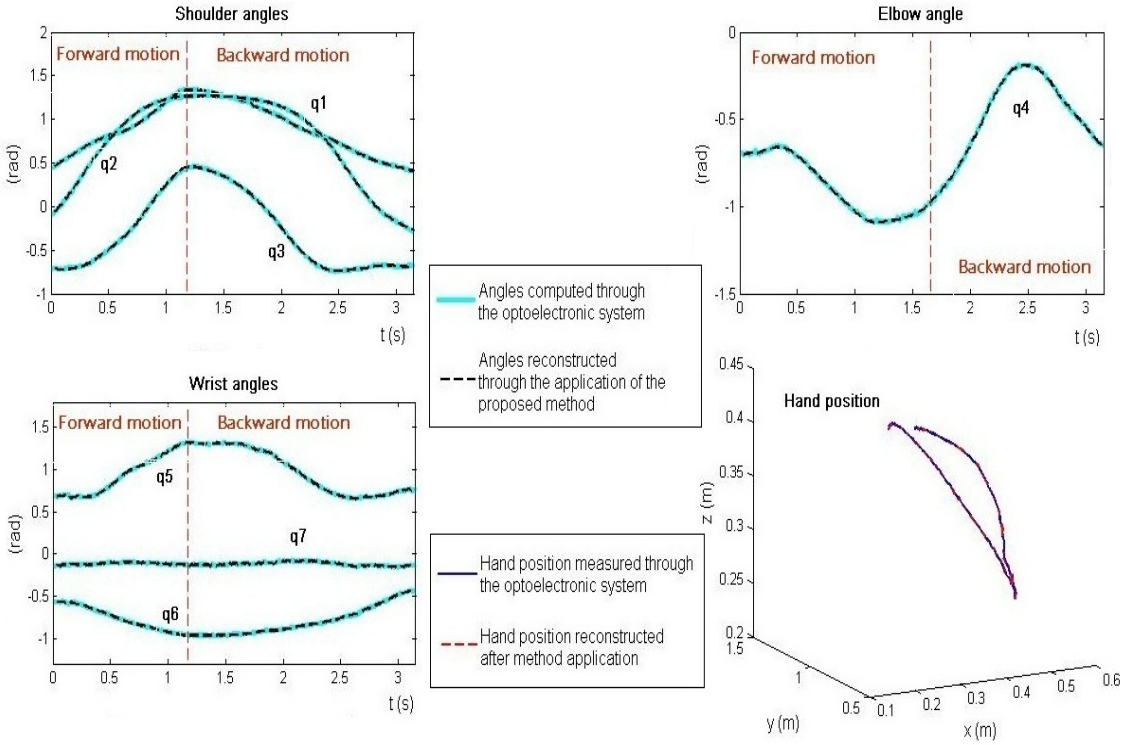

FIGURE 4.6: Shoulder and elbow angles (above) and wrist angles (lower left) reconstructed with the proposed method (dotted black line) and measured through the optoelectronic system (light blue line). Lower right: hand position computed by applying the arm forward kinematic function to the angles reconstructed with the proposed method (dotted red line) and measured through the optoelectronic system (blue line). All data refer to a *forward/backward movement* performed by one of the tested subjects

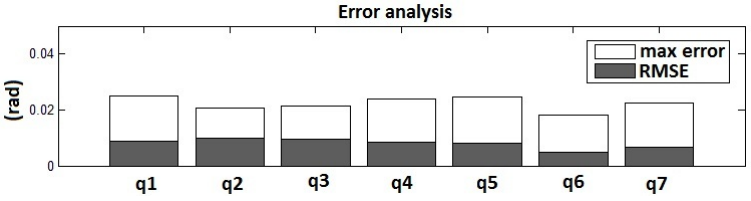

FIGURE 4.7: RMSE (grey) and maximum error (white) between joint angles computed with the proposed method and obtained via the optoelectronic system

4.5.2 Experimental results of robot-aided rehabilitation

Figure 4.8 reports the joint kinematic reconstructions of healthy and stroke subjects during the circle-drawing tasks performed with the InMotion2 robot. In particular, the Figure 4.8 shows the reconstructed shoulder angles q_1, q_2, q_3 in the top, elbow angle q_4 in the middle and the hand positions provided by the robot in the bottom. Wrist angles are not reported being negligible their variations during planar tasks with the InMotion2.

Healthy subjects' trajectories have been reported as "healthy bands", thus defining a reference behaviour for evaluating patients motion. Patients' trajectories are related to the phases of pre-treatment assessment (blue line) and the post-treatment assessment (red line). They have been averaged over all the five task repetitions and reported for both patients in two different columns.

It clearly emerges from Figure 4.8 that hand trajectories close to those of healthy subjects are obtained with joint trajectories that tend to the "healhty bands" of the angles; further, they are characterized by high variability. As can be noticed, the outcomes for the two tested patients are different: patient 1 performance in drawing the circle at the end of the treatment is higher than patient 2. This result seems to be controversial with the clinical scales reported in Table 4.2 (at the discharge, patient 2 has higher clinical scores than patient 1). The inspection of all the items of the clinical scales has revealed that the score of patient 2 is due to the improvement of 2 points on the FM scale for forearm pronation-supination; this is a DoF that is not exploited during the evaluation task performed with the InMotion2 robot, thus its improvement does not contribute to circle drawing.

Finally, results point out, on the one hand, the coherence between the obtained kinematic reconstructions and the clinical scores provided by the clinicians, on the other hand, the capability of identifying from patients' plots movement features in the joint space that are responsible for hand motion far from the "healthy bands". In particular:

- The coordination of shoulder and elbow joints during circle-drawing tasks is a key point. A higher correlation between arm joints can be observed in patient 1 than in patient 2 (who mainly improves forearm pronation-supination not involved in the analyzed tasks).
- The difficulty of patients to draw large circles is mainly due to their inability to properly extend the elbow joint.
- The meager movement smoothness in the Cartesian space clearly originates from a low smoothness in the joint space.

Eugenia Papaleo

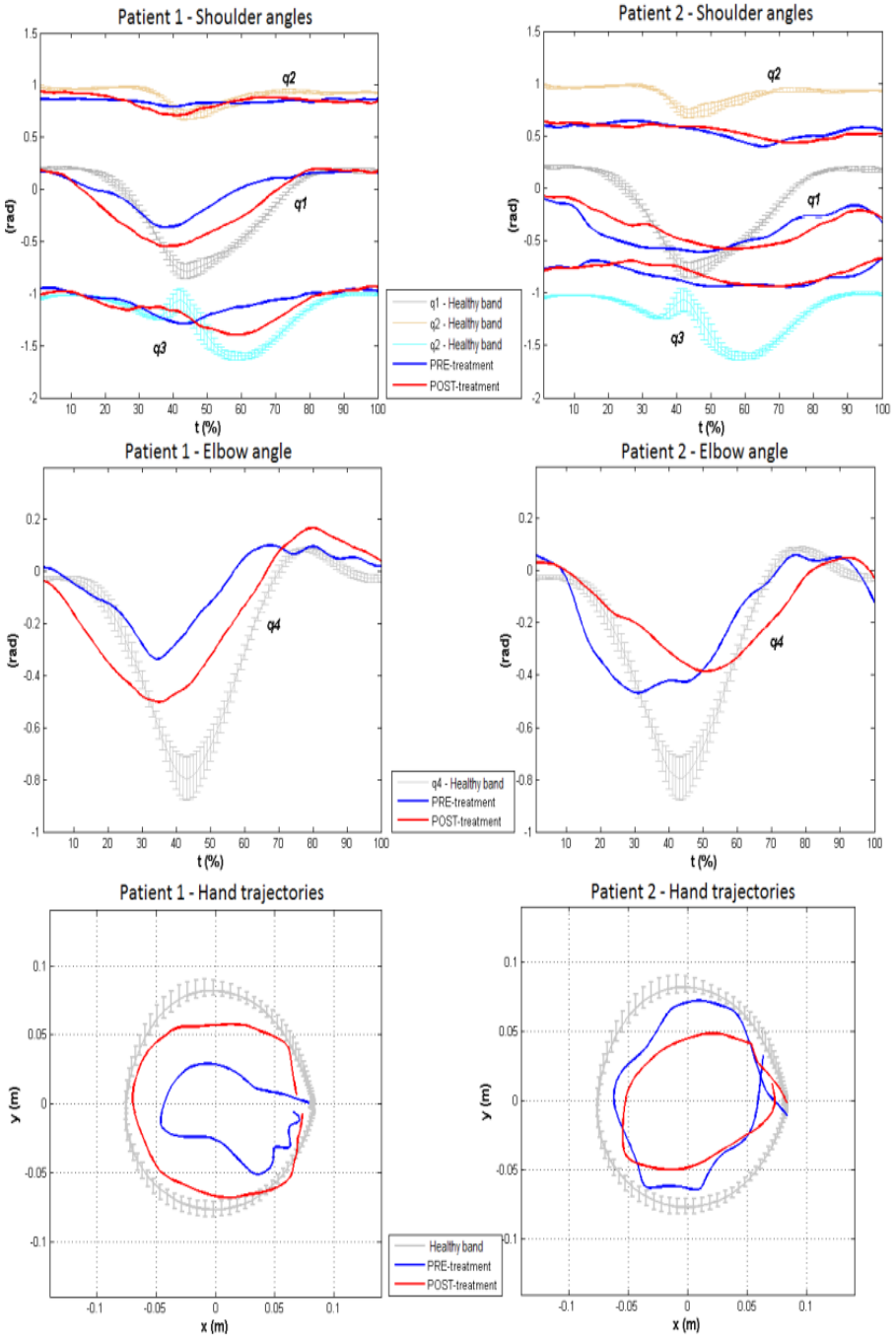

FIGURE 4.8: Shoulder and elbow angles and hand trajectories of healthy and stroke subjects. Healthy subjects trajectories are depicted as "healhty bands"; stroke patients' data are averaged over all the five task repetitions. Blue: pre-treatment; red: post-treatment.

Chapter 5

Application of the bio-cooperative system to 3D robot-aided rehabilitation

This Chapter presents a robotic system for 3D upper-limb robot-aided rehabilitation, grounded on the proposed bio-cooperative system: it real-time adapts therapy characteristics to patient needs, by including the patient in the control loop. The system is composed of a 7-DoF robot arm, the adaptive interaction control system and the multimodal interface, that acquires patient biomechanical data and evaluates the global biomechanical performance. This is fed back to the robot controller for the adaptation of task complexity in the 3D space.
The experimental validation of the application here proposed is carried out on healthy subjects and results in 2D and 3D space are provided.

The Chapter is structured as follows. Section 5.2 illustrates the proposed bio-cooperative robotic system. The experimental validation of the system is presented in Section 5.3: it has been carried out on healthy subjects, behaving as normal subjects and simulated post-stroke patients. Both the experimental protocol and the experimental results are reported in Sections 5.3.1 and 5.3.2, respectively.

5.1 Background

As discussed in Chapter 2, in the last decades the use of robotic systems for upper-limb rehabilitation is widely increased, as it fosters cortical re-organization, supplies meaningful measures on task fulfilment, provides objective evaluations of motor recovery and impact of the therapeutic approach, takes charge of the

Eugenia Papaleo

physically demanding parts of treatment, favors the active role of patients; moreover, robots allow administering repetitive and accurate exercises, exploiting data logged by their position and force sensors, aiding patient as he needs [107], [33], [39]. But what is still poorly faced in the current rehabilitation robotic machines is the combination of physical therapy with the identification of patient needs and global status, thus re-planning, re-adapting the training with respect to them [32] and enhancing patient involvement and active role in the therapy, with a consequent improvement of therapy outcomes.

Moreover, the standard robot-aided rehabilitation is very task-specific, typically consisting of a robot waiting for the onset of the patient voluntary motion and then guiding the patient to accomplish predetermined analytical movements (such as point-to-point motion). It is shown in [108] that the specificity of traditional robot-aided training has a limiting effect on cortical plasticity, since the primary sensorimotor cortex representational map for the practiced task increases substantially over time, while the size of the map for a not practiced task does not change.

The work presented in this Chapter wants to face the above-mentioned issues by (i) extending training exercises to 3D space and to activities of daily living (ADLs), thus involving more cortical areas and stimulating generalization; (ii) proposing a patient-tailored adaptive therapy that includes the patient in the control loop, thus monitoring his state and accordingly changing robot behaviour. The main expected results are to maximize patients involvement in the therapy by encouraging them to use all their residual capabilities, to progress movement performance and to increase the rate of motor re-learning.
To this purpose, the novel bio-cooperative system for 3D upper-limb robot-aided rehabilitation presented here joins together

- a 7-DoF robot arm, enabling therapy delivery in 3D space and execution of ADL tasks;
- the adaptive robotic controller proposed in Chapter 3, to modulate the level of assistance and deliver patient-tailored therapy;
- the multimodal interface proposed in Chapter 3, to acquire biomechanical data from the patient and provide the robot with real-time information on patient behaviour for adaptively and dynamically changing the difficulty level of the task.

Eugenia Papaleo

As anticipated in Chapter 2, currently only a few attempts of robotic systems for motor therapy can be found in the literature collecting multimodal sensory signals from the patient for assessment and control, or aiming at closing the patient in the control loop [66], [109], [68], [110], [67], [5], [69].
The first work on this line dates back to several years ago [66]. It proposed a *performance-based* impedance control algorithm using patient active power and motion accuracy measures to define the level of robot assistance at the beginning of a new block of exercises; it was conceived for planar analytical exercises with the MIT-Manus robot. Performance measures were carried out on a set of reaching movements in different directions.
Later works by Novak [67] and Koenig [68] proposed to use psycho-physiological measurements of patient state and task performance analysis to adjust the difficulty of a task administered by the Haptic Master robot; the results showed that patient psycho-physiological measurements alone cannot be efficiently used to update the robot behaviour; they can provide just supplementary information with respect to motor data.

In the bio-cooperative system here proposed, first complete pictures of patient biomechanical performance, one for each movement direction, are reconstructed by the multimodal interface; then, the adaptive robotic controller modulates the complexity of the task in the 3D space, according to the estimated patient global performance.

5.2 The proposed bio-cooperative robotic system

5.2.1 System components

The bio-cooperative robotic system is composed of the following main components.

1. The multimodal interface proposed in Chapter 3 - Section 3.1.
2. The adaptive control system proposed in Chapter 3 - Section 3.2.
3. The anthropomorphic 7-DoF Light Weight Robot (LWR) from KUKA, its controller (KRC 2lr) and control panel (KCP) (Figure 5.1). The LWR is a robot characterized by high dynamic performance; moreover, its elastic joints ensure an intrinsic compliance that enforces safety in the interaction.
4. A mounting flange opportunely designed for attaching user wrist to the KUKA LWR end-effector (Figure 5.2). The flange is made of a holding

Eugenia Papaleo

FIGURE 5.1: KUKA Light Weight Robot with robot controller (KRC 2lr) and control panel (KCP)

magnet (GMHX 050 X20 A01, MAGNET-SCHULTZ), a wrist support conceived in order to leave the hand free of moving and velcro straps that lightly hold the patient forearm secure.

FIGURE 5.2: The designed mounting flange for connecting the robot end-effector and the patient's wrist

5. A software package, named Fast Research Interface (FRI), enabling robot remote programming in C++ and communication with the robot controller through a UDP protocol.

6. A PC where the FRI and the Simulink scheme of the multimodal interface can simultaneously run.

7. Two miniaturized magneto-inertial sensors (MTx sensors, from Xsens - full scale: $pm5g$) (Figure 5.3) placed on the subject arm and employed for the on-line reconstruction of the upper-limb kinematics. In particular, one sensor is

Eugenia Papaleo

used for acquiring upper arm acceleration data, the other sensor is exploited for recording data on hand orientation.

FIGURE 5.3: MTx sensor from Xsens

Figure 5.4 shows some of the main components of the bio-cooperative system during the execution of a motor task.

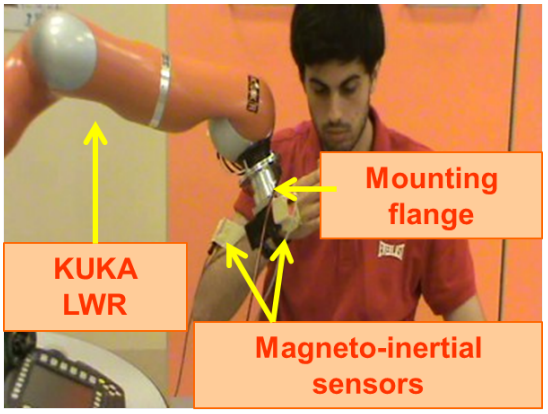

FIGURE 5.4: Motor task execution at the bio-cooperative robotic system; some of the main components are indicated

In order to increase safety in the interaction, two expedients have been used: i) an emergency stop button, to be used in case of dangerous situation to interrupt the power supply of the holding magnet embedded in the mounting flange, thus causing the immediate release of user wrist; ii) limitation of control commands so that, if the value in norm of the force exerted by the robot at the end-effector level exceeds a predetermined value (fixed at about $15N$), the control system immediately halts the movement.

Eugenia Papaleo

5.2.2 Communication between system modules

The communication between the different system modules is illustrated in Figure 5.5.

The communication between the PC and the KUKA robot controller is established via the FRI, using an Ethernet cable, with a sample time of 30 ms. On the same PC, the Simulink scheme of the multimodal interface, running at 100 Hz, receives information from: i) MTx sensors placed on the subject arm, via USB connection, and ii) robot sensors, via UDP communication. The multimodal interface Simulink scheme real-time:

- reconstructs the upper-limb kinematics,
- computes the kinematic and dynamic performance indicators,
- evaluates the patient global biomechanical state,
- displays the virtual reality environment relative to the execution of the assigned task,
- communicates with the FRI via UDP.

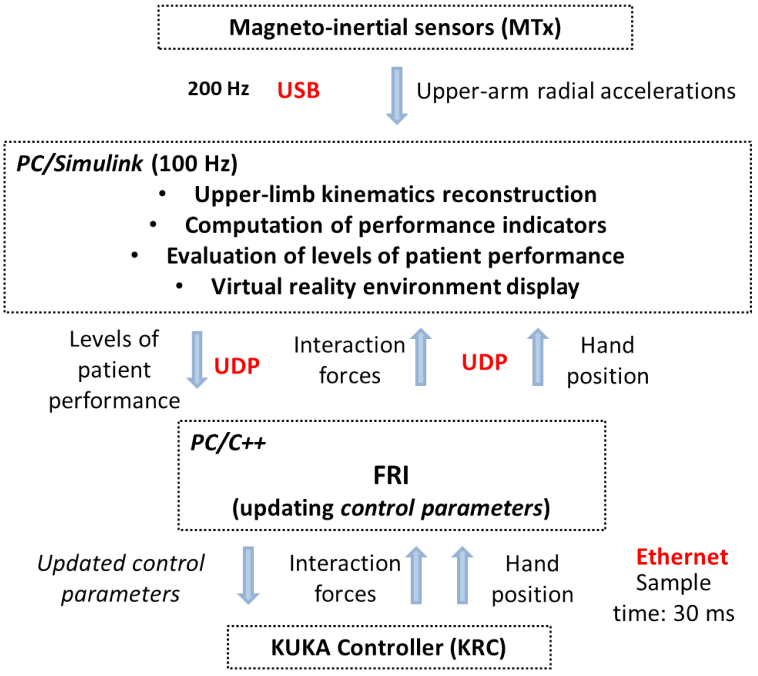

FIGURE 5.5: Functional architecture of the communication among all the main modules of the bio-cooperative system

5.2.3 Estimation of patient biomechanical performance

The global patient biomechanical state is estimated through the computation of the following performance indicators:

- *aiming angle* (ϕ),
- *Mean Arrest Period Ratio (MAPR)*,
- *Inter-joint coordination* ($q_{corr_{i,j}}$),
- *Useful Mean Force (UMF)*,
- *Useful Peak Force (UPF)*.

Performance indicators are normalized with respect to their maximum and adjusted in order to increase with motor recovery; then, they are used to update control parameters through opportune modulation functions.
Among all the indicators, the *aiming angle* index is employed only in the function for modulating robot stiffness, since it quantifies the direction of the fulfilled movement; on the other hand, the *MAPR* index is used only in the function that updates task duration, as it accounts for movement smoothness (describing the percentage of stops during task execution). All the other indicators are employed in both the modulation functions.

5.2.4 Modulation functions of control parameters

As anticipated in Chapter 3, the two modulation functions for K and t are computed as weighted sums of the selected indicators, where weights have been chosen through a "trial and error" approach. A weight configuration that allows discriminating between different quality levels of the executed movements has been selected. Greater weights have been given to *aiming angle* and *MAPR* in K and t, respectively, with respect to the other indicators because they are more indicative of a pathological behaviour versus a healthy behaviour.
In detail, the two functions are expressed as

$$C_K = \frac{1}{2}\phi + \frac{1}{8}q_{corr_{1,4}} + \frac{1}{8}q_{corr_{2,4}} + \frac{1}{8}UMF + \frac{1}{8}UPF \tag{5.1}$$

and

$$C_t = \frac{1}{2}MAPR + \frac{1}{8}q_{corr_{1,4}} + \frac{1}{8}q_{corr_{2,4}} + \frac{1}{8}UMF + \frac{1}{8}UPF, \tag{5.2}$$

Eugenia Papaleo

where $q_{corr_{1,4}}$ and $q_{corr_{2,4}}$ are the Inter-joint coordination indices between shoulder abduction/adduction and elbow flexion/extension and shoulder flexion/extension and elbow flexion/extension, respectively.

Considering that C_K and C_t continuously vary in the interval $[0, 1]$, a threshold strategy has been implemented to define the discrete values needed to the robot controller for updating the control parameters. Therefore, the discrete levels of patient performance for updating K and t are related to the output of functions (5.1) and (5.2) as

$$L_i = \begin{cases} 1 & 0 \leq C_i < 0.5 \\ 2 & 0.5 \leq C_i < 0.75 \\ 3 & 0.75 \leq C_i < 1 \end{cases} \tag{5.3}$$

where $i = K, t$.

The values of L_k and L_t are sent to the robot control and are automatically associated to predetermined values of stiffness and task duration. In particular, stiffness K could assume the three values 0.1, 300 or 1000 N/m, corresponding to the three discrete levels of L_K, while task duration could be equal to 5, 7.5 or 10 s, according to the discrete value of L_t.

Finally, the implemented bio-cooperative system evaluates subject performance and adjusts control parameters after each task execution, not strictly in real-time. This choice is due to a twofold reason: i) since robot dynamic features in the 3D space are anisotropic (especially inertia), task difficulty can not be the same in all the directions and different levels of assistance can be required; ii) the capability of each patient to accomplish a task can obviously vary with task direction.

5.3 Experimental validation

The proposed bio-cooperative rehabilitation system has been experimentally tested on healthy subjects in a laboratory setting. This is a fundamental preliminary step to the application to stroke patients. In fact, although the developed system has been conceived for delivering 3D space exercises and ADL tasks, in this early evaluation of the system it has been chosen i) to evaluate its performance and viability during the execution of simple 3D tasks (i.e. point-to-point movements), ii) to carry out an initial validation only on healthy subjects in order to assess

Eugenia Papaleo

control performance and safety issue. The natural extension is to test ADL tasks and include the robotic system in a clinical setting for an extensive validation on post-stroke patients.

5.3.1 Experimental protocol

Two healthy subjects has been tested, aged 24 and 27 years respectively. Subjects, while seated on a chair and with the right wrist connected to the robot end-effector, performed the 2D and 3D motion tasks described in the following:

- Planar clock game, entailing point-to-point movements in 8 different directions from North (N) to North-West (NW), spaced 40° apart. In order to obtain high stiffness in the vertical direction and enable planar motion, the Cartesian stiffness along the vertical axes has been set to 5000 N/m;
- 3D clock game, entailing point-to-point movements in the space in 4 different directions, spaced 90° apart.

Consistently with the robot workspace (and with the traditional clock game [93]), each point-to-point movement had a length of 0.14 m.

Subjects have been required to exhibit two different behaviours:

1. *Healthy behaviour*, aimed at evaluating system response when the user performs a correct motion; in this case subjects have been required to perform the motion with a self-paced velocity;
2. *Simulated post-stroke behaviour*, aimed at preliminary testing the patient-tailored approach by simulating the behaviour of a stroke subject. To this purpose, subjects have been required to intentionally fail to perform the motion (especially that involving elbow extension), going in the wrong direction or repeatedly stopping during the task execution, trying to emulate motion difficulty of stroke subjects.

Tests have been conducted in the following way:

- Subjects executed two unassisted clock games in the two conditions (i.e. healthy and pathological); in order not to provide assistance, the stiffness value has been chosen very low ($K = 0.1N/m$).

Eugenia Papaleo

- The global biomechanical performance have been evaluated first through the computation of performance indicators and, then, through equations (5.1) and (5.2).
- The control parameters have been updated according to equation (5.3).
- The training tasks have been executed again with the required level of robot assistance and performance indicators and biomechanical states have been anew computed.

5.3.2 Experimental results

Figures 5.6 and 5.7 show the Cartesian position in the plane during the clock exercise for subject 1 and 2, respectively, during the healthy behaviour and the simulated post-stroke behaviour. In particular, the desired motion is shown with a dotted black line, the healthy motion is in blue, the unassisted post-stroke behaviour is in red and the assisted post-stroke behaviour is in green. It seems needless to point out that after the adaptation of control parameters post-stroke simulated trajectories tend to the healthy ones.

Table in Figure 5.8 reports the values of the computed performance indicators and of C_K and C_t (biomechanical states) calculated through equations (5.1) and (5.2), for each task direction (planar and 3D) executed by subject 1 during the initial unassisted phase; results are reported for both the conditions of *Healthy behaviour* and *Simulated post-stroke behaviour*. Analogously, table in Figure 5.9 reports the same values for subject 2.
As expected, performance indicators, C_K and C_t assume greater values in the case of healthy motion than in the case of simulated pathological behaviour, thus not causing the update of robot control parameters. On the other hand, the simulated post-stroke behaviour produces globally lower values of the performance indicators than a healthy behaviour, but different in each direction, depending on the predominance of elbow flexion or extension. For instance, table of Figures 5.8 and 5.9 point out that in directions South (S), South-West (SW) and West (W) of the planar clock game, which mainly involve elbow flexion, the value of the indicators and the levels of the biomechanical states are higher than in the other directions (involving elbow extension, which is typically more limited than flexion in post-stroke subjects [111]). Future tests on post-stroke patients will be carried out to further investigate this issue and perform a statistical analysis of the collected data.

Eugenia Papaleo

Results about the modulation of robot behaviour are reported in the tables in Figures 5.10 and 5.11 for subject 1 and 2, respectively. Tables report data in the simulated post-stroke behaviour obtained during assisted motion, after updating control parameters; thus, the values defined for K and t after the assessment of subject biomechanical states during unassisted tasks are reported together with the new values of performance indicators and biomechanical states.

One can observe that the values of the biomechanical states significantly increase as a consequence of the increased values of the performance indicators. Moreover, it is worth noticing that the dynamic indicators, which quantify the amount of force directed towards the target, do not considerably grow, except for the case of planar movements which require elbow flexion (S, SW, W) and are easier than 3D tasks: in all the other planar movements, mainly involving elbow extension, and in 3D tasks subjects tend to be moved by the robotic device. This suggests that the dynamic performance indicators can be more fruitfully employed in resistive tasks, in which subject strength is always stimulated.

Eugenia Papaleo

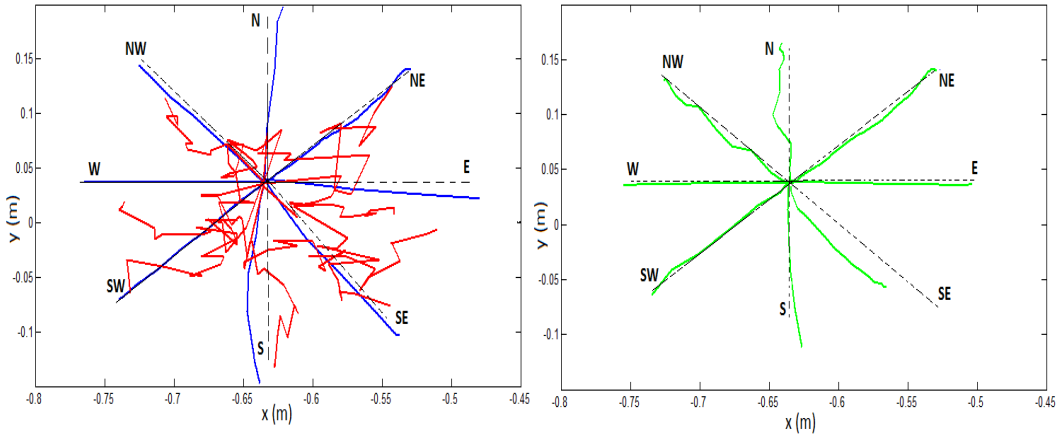

FIGURE 5.6: Planar clock game: Movements executed by subject 1 for the healthy and the simulated post-stroke behaviours and desired motion (dotted black line). Left: unassisted tasks for healthy (blue) and post-stroke motion(red). Right: tasks performed simulating post-stroke behaviour after the updating of the control parameters (green)

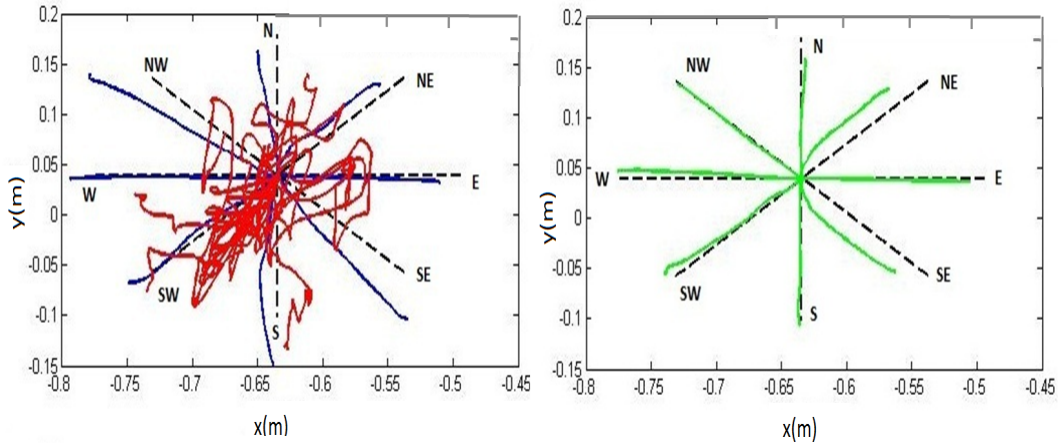

FIGURE 5.7: Planar clock game: Movements executed by subject 2 for the healthy and the simulated post-stroke behaviours and desired motion (dotted black line). Left: unassisted tasks for healthy (blue) and post-stroke motion(red). Right: tasks performed simulating post-stroke behaviour after the updating of the control parameters (green)

Unassisted tasks								
Planar clock game								
P-T-P	**ϕ**	**MAPR**	**$q_{corr\ 1,4}$**	**$q_{corr\ 2,4}$**	**UMF**	**UPF**	**C_K**	**Ct**
Subject 1 (Healthy)								
N	0.97	0.80	1	0.79	0.70	0.79	0.90	0.80
NE	0.95	0.86	0.97	0.92	0.88	0.82	0.92	0.88
E	0.96	0.75	0.87	0.89	0.86	0.96	0.93	0.82
SE	0.94	0.90	0.97	0.49	0.75	0.91	0.86	0.84
S	0.98	0.73	0.99	0.92	0.65	0.78	0.91	0.78
SW	0.98	0.89	0.99	0.99	0.88	0.90	0.97	0.92
W	1	0.80	0.73	0.77	0.97	0.99	0.93	0.83
NW	0.97	0.67	1	1	0.88	0.88	0.95	0.80
Subject 1 (Simulated post-stroke)								
N	0.72	0.30	0.004	0.49	0.50	0.97	0.60	0.39
NE	0.80	0.76	0.63	0.54	0.42	0.25	0.63	0.61
E	0.44	0.70	0.03	0.67	0.57	0.06	0.39	0.52
SE	0.71	0.46	0.96	0.02	0.48	0.61	0.61	0.49
S	0.59	0.50	0.98	0.18	0.51	0.68	0.59	0.55
SW	0.46	0.58	0.90	0.38	0.55	0.76	0.55	0.62
W	0.58	0.62	0.31	0.08	0.70	0.93	0.54	0.56
NW	0.66	0.65	0.80	0.28	0.59	0.69	0.63	0.62
3D clock game								
P-T-P	**ϕ**	**MAPR**	**$q_{corr\ 1,4}$**	**$q_{corr\ 2,4}$**	**UMF**	**UPF**	**C_K**	**Ct**
Subject 1 (Healthy)								
NE	0.86	0.82	0.99	0.77	0.83	0.76	0.85	0.83
SE	0.92	0.86	0.95	0.49	0.94	0.98	0.88	0.85
SW	0.84	0.77	1	1	0.77	0.84	0.87	0.83
NW	0.81	0.92	0.99	0.55	0.84	0.85	0.8	0.85
Subject 1 (Simulated post-stroke)								
NE	0.27	0.75	0.53	0.61	0.48	0.35	0.39	0.62
SE	0.61	0.58	0.95	0.56	0.70	0.68	0.66	0.65
SW	0.67	0.62	0.24	0.63	0.54	0.65	0.59	0.57
NW	0.75	0.76	0.16	0.30	0.48	0.65	0.52	0.57

FIGURE 5.8: Unassisted tasks (K=0.1N/m): Values of performance indicators and biomechanical states for subject 1 during unassisted tasks for healthy and simulated post-stroke conditions

Unassisted tasks								
Planar clock game								
P-T-P	**ϕ**	**MAPR**	**$q_{corr\ 1,4}$**	**$q_{corr\ 2,4}$**	**UMF**	**UPF**	**C_K**	**Ct**
Subject 2 (Healthy)								
N	0.96	0.81	0.85	1	0.70	0.78	0.90	0.82
NE	0.98	0.79	0.86	1	0.66	0.75	0.90	0.80
E	0.99	0.90	0.97	0.98	0.85	0.87	0.95	0.91
SE	0.98	0.73	0.99	0.99	0.66	0.66	0.90	0.78
S	0.98	0.89	0.56	1	0.69	0.72	0.86	0.82
SW	0.99	0.92	0.92	1	0.78	0.79	0.93	0.89
W	0.99	0.94	0.80	0.89	0.98	0.99	0.95	0.93
NW	0.96	0.91	0.99	0.99	0.87	0.86	0.94	0.92
Subject 2 (Simulated post-stroke)								
N	0.94	0.20	0.37	0.14	0.49	0.29	0.63	0.26
NE	0.77	0.58	0.61	0.98	0.49	0.08	0.65	0.56
E	0.16	0.61	0.76	0.88	0.51	0.58	0.42	0.65
SE	0.61	0.81	0.76	0.99	0.48	0.42	0.64	0.74
S	0.79	0.96	0.30	0.98	0.50	0.78	0.71	0.80
SW	0.92	0.71	0.23	0.98	0.62	0.19	0.71	0.61
W	0.75	0.57	0.05	0.92	0.61	0.95	0.69	0.60
NW	0.45	0.81	0.06	0.98	0.49	0.32	0.29	0.64
3D clock game								
P-T-P	**ϕ**	**MAPR**	**$q_{corr\ 1,4}$**	**$q_{corr\ 2,4}$**	**UMF**	**UPF**	**C_K**	**Ct**
Subject 2 (Healthy)								
NE	0.88	0.75	0.91	1	0.85	0.96	0.90	0.84
SE	0.84	0.75	0.59	1	0.96	0.95	0.86	0.81
SW	0.78	0.71	0.90	0.81	0.72	0.70	0.79	0.76
NW	0.73	0.82	0.92	1	0.84	0.76	0.82	0.85
Subject 2 (Simulated post-stroke)								
NE	0.29	0.77	0.01	0.52	0.55	0.80	0.38	0.62
SE	0.52	0.16	0.93	0.91	0.43	0.30	0.58	0.40
SW	0.78	0.81	0.25	0.09	0.62	0.76	0.61	0.62
NW	0.32	0.31	0.91	1	0.65	0.78	0.58	0.57

FIGURE 5.9: Unassisted tasks (K=0.1N/m): Values of performance indicators and biomechanical states for subject 2 during unassisted tasks for healthy and simulated post-stroke conditions

Eugenia Papaleo

Assisted tasks										
Planar clock game										
P-T-P	***K [N/m]***	***t [s]***	***ϕ***	***MAPR***	***$q_{corr\ 1,4}$***	***$q_{corr\ 2,4}$***	***UMF***	***UPF***	***C_K***	***Ct***
Subject 1 (Simulated post-stroke)										
N	300	10	0.90	0.77	1	0.50	0.14	0.08	0.63	0.56
NE	300	7.5	0.99	0.87	0.88	0.85	0.40	0.23	0.79	0.73
E	1000	7.5	0.99	0.65	0.98	0.99	0.04	0.01	0.70	0.53
SE	300	10	0.94	0.79	0.98	0.11	0.17	0.11	0.60	0.53
S	300	7.5	0.97	0.47	0.99	0.98	0.61	0.72	0.91	0.66
SW	300	7.5	0.99	0.71	0.99	0.94	0.53	0.83	0.88	0.74
W	300	7.5	0.99	0.90	0.90	0.92	0.66	0.77	0.92	0.87
NW	300	7.5	0.96	0.81	0.99	0.98	0.45	0.27	0.79	0.71
3D clock game										
P-T-P			**ϕ**	**MAPR**	**$q_{corr\ 1,4}$**	**$q_{corr\ 2,4}$**	**UMF**	**UPF**	**C_K**	**Ct**
Subject 1 (Simulated post-stroke)										
NE	1000	7.5	0.97	0.92	0.90	0.94	0.32	0.27	0.76	0.73
SE	300	7.5	0.92	0.76	1	0.94	0.50	0.64	0.82	0.74
SW	300	7.5	0.94	0.89	0.98	0.94	0.30	0.27	0.75	0.72
NW	300	7.5	0.96	0.77	0.98	0.97	0.09	0.05	0.69	0.59

FIGURE 5.10: Assisted tasks for simulated post-stroke motion of subject 1: Values of K and t (defined as a function of the biomechanical states evaluation during unassisted tasks), the new values of performance indicators and biomechanical states

Assisted tasks										
Planar clock game										
P-T-P	***K [N/m]***	***t [s]***	***ϕ***	***MAPR***	***$q_{corr\ 1,4}$***	***$q_{corr\ 2,4}$***	***UMF***	***UPF***	***C_K***	***Ct***
Subject 2 (Simulated post-stroke)										
N	300	10	1	0.92	0.99	1	0.32	0.28	0.82	0.78
NE	300	7.5	0.92	0.82	0.94	1	0.16	0.13	0.74	0.69
E	1000	7.5	0.99	0.91	0.99	0.96	0.24	0.22	0.80	0.76
SE	300	7.5	0.96	1	0.91	0.99	0.22	0.21	0.77	0.79
S	300	5	0.99	0.89	0.97	1	0.56	0.64	0.89	0.84
SW	300	7.5	0.97	0.78	0.90	1	0.68	0.82	0.91	0.81
W	300	7.5	0.97	0.86	0.79	0.75	0.78	0.81	0.88	0.82
NW	1000	7.5	1	0.73	0.99	1	0.50	0.63	0.89	0.75
3D clock game										
P-T-P			**ϕ**	**MAPR**	**$q_{corr\ 1,4}$**	**$q_{corr\ 2,4}$**	**UMF**	**UPF**	**C_K**	**Ct**
Subject 2 (Simulated post-stroke)										
NE	1000	7.5	0.97	0.80	0.99	0.91	0.05	0.03	0.74	0.65
SE	300	10	0.85	0.86	0.87	1	0.31	0.30	0.73	0.74
SW	300	7.5	0.93	0.87	0.04	0.95	0.07	0.05	0.61	0.57
NW	300	7.5	0.90	0.71	0.94	0.98	0.18	0.18	0.74	0.64

FIGURE 5.11: Assisted tasks for simulated post-stroke motion of subject 2: Values of K and t (defined as a function of the biomechanical state evaluation during unassisted tasks), the new values of performance indicators and biomechanical states

Eugenia Papaleo

Chapter 6

Application of the multimodal interface to the quantitative evaluation of chronic stroke patients

In this Chapter a further application of the system proposed in Chapter 3 is presented. In particular, the developed multimodal interface is used for the quantitative evaluation of the outcomes of a novel rehabilitation treatment that joins together transcranial Direct Current Stimulation (tDCS) and upper-limb robotic therapy.
The application of the multimodal interface to quantitative evaluation has the following twofold objective:

1. Couple the clinical evaluation of patients with the quantitative evaluation of their performance;
2. Test the correlation between the performance indicators extracted by the multimodal interface and the clinical scales commonly employed in the clinical practice.

The Chapter is structured as follows. First study background (Section 6.1) and methodology (study design, participants' selection, robotic and stimulation systems - Section 6.2) are presented. Then, the tools for measuring the outcomes of the treatment are illustrated (Section 6.3) and the preliminary results on chronic stroke patients are reported (Section 6.4).

Eugenia Papaleo

6.1 Background

As discussed in Chapter 2, following a stroke most people survive but motor functions, speech, attention, cognitive or sensory functions are often compromised. Recovery of motor disabilities can be promoted by physical therapy and rehabilitation; in particular, robot-assisted therapy represents a particularly powerful tool to promote functional recovery. However, despite such interventions, residual disabilities often persist.

In last decade, the idea has arisen that adjunct non-invasive interventions, such as the electrical brain stimulation, might be used to speed-up and maximize the potential benefit of rehabilitation treatments [112] [113] [114].
The rationale of this idea originates from the fact that, after a stroke affecting the primary motor cortex (M1), patients' motor cortex excitability is reduced in the damaged hemisphere and increased in the contralateral side [115], while, in physiological conditions, the two hemispheres are in a state of electrical balance due to the existent mutual inhibition [116].

Recently, it has been pointed out that tDCS, if applied on M1 through a *bi-hemispheric* configuration, can produce changes in motor performance due to the simultaneous facilitatory effect, under the anode location, and inhibitory effect, under the cathode location (contralesional side) [117]. This can be fruitfully exploited in stroke: an anodic polarization can be used for opposing the ipsilesional inhibition, while a concurrent cathodic polarization can be exploited for toning down the excessive excitability of the contralesional hemisphere [118].
Moreover, the study reported in [114] suggested that, combining anodic tDCS with wrist robot-aided therapy, the increased excitability of the lesioned M1 still persists after therapy and, hence, the changes promoted by tDCS on the M1 excitability can co-exist with the motor learning associated to a repetitive motor training.

Therefore, the experimental study here presented (proposed by the Laboratory of Biomedical Robotics and Biomicrosystems, the Unit of Physical Medicine and Rehabilitation and the Unit of Neurology of the Università Campus Bio-Medico di Roma, and approved by the Ethical Committee of the University on June 2012) aims at evaluating the effects of robot-aided wrist training coupled with tDCS on chronic stroke patients. The hypothesis to test is if a training regimen over 6 weeks can lead to a significant improvement in motor functions.
In particular, the objective of this experimental study is twofold:

Eugenia Papaleo

1. To propose a novel strategy that can lead to long lasting improvements in motor function of stroke patients, i.e. tDCS coupled with robotic motor training;

2. To test if this strategy can be more effective than robotic training alone in promoting motor recovery.

The recovery of patients is assessed through widely accepted clinical scales, commonly employed parameters of cortical excitability and quantitative indicators of motor performance extracted by the multimodal interface.

Finally, no reported studies of tDCS have investigated physiological interactions with a highly controlled motor training. Therefore, this study represents an innovative approach to understand mechanisms and characteristics of an emerging stroke rehabilitation therapy.

6.2 Methodology

6.2.1 Study design

The experimental study, started in January 2013, is a 2-year, double-blind, randomized study in which a total number of 24 chronic stroke patients will be enrolled.

Patients are randomized into three groups; all groups receive wrist motor therapy with the InMotion3-Wrist robot (Section 6.2.3), but they can receive *real* or *sham* tDCS, according to the following randomization:

- Group A - Robotic training with InMotion3 and simultaneous tDCS *real*, followed by tDCS *sham*;
- Group B - Robotic training with InMotion3 and simultaneous tDCS *sham*, followed by tDCS *real*;
- Group C - Robotic training with InMotion3 and simultaneous tDCS *sham*, followed by tDCS *sham*.

Real tDCS is delivered at $1mA$ for $20'$, while *sham* tDCS is fictitiously delivered in three steps: $1mA$ for $30''$, $0mA$ for $19'$ and $1mA$ for $30''$.

Eugenia Papaleo

A graphical representation of the experimental protocol timetable is shown in Figure 6.1. After patient recruitment, according to the inclusion criteria described in Section 6.2.2, the evaluation phase is carried out three times (T_{00}, T_{01} and T_{02}), separated by one week, to ensure reliability and stability of measures. The evaluation phase consists of:

- Clinical measures,

- Robot-aided evaluation at InMotion2-Shoulder/Elbow robot (Section 6.2.3) and InMotion3-Wrist robot and computation of the performance indicators extracted by the developed multimodal interface (Chapter 3 - Section 3.1).

Then, 18 1-hour sessions of robotic therapy are administered to the patient three times a week, in alternate days.

Finally, the evaluation phase is repeated twice: at the end of the training phase (T_1) and after 6 months (T_2-follow up).

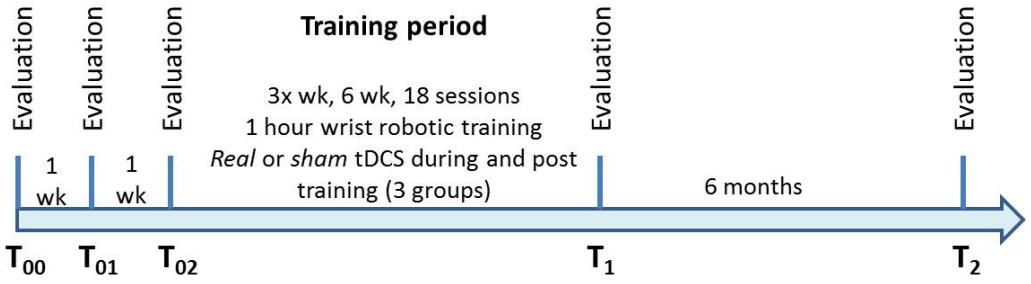

FIGURE 6.1: Graphical representation of the experimental protocol timetable; the evaluation and training phases are indicated

6.2.2 Participants

Patients are recruited from the Unit of Physical Medicine and Rehabilitation of the Università Campus Bio-Medico di Roma. Patients have to meet the following inclusion criteria:

- A first single focal unilateral lesion with diagnosis verified by brain imaging (MRI or CT scans), occurred at least 6 months prior;
- Cognitive functions sufficient to understand the experiment and follow instructions, i.e. Mini-Mental Status Examination (see below) of 22 or higher;

Eugenia Papaleo

- Fugl-Meyer assessment (see below) 7 to 36 out of 66 (neither hemiplegic nor fully recovered motor function in the muscles of the shoulder and elbow and wrist);
- Acceptance of the informed consent to participate in the study.

Patients are excluded from the study if they have:

- A fixed contraction deformity in the affected limb;
- A complete and total flaccid paralysis of all shoulder and elbow motor performance;
- A haemorrhagic stroke;
- Psychoactive medications, such as stimulants, antidepressants, and antipsychotic medications;
- Additional potential tDCS (or TMS - Transcranial Magnetic Stimulation) risk factors:
  - Damaged skin at the site of stimulation,
  - Presence of an electrically, magnetically or mechanically activated implant (including cardiac pacemaker),
  - Metal in any part of the body (jewels must be removed during stimulation),
  - A history of medication-resistant epilepsy in the family,
  - Past history of seizures or unexplained spells of loss of consciousness.

6.2.3 Robotic devices

The InMotion3-Wrist robot (Figure 6.2) and InMotion2-Shoulder/Elbow robot (Figure 6.3) (briefly InMotion robots) are FDA approved rehabilitation robotic devices designed to move patient wrist-forearm and shoulder-elbow, respectively. The patient seats in a foam-padded chair, grasping the robot handle and facing a video screen. During treatment, the patient, while attached to the robot handle, performs a series of point-to-point movements shown on the video screen: motion targets and a cursor tracking patient hand movement are displayed.
A single training session consists of different motor tasks during which the robot

Eugenia Papaleo

can either assist, guide or oppose patient motion, according to the planned treatment.

A key feature of the InMotion robots is the low, near isotropic inertia and the reduced friction; the force required to move the robotic arms, in fact, is minimal, compared to moving unrestricted.

The InMotion3-Wrist robot is conceived to train 3 upper-limb joint angles, i.e. pronation-supination of the forearm, ulnar-radial deviation of the hand and flexion-extension of the hand. In the study here presented, the Wrist robot is used in both the training phase and the evaluation phase.

The InMotion2-Shoulder/Elbow robot is conceived for proximal training, as it moves shoulder and elbow joints. In the study here presented, this robot is employed only in the evaluation phase for therapy outcome measures.

FIGURE 6.2: The InMotion3-Wrist robot

FIGURE 6.3: The InMotion2-Shoulder/Elbow robot

Eugenia Papaleo

6.2.4 Transcranial Direct Current Stimulation

tDCS is delivered through surface rubber-carbon electrodes (area: $35cm^2$), equipped with saline soaked sponges ($0.9\%NaCl$), by a battery driven constant current stimulator (BrainSTIM®- Figure 6.4). As anticipated, *real* tDCS consists of $20'$ stimulation, with the anode placed over the site for flexor carpi radialis and cathode on the contralateral motor area.

FIGURE 6.4: The BrainSTIM®system for tDCS delivering

6.3 Patient evaluation

6.3.1 Clinical evaluation

During the evaluation phase at T_{00}, patient medical history, personal and anthropometric data are registered.

The clinical evaluation includes:

1. The administration of clinical scales for the evaluation of motor impairment,
2. The applications of specific magnetic stimulation protocols for the assessment of excitability and plasticity of M1.

As regards point 1., the following clinical scales are administered by therapists:

- Mini-Mental Status Examination - It is a brief 30-point questionnaire used to screen for cognitive impairment;
- Fugl-Meyer Assessment Upper Extremity (FMA-UE) - It evaluates upper-limb motor impairment through five sub-scales (i.e. Motor, Balance, Sensation, Joint Range of Motion and Pain);

Eugenia Papaleo

- Motor Power scale (MP) - It evaluates tone and power of upper-limb muscles;
- Modified Ashworth scale - It assesses spasticity by feeling the resistance of the muscles to passive lengthening;
- Nine Hole Peg Test - It evaluates the fine manual dexterity.

Regarding point 2., specific TMS protocols are used by neurologists for the evaluation of the functional modifications in motor cortex. Stimulation is delivered through the Magstim 200 (from Magstim), while the position of the TMS coil is controlled by a neuronavigation system. At the same time, two types of electrical recordings are performed: (i) the EMG activity of hand muscles, (ii) a 32-channels electroencephalographic (EEG) recording, for the assessment of the modifications produced by TMS stimulations on cerebral activity [119].

The following neurological parameters are measured.

- Motor Evoked Potentials (MEP) - They are used to evaluate the basic ipsi- and contralesional excitability of M1 after a focal stimulation of the cortical area relative to hand motor control.
- Short Interval Cortical Inhibition (SICI) and Intracortical Facilitation (ICF) - They are used to evaluate intracortical inhibition and facilitation processes.

Finally, in order to evaluate motor cortex response to neuroplastic phenomena, the same neurological parameters are measured after conditioning the lesioned motor cortex through a repetitive stimulation protocol (rTMS) with facilitatory function.

6.3.2 Quantitative evaluation

The developed multimodal interface is re-adapted for carrying out a quantitative evaluation of the motor performance of the patients recruited in the experimental study.
To this purpose, different signals are acquired:

- Motion data from position sensors of InMotion robots - only data relative to unassisted (i.e. robot motors are switched off) clock games are considered;
- Upper arm radial accelerations from a MTx sensor (Xsens) placed on the patient arm - they are used for reconstructing the upper-limb kinematics as explained in Chapter 4;

Eugenia Papaleo

- Electromyographyc signals from two couples of antagonist muscles of the upper-limb:
  - Deltoid muscle and pectoral muscle - they are involved in shoulder extension and flexion, respectively,
  - Triceps muscle and biceps muscle - they are involved in elbow extension and flexion, respectively.

Synchronization between signals is obtained through a purposely generated square wave sent from the robot controller to both the EMG acquisition board and the acquisition software of the MTx sensor.

The system used for recording EMG signals is composed of (Figures 6.5):

1. Wire surface EMG electrodes - 12 electrodes are employed for *bipolar* acquisitions from the selected 4 muscles (each recording channel consists of 2 electrodes for differential acquisition and 1 electrode as neutral).
2. A workstation embedding the acquisition board and the Analogical Digital Converters (ADC) (one for each recording channel).
3. A software package (implemented in LabVIEW, National Instruments) that allows logging EMG data and realtime displaying them on a video screen.

Figure 6.6 shows a patient performing the robot-based evaluation tasks at InMotion2 robot; the sensory systems employed for the quantitative evaluation of motor performance are indicated.

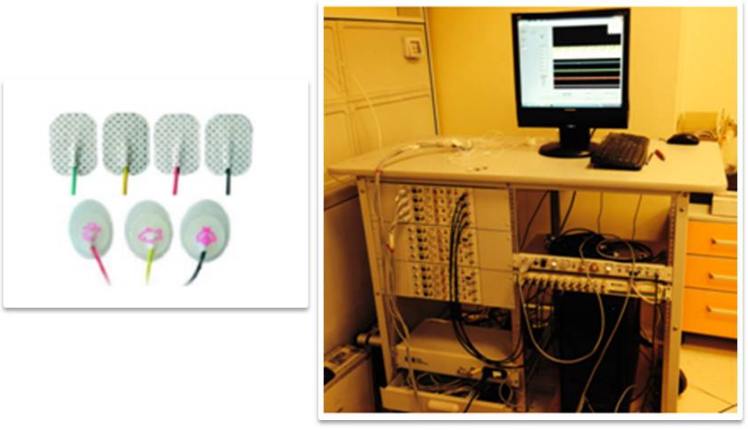

FIGURE 6.5: EMG recording system. Left: wire surface electrodes; right: the workstation embedding acquisition board and ADCs

Eugenia Papaleo

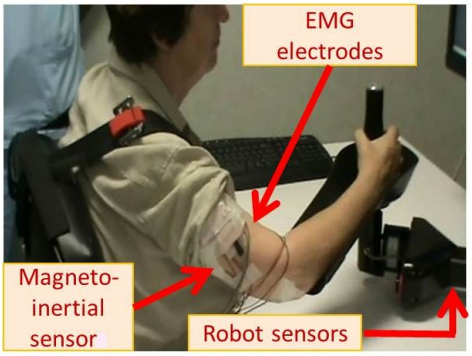

FIGURE 6.6: A patient enrolled in the experimental study performing evaluation tasks at InMotion2 robot; sensory systems are highlighted

Before extracting performance indicators from the recorded signals, the multimodal interface:

- Reconstructs shoulder and elbow joint angles exploiting hand position data provided by the InMotion2 robot (wrist angles are easily derived from InMotion3 robot sensors);
- Processes the acquired EMG data according to the processing procedure described in Chapter 3 - Section 3.1.1.3.

Once processed, data are ready for the extraction of the performance indicators listed in the following (note that, in this application, indicators are neither normalized with respect to their maximum nor adapted so that they all increase with recovery).
It is worth observing that at this stage several, and redundant, performance indicators have been extracted. In fact, one of the objectives of the proposed application is to test the correlation between the proposed performance indicators and the scores of the commonly employed clinical scales with the aim of selecting, among all, the most appropriate indicators for quantitatively evaluating patient recovery from the motor and the functional view points. Moreover, also the correlation with well-know functional scales, that, as explained in the following, are going to be added to the clinical evaluation, is of very importance.

- Kinematic indicators in the Cartesian space:
  - *aiming angle* (ϕ) - It is expected to decrease as movement direction improves during recovery;

Eugenia Papaleo

- *normalized Mean Deviation (nMD)* - As patient recovers, the deviation of his/her trajectory from the desired path is expected to decrease;
- *AREA* - The area between the desired and the actual trajectory performed by the patient is expected to decrease as movement accuracy increases with recovery;
- *Speed Metric (SM)* - As patient recovers, the normalized mean velocity increases due to the reduction of peaks and valleys in the velocity profile;
- *Mean Arrest Period Ratio (MAPR)* - The deep valleys (percentage of pauses during motion) in the velocity profile of patient hand are expected to reduce as movement smoothness improves with recovery;
- *Deviation from Ratio between Velocities (DRV)* - It is expected to reduce with recovery since patient velocity profile tends to the bell-shaped velocity profile of *minimum jerk* trajectory;
- *Success Rate (SR)* - As patient recovers, he/she learns to successfully complete the assigned motor tasks, so the success rate increases;
- *Movement Duration (MD)* - As patient recovers, movement duration decreases as a consequence of the augmented efficiency;
- *Path Length (PL)* - It is expected that during recovery the actual patient curve tends to the desired path and, hence, their ratio tends to one;
- *Manipulability Index* (w_1) - It it expected that the volume of the manipulability ellipsoid of the upper-limb increases as the global hand capacity of velocity generation improves.

- Kinematic indicators in the joint space:
  - *Inter-joint coordination* ($q_{corr_{i,j}}$) - It is expected to increase as the coordination between patient upper-limb joint angles improves. The following couples of adjacent joint angles are here considered:
    - shoulder abduction/adduction and elbow flexion/extension ($q_{corr_{1,4}}$),
    - shoulder flexion/extension and elbow flexion/extension ($q_{corr_{2,4}}$),
    - wrist abduction/adduction and wrist flexion/extension ($q_{corr_{6,7}}$).

- EMG indicators:
  - *Root Mean Square value (RMS)* - It is expected to increase with recovery since patient muscular force increases;
  - *Power Spectrum (PS)* - As patient recovers, his/her muscular power is expected to increase;

Eugenia Papaleo

- *Co-Contraction Index (CCI)* - As patient recovers, it is expected to decrease as the simultaneous activation of antagonist muscles crossing a joint reduces.
- *Median Frequency (MF)* - It is expected to increase with patient recovery as his/her muscular force and resistance to fatigue improve.
- *Fatigue index (FI)* - As patient recovers, his/her fatigue level grows more slowly, so fatigue index is expected to decrease.

It is opportune to clarify that, basing on previous experience in the use of dynamic indicators for unassisted tasks (Chapter 5 - Section 5.3.2), it has been chosen to limit dynamic indicators to resistive tasks.

6.3.3 Statistical analysis

Prior to study termination, demographic, clinical, kinematic, electromyographic and tDCS variables between *real* and *sham* groups will be compared, using *t-tests* and *chi-squared tests*, in order to evaluate if the proposed novel therapy strategy (i.e. tDCS+robot-aided therapy) can be more effective then robotic training alone in promoting upper-limb motor recovery.

Moreover, a statistical analysis based on repeated measures ANOVA will be carried out to assess the significance of the change in clinical scores and quantitative indicators from patients admission to discharge.

Finally, a correlation analysis between clinical scores and quantitative measures will be carried out in order to test the correlation between the performance indicators extracted by the multimodal interface and the clinical scales commonly employed in the clinical practice.

6.4 Preliminary results

The preliminary results reported in this Section are relative to the patients that have completed the training period and performed (at least) the evaluation phase at T_1. In particular, such patients are distributed among groups as follows:

- Group A: 3 patients, all men, mean age = 60.3 ± 4.1 years;
- Group C: 3 patients, 2 women and 1 man, mean age = 63.6 ± 5.8 years.

Eugenia Papaleo

In the following, the scores of the clinical scales and the performance indicators computed by the multimodal interface are reported for both the above-mentioned groups.

6.4.1 Clinical outcome measures

In this Sub-Section, the clinical scores relative to the administered Fugl-Meyer Assessment Upper Extremity (FMA-UE) and the Motor Power scale (MP) are reported.

Figure 6.7 report the mean scores of both the scales for patients of group A and C, before (T_{02}) and after (T_1) training administration. It can be noticed that the increase of clinical scores is higher in the group A (that receives 20′ of tDCS during wrist robotic training) than in the group C (no stimulation, neither during robotic therapy nor after), although the values of both the scales were already greater prior to therapy administration.

Figure 6.8 reports the details on the FMA-UE of all the patients of group A (top) and group C (bottom). The values in the tables are relative to the shoulder-elbow (SE) complex, the wrist-hand (WH) complex and the whole arm (*Total*); both the pre-training scores at T_{02} and the post-training scores at T_1 are reported.

On the other hand, the scores obtained through the administration of the MP scale are shown in Figure 6.9, for the group A (top) and group C (bottom). Data relative to the pre-training evaluation and the post-training evaluation are reported.

	FMA-UE		MP	
	T_{02}	T_1	T_{02}	T_1
Group A	28±6	35±8	45±8	48±6
Group C	17±3	19±2	40±8	43±9

FIGURE 6.7: Mean scores of pre-training and post-training FMA-UE and MP scale

Eugenia Papaleo

FMA-UE

Group A	SE T_{02}	WH T_{02}	*Total* T_{02}	SE T_1	WH T_1	*Total* T_1
Pat 1	17	10	27	25	17	42
Pat 2	19	4	23	22	5	27
Pat 3	19	15	34	21	16	37
Group C	**SE T_{02}**	**WH T_{02}**	***Total* T_{02}**	**SE T_1**	**WH T_1**	***Total* T_1**
Pat 1	18	1	19	19	1	20
Pat 2	10	4	14	11	5	16
Pat 3	1	8	19	12	8	20

FIGURE 6.8: Detailed scores of FMA-UE for all the recruited patients

MP scale

Group A	T_{02}	T_1
Pat 1	40	46
Pat 2	54	55
Pat 3	42	43
Group C	**T_{02}**	**T_1**
Pat 1	36	38
Pat 2	35	38
Pat 3	49	53

FIGURE 6.9: Detailed scores of MP scale for all the recruited patients

6.4.2 Quantitative evaluation

6.4.2.1 Data processing

In this Sub-Section, data relative to the processing procedure of the acquired signals, preparatory to the computation of the set of performance indicators, are reported.

Eugenia Papaleo

As regards kinematic data, Figure 6.10 shows the hand trajectories in the XY plane of one patient of the group A (top) and one patient of the group C (bottom) during the clock game with the InMotion2 robot. The reported data are provided by robot position sensors and refer to the pre-training evaluation at T_{02} (left) and the post-training evaluation at T_1 (right).

As it can be noticed, movement accuracy and smoothness increase with therapy more in the patient of the group A than in the patient of the group C.

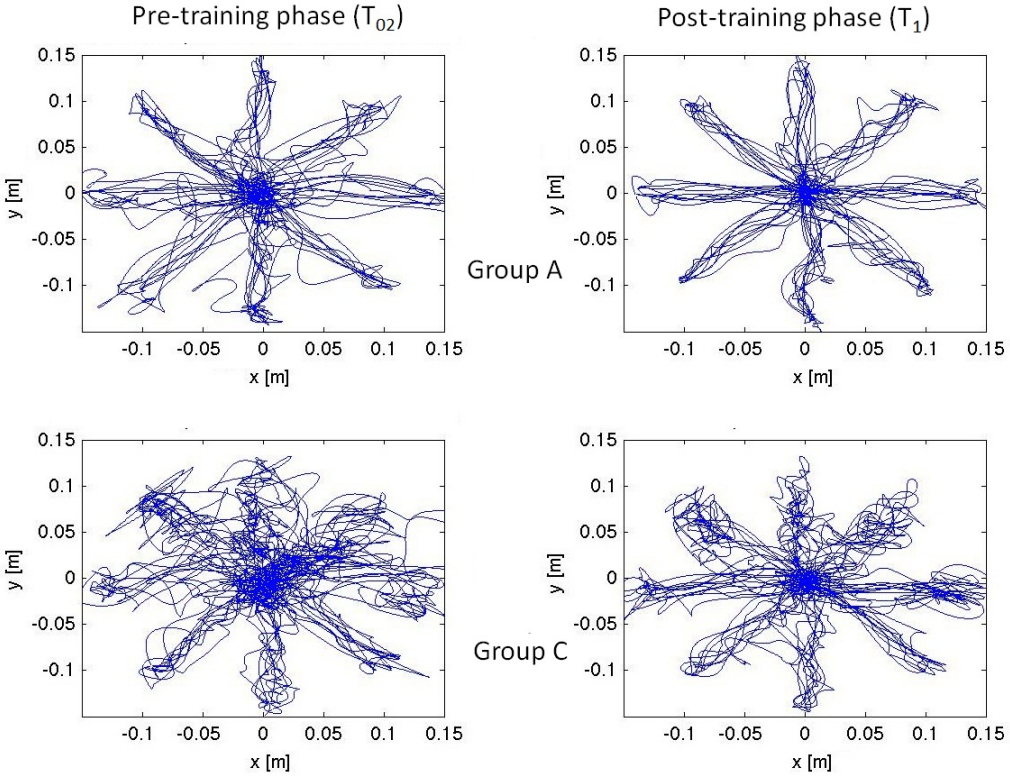

FIGURE 6.10: Hand trajectories of one patient of group A (top) and one patient of group C (bottom) during clock game. Left: pre-training evaluation; right: post-training evaluation

Referring to the same two patients and the same pre-training (T_{02}) and post-training (T_1) phases, the hand speed profiles, needed for the computation of some kinematic performance indicators (i.e. SM, MAPR, DRV), are shown in Figure 6.11.

For clarity of presentation, it has been chosen to report only the velocity profile averaged over five repetitions of one point-to-point movement; in particular, it has been considered the movement from the center of the clock game to 12 o'clock.

Both the components of the hand velocity in the XY plane (v_x and v_y) are reported; they are provided from the differential kinematics module of the InMotion2 robot.

Eugenia Papaleo

As it can be observed, the speed profile of the patient of the group A (top) is characterized by a very low number of pauses, indicating a good motion smoothness; conversely, the patient of the group C repeatedly stops during the point-to-point task.

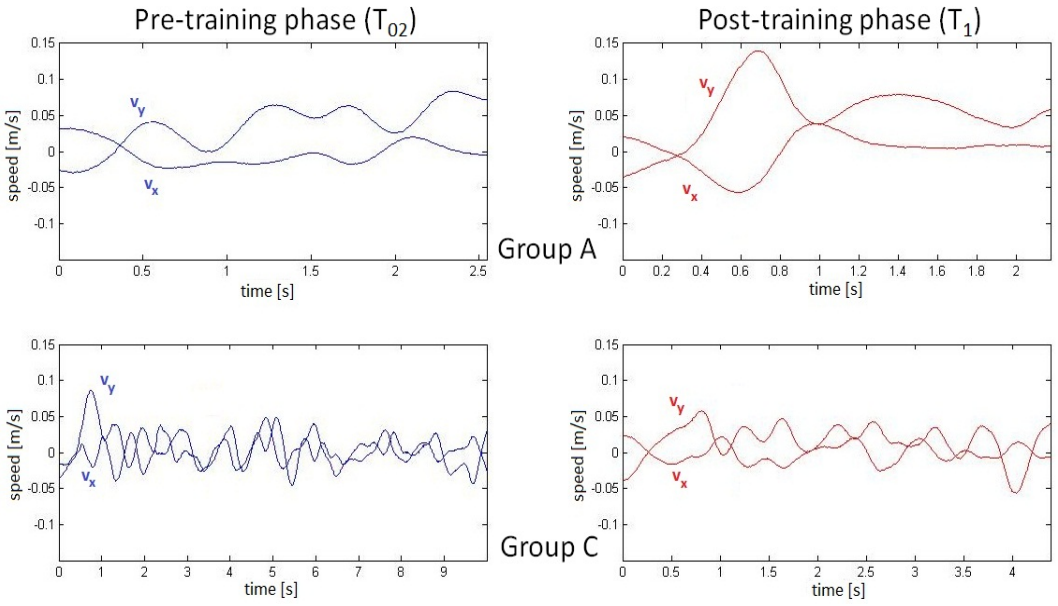

FIGURE 6.11: Hand velocity profiles, averaged over five repetitions of the point-to-point movement towards the target in North, of one patient of group A (top) and one patient of group C (bottom). Left: pre-training evaluation; right: post-training evaluation

As regards the reconstruction of the kinematics of patients' upper-limb, Figure 6.12 shows shoulder and elbow joint angles relative to the point-to-point motion. Data refer to the same two patients of previous Figures; joint angles of the pre-training evaluation phase at T_{02} (left) and the post-training evaluation phase at T_1 (right) are illustrated. In particular, as reported in Chapter 4, q_1 represents the shoulder abduction/adduction, q_2 is the shoulder flexion/extension, q_3 is the shoulder internal-external rotation and q_4 represents the elbow flexion/extension. Moreover, Figure 6.13 shows wrist joint angles provided by the InMotion3 robot during the point-to-point movement towards North executed in the pre-training evaluation (left) and the post-training evaluation (right) by the same two patients. In particular, q_5 represents the forearm pronation-supination, q_6 is the hand ulnar-radial deviation and q_7 is the hand flexion-extension.

As regards the processing of the electromyographic signals, Figures 6.14 and 6.15 show the EMG signals of one of the recruited patients (group A), acquired during a point-to-point task by the electrodes placed on pectoral muscle and triceps muscle, respectively. The Figures, besides the raw signal (blue line), report data

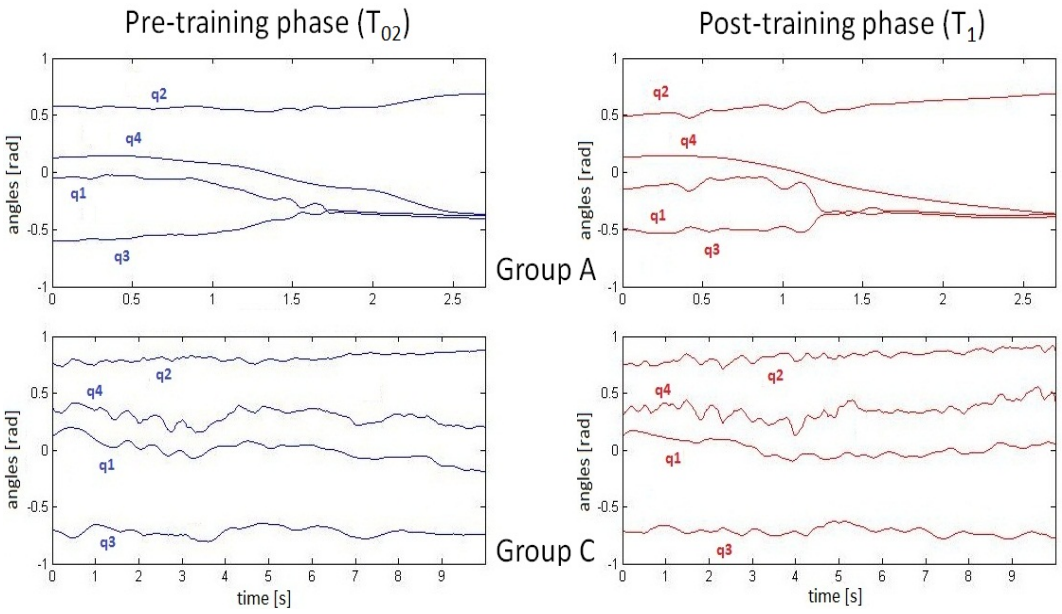

FIGURE 6.12: Reconstructed shoulder and elbow joint angles during a point-to-point movement towards the target in North. Data refer to one patient of group A (top) and one patient of group C (bottom). Left: pre-training evaluation; right: post-training evaluation

obtained through the processing procedure preliminary to the computation of the EMG indicators in the time domain (i.e. RMS, CCI), that is: the rectified signal (pink line), the signal obtained from the normalization on the Maximum Voluntary Contraction (red line), measured before task' execution as explained in Chapter 3-Section 3.1.1.3, and the signal envelope (black line) obtained through a low-pass filtering (cutoff frequency: $10Hz$ - Butterworth, 3rd order). Data relative to both the evaluation phase at T_{02} (top) and the evaluation phase at T_1 (bottom) are illustrated.
Figures show that, after treatment, the signal amplitude and the muscular activation augment, causing an increase of the RMS value (as reported in the following Sub-Section) and, hence, of muscular force and muscular power.

Finally, as stated in Chapter 3, the signal processing preliminary to the computation of EMG indicators in the frequency domain (i.e. MF, PS, FI) consists of the application of a band-pass Butterworth filter (cutoff frequencies:$10-500HZ$). The spectrum of pectoral and triceps EMG signals (shown in the previous Figures) are reported in Figures 6.16 and 6.17, respectively. The spectrum of the raw signal (blue line) and the spectrum of the filtered signal (black line) are illustrated.
Figures suggest that, after treatment, the signal energy content and, hence, the muscular power increase.

Eugenia Papaleo

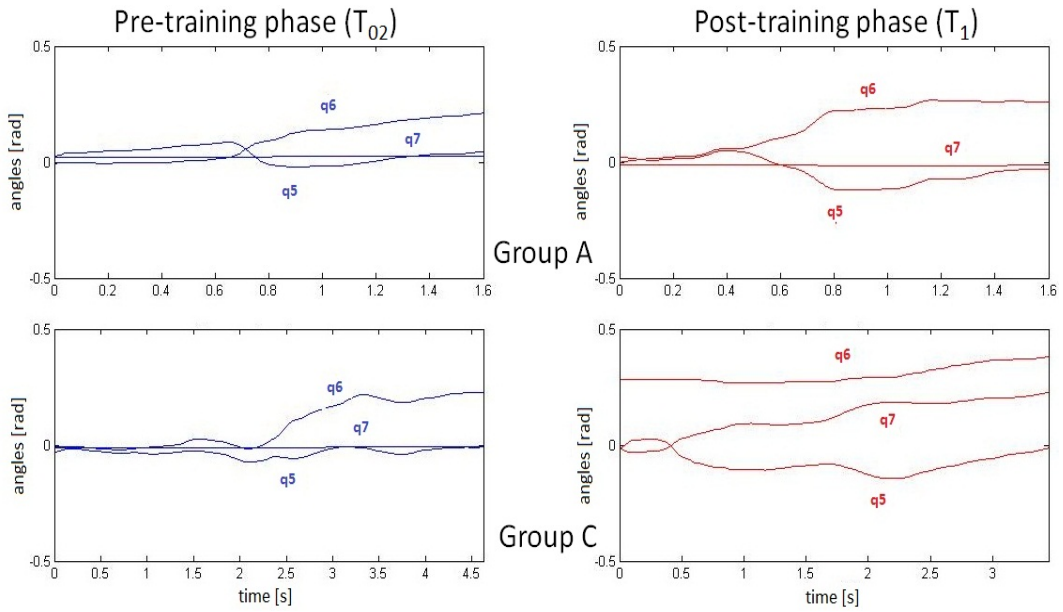

FIGURE 6.13: Wrist joint angles acquired by InMotion3 robot sensors during a point-to-point movement towards the target in North. Data refer to one patient of group A (top) and one patient of group C (bottom). Left: pre-training evaluation; right: post-training evaluation

6.4.2.2 Performance indicators

In this Sub-Section the performance indicators relative to the patients that have completed the experimental protocol are reported.

Figure 6.18 reports the mean values of the kinematic indicators in the Cartesian space computed from data provided by the InMotion2 robot; the table above is relative to the group A, while the table below refers to the group C. The second row of the tables indicates the expected trend of each indicator, i.e. if it is expected to increase (up-arrow) or decrease (down-arrow) with recovery. The values of the kinematic indicators relative to the evaluation phase at T_{02} and the evaluation phase at T_1 are reported.
It clearly emerges that in both the groups the kinematic indicators in the Cartesian space follow the expected trend; this indicates an improvement of patients' biomechanical performance due to the administered therapies. Moreover, it can be observed in general a greater increase of motor performance in the group A.

The mean values of the kinematic indicators in the joint space are reported in Figure 6.19; the first two columns of indicators are computed after reconstructing shoulder and elbow joint angles through the method proposed in Chapter 4, while

Eugenia Papaleo

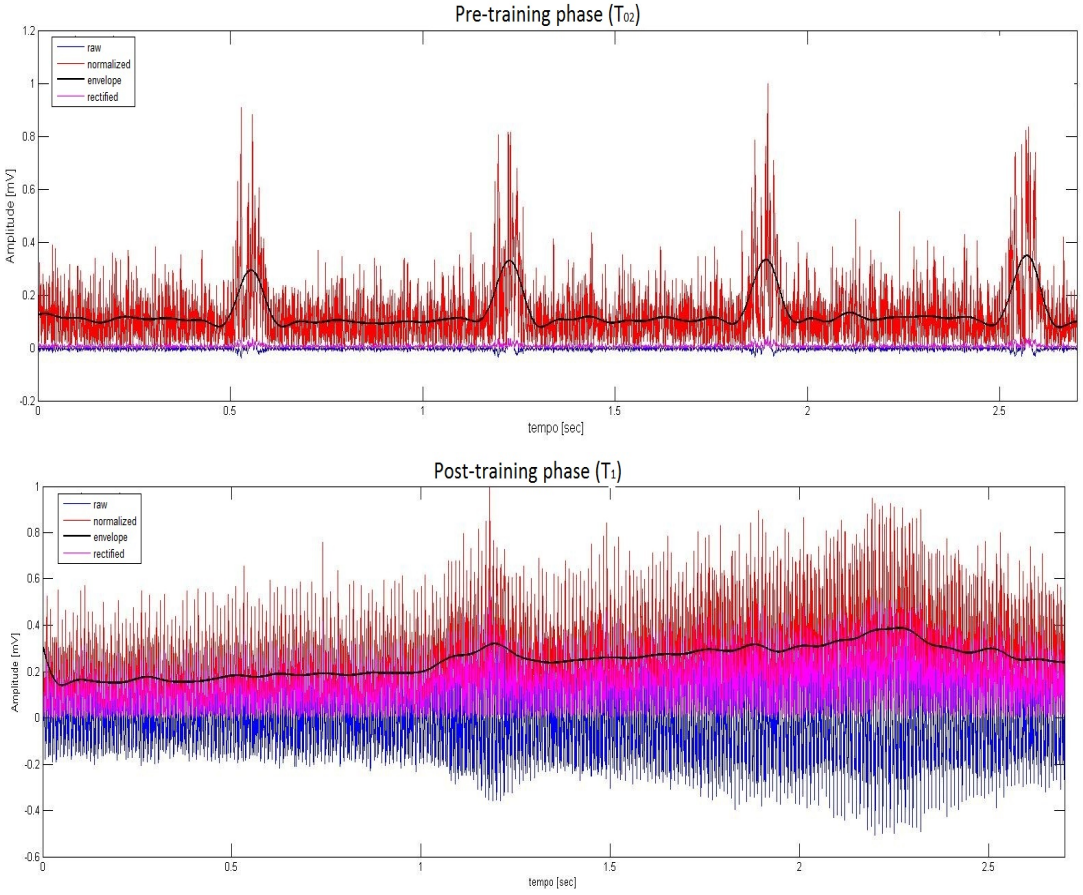

FIGURE 6.14: Processing of pectoral EMG signal: raw signal (blue line), rectified signal (pink line), signal normalized on the MVC (red line), signal envelope (black line). Data refer to a point-to-point movement towards the target in North performed by one of the recruited patients (group A). Top: pre-training evaluation; bottom: post-training evaluation

the indicators in the third column are computed from the wrist joint angles acquired by the InMotion3 robot position sensors.
However, all the kinematic indicators in the joint space show an improvement of the upper-limb inter-joint coordination as a consequence of the administered treatments in both groups. As before, motor improvement is higher in the group A than in the group C.

Finally, the mean electromyographic indicators are shown in Figure 6.20; they are computed after processing the EMG signals. The EMG indicators follow the expected trend in both the groups and, in particular, patients of the group A improve muscular features more than patients of the group C.

The analysis of all the computed performance indicators clearly suggests two key points that need to be confirmed through the analysis of a more rich number of

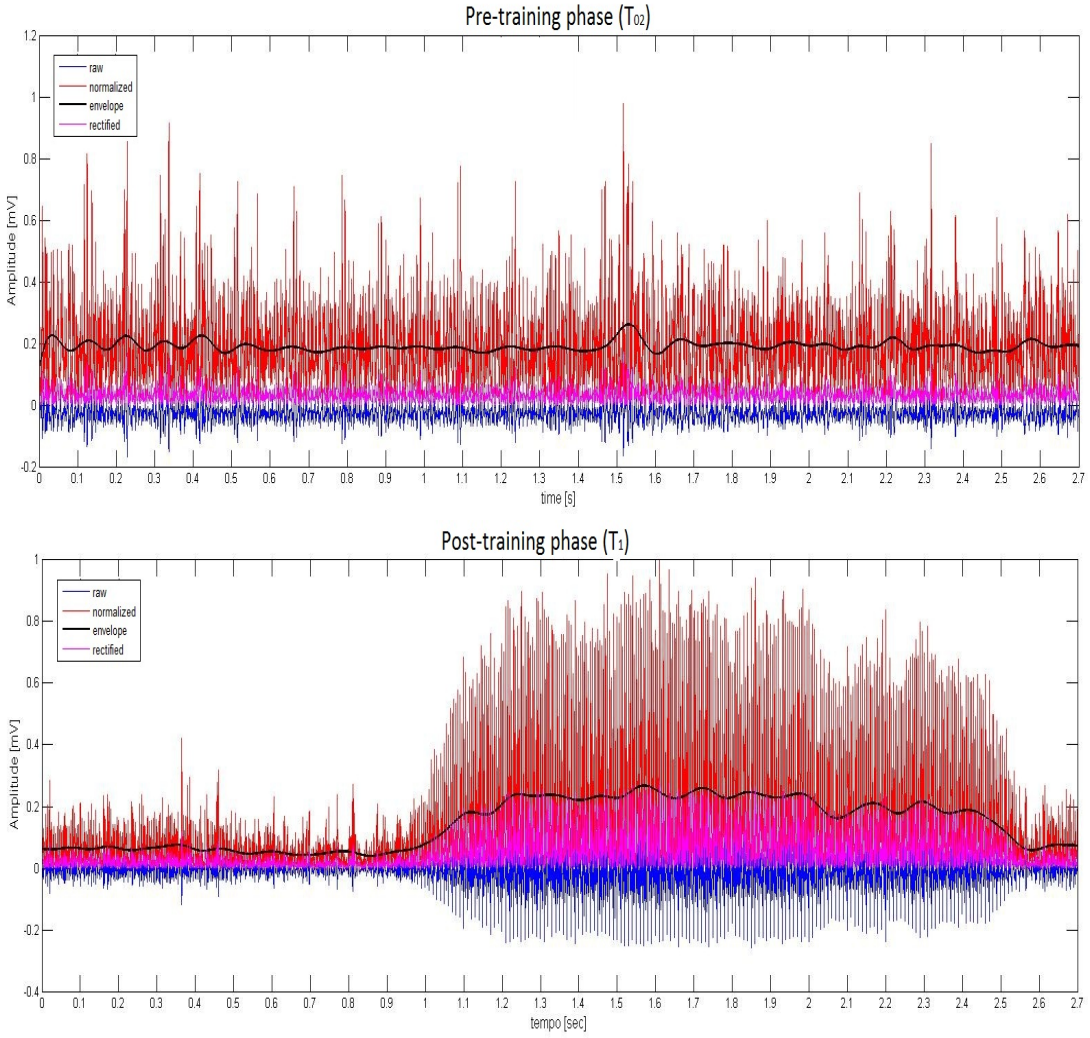

FIGURE 6.15: Processing of triceps EMG signal: raw signal (blue line), rectified signal (pink line), signal normalized on the MVC (red line), signal envelope (black line). Data refer to a point-to-point movement towards the target in North performed by one of the recruited patients (group A). Top: pre-training evaluation; bottom: post-training evaluation

patients:

1. The performance indicators follow the expected trends where patient motor impairment reduces (as confirmed by clinical scales);
2. The improvements of biomechanical and EMG indicators are higher in the patients that receive 20′ of tDCS during wrist robotic therapy.

The first point is in line with one of the objectives of the application of the multimodal interface in the experimental study, i.e.: to test the correlation between the performance indicators and the scores of the commonly employed clinical scales.

Eugenia Papaleo

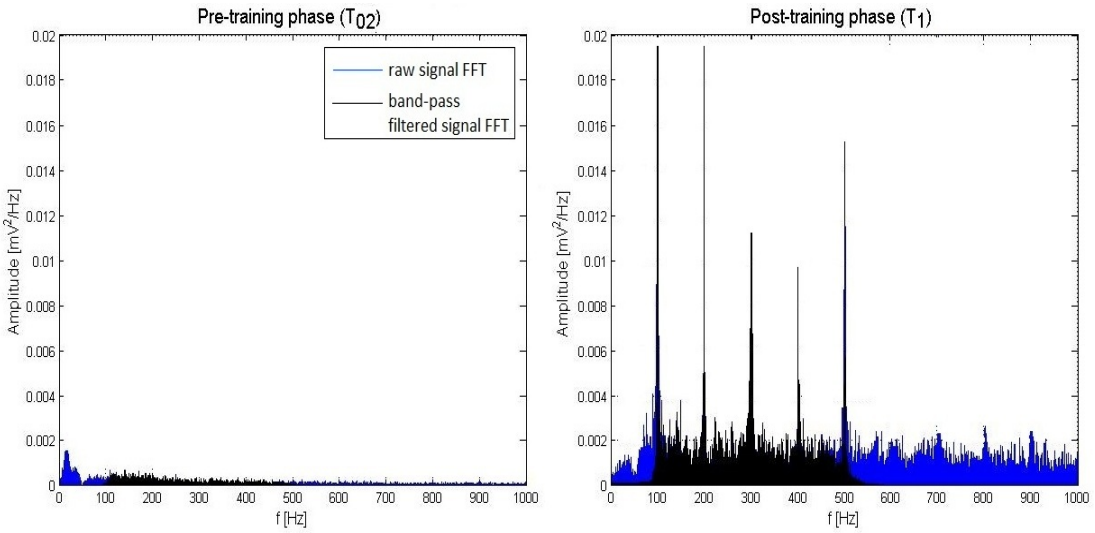

FIGURE 6.16: Spectrum of the pectoral EMG signal of Figure 6.14: raw signal (blue line), band-pass filtered signal (black line). Left: pre-training evaluation; right: post-training evaluation

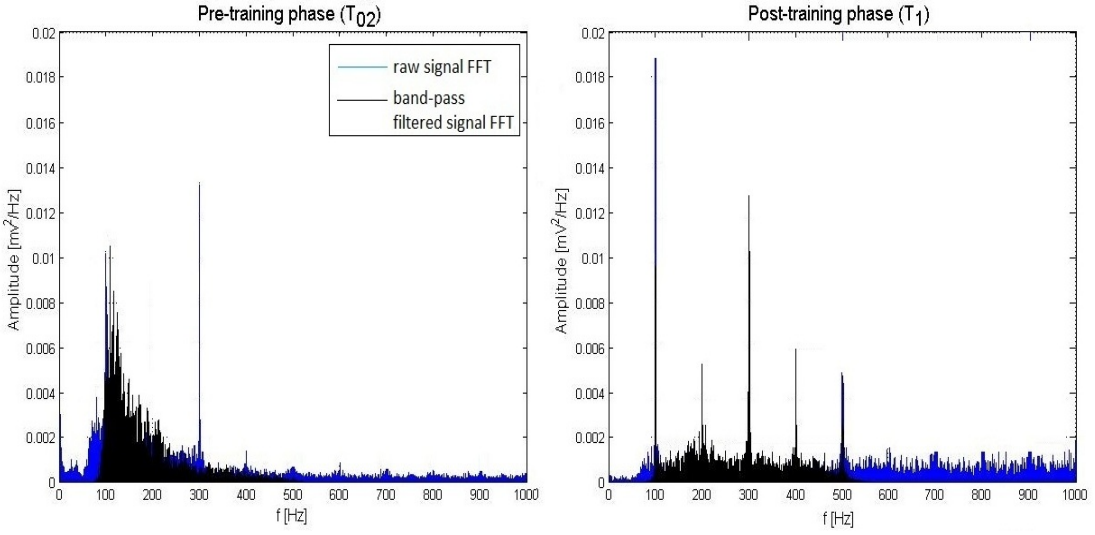

FIGURE 6.17: Spectrum of the triceps EMG signal of Figure 6.15: raw signal (blue line), band-pass filtered signal (black line). Left: pre-training evaluation; right: post-training evaluation

The second point, instead, is in line with one of the aims of the experimental study: to test if the proposed therapy strategy (tDCS coupled with wrist robotic training) can be more effective than robotic training alone in promoting motor recovery. As shown, this second result is confirmed also by clinical scores.

However, a correlation analysis between the computed set of performance indicators and the obtained clinical scores cannot be applied in the current status due to the very small number of patients that have completed the experimental protocol.

Eugenia Papaleo

Group A	ϕ	nMD	AREA [m^2]	SM	MAPR	DRV	SR	MD [s]	PL	w_1
Expected trend	↓	↓	↓	↑	↓	↓	↑	↓	↓	↑
T_{02}	0.16 ±0.02	0.44 ±0.05	0.1±0.02	0.46 ±0.02	0.08 ±0.02	0.5 ±0.09	0.98 ±0.01	3.06 ±0.4	0.73 ±0.09	0.034 ±0.007
T_1	0.13 ±0.03	0.39 ±0.07	0.07±0.01	0.49 ±0.03	0.06 ±0.01	0.42 ±0.08	1±0	2.48 ±0.2	0.78 ±0.09	0.035 ±0.006
Group C	ϕ	nMD	AREA [m^2]	SM	MAPR	DRV	SR	MD [s]	PL	w_1
Expected trend	↓	↓	↓	↑	↓	↓	↑	↓	↓	↑
T_{02}	0.5 ±0.2	0.56 ±0.09	0.7±0.5	0.4 ±0.1	0.19 ±0.15	1.9 ±1.5	0.5 ±0.3	6±1	0.4 ±0.2	0.028 ±0.003
T_1	0.4 ±0.2	0.5 ±0.1	0.5±0.4	0.4 ±0.1	0.18 ±0.2	1.8 ±1.5	0.6 ±0.4	5.0±1.7	0.58 ±0.08	0.029 ±0.002

FIGURE 6.18: Mean and standard deviation of the kinematic indicators in the Cartesian space

Current efforts are addressed to the introduction of functional scales (in addition to the motor scales) with the aim of identifying performance indicators that could be potentially employed for providing a quantitative evaluation of the patient also from the functional point of view.

Finally, differently from what the clinical scores on shoulder and elbow indicate (see Figure 6.8), the kinematic indicators in the Cartesian space show a limited improvement of all the enrolled patients in the execution of tasks at InMotion2 robot. However, it is plausible that patients, accustomed (because of the training) to execute tasks with the wrist robot, when evaluated at the InMotion2 Shoulder/Elbow robot cannot fully express their abilities.
For this reason, it is currently under evaluation the idea of extending the training protocol also to the InMotion2 robot.

Eugenia Papaleo

Group A	$q_{corr1,4}$	$q_{corr2,4}$	$q_{corr6,7}$
Expected trend	↑	↑	↑
T_{02}	0.78±0.03	0.67±0.04	0.53±0.04
T_1	0.81±0.01	0.70±0.01	0.75±0.02

Group C	$q_{corr1,4}$	$q_{corr2,4}$	$q_{corr6,7}$
Expected trend	↑	↑	↑
T_{02}	0.72±0.03	0.53±0.2	0.6±0.1
T_1	0.80±0.04	0.67±0.04	0.7±0.1

FIGURE 6.19: Mean and standard deviation of the kinematic indicators in the joint space

Group A	RMS [V]	PS [mV^2/Hz]	CCI	MF [Hz]	FI [Hz/s]
Expected trend	↑	↑	↓	↑	↓
T_{02}	0.7±0.5	$(1.4\pm0.2)\cdot10^{-6}$	0.7±0.4	196±27	-0.07±0.05
T_1	3±1	$(4\pm2)\cdot10^{-5}$	0.4±0.3	247±9	-0.09±0.07

Group C	RMS [V]	PS [mV^2/Hz]	CCI	MF [Hz]	FI [Hz/s]
Expected trend	↑	↑	↓	↑	↓
T_{02}	0.5±0.2	$(7\pm3)\cdot10^{-7}$	0.4±0.2	231±18	0.06±0.01
T_1	0.6±0.2	$(2\pm1)\cdot10^{-5}$	0.4±0.3	238±27	-0.14±0.09

FIGURE 6.20: Mean and standard deviation of the EMG indicators

Eugenia Papaleo

Chapter 7

Conclusions

The employment of bio-cooperative control systems for the administration of robot-aided therapy to stroke patients represents a real breakthrough and the interest in this field is continuously growing. Such systems place the patient in the control loop, by feeding back his/her biomechanical and physiological state, and adapt therapy characteristics to patient needs; in this way, the patient is motivated in an engaging and challenging way and a faster learning and recovery time can be obtained.

This dissertation thesis presents the design and the development of a bio-cooperative system for upper-limb robot-aided therapy, consisting of two main modules:

- A multimodal interface, able to evaluate patient performance and realtime display a virtual reality environment relative to the execution of the assigned task,
- An adaptive robot control system, able to modulate the complexity of the assigned motor task, allowing the administration of a patient-tailored therapy.

A special attention has been paid to the development of an unobtrusive system for delivering motor therapy without altering user natural motion.
Both modules of the developed system have been presented in Chapter 3. The functional architecture of the multimodal interface has been illustrated and the methods for motion, force and electromyographic data acquisition and processing as well as for the extraction of performance indicators have been described. Moreover, the modulation functions for updating control parameters and the implemented virtual reality software have been discussed. Finally, the adaptive robot

Eugenia Papaleo

control system has been illustrated.

In order to deal with the lack of knowledge on human joint motion when end-effector robots are employed in the proposed bio-cooperative system, a method for reconstructing the entire upper-limb kinematics has been presented and experimentally validated in Chapter 4. It is grounded on an analytical procedure of inverse kinematics borrowed from the robotic domain and based on an Augmented Jacobian matrix. For the computation of an additional constraint needed to solve the redundant arm inverse kinematics, the coupled use of the rehabilitation robot with an accelerometer is proposed in order to record hand pose data, with the robot, and radial acceleration of the upper arm segment, with the wearable sensor.
The experimental validation of the algorithm, aimed at measuring its accuracy and testing its applicability to robot-aided rehabilitation, has been carried out.

- As regards method accuracy, the algorithm has revealed good results in reconstructing all the arm angles with a RMSE error of $8.3 * 10^{-3} rad$ (and variance of $1.8 * 10^{-3} rad$) with respect to the measures performed with a commercial optoelectronic motion capturing system.
- As regards the application to robot-aided rehabilitation, four healthy subjects and two patients have been evaluated and the reported plots have shown a clear difference between healthy and pathological behaviour, i.e.: when patients are not able to fulfill a correct motion in the Cartesian space, the joint angles are clearly far from "healthy bands".

Two applications of the developed bio-cooperative system for upper-limb robot-aided therapy have been proposed:

1. A robotic system for 3D upper-limb rehabilitation (Chapter 5),
2. The quantitative evaluation of the outcomes of a clinical study on chronic stroke patients (Chapter 6).

As regards the first application, the system, grounded on the multimodal interface and on the adaptive control approach, is able to update therapy characteristics according to patient needs and performance. The presented system employs an industrial 7-DoF robot arm and a purposely developed mounting flange to connect subject wrist with robot end-effector. During robot-aided motor tasks, the system acquires patient biomechanical data, computes performance indicators, evaluates

Eugenia Papaleo

patient biomechanical state and adjusts robot control parameters for modifying task complexity in the 3D space.
The results of the experimental validation carried out on healthy subjects, although preliminary, are very encouraging as they show:

- the capability of the multimodal interface to correctly online evaluate subject behaviour,
- the validity of the controller to online adapt to subject biomechanical features in a safe way, thus driving him/her towards the target, with a level of assistance that is tuned on his/her motor abilities.

Although the experimental validation has been shown for point-to-point motion in 2D and 3D space, the approach has the further benefit of being easily extended to functional training, through the execution of activities of daily living (ADLs).
Future activities will be addressed to:

1. Perform an experimental validation on post-stroke patients;
2. Define continuous functions (instead of discrete levels) for modulating robot control parameters;
3. Extend the multimodality of the platform by:
   - acquiring also upper-limb electromyographic signals, thus computing EMG indicators on muscle force, muscle power and muscle fatigue,
   - selecting further physiological signals apt to quantitatively assess the subject physiological/psycho-physiological state,
   - introducing acoustic feed-back and motivational rewards for the patient;
4. Execute also ADL tasks.

Regarding the second application, the developed multimodal interface has been re-adapted and employed for the quantitative evaluation of the motor performance of chronic stroke patients undergoing a novel experimental protocol at Università Campus Bio-Medico di Roma. The protocol aims at assessing if tDCS coupled with wrist robotic training can be more effective than robot-aided therapy alone in promoting motor recovery.
The objective of this application of the multimodal interface is twofold: (i) adding to the clinical evaluation of the patients the quantitative evaluation of their motor performance, (ii) testing the correlation between the performance indicators extracted by the multimodal interface and the clinical scales commonly employed in the clinical practice.
The analysis of the performance indicators and of the clinical scores obtained in the pre- and post-training evaluation phases suggests:

Eugenia Papaleo

- The efficacy of joining tDCS to robotic training - clinical scores and performance indicators mainly increase in patients that receive tDCS during robotic therapy;
- The possibility to fruitfully employ the set of computed indicators together with the clinical evaluation in order to obtain an exhaustive picture of the patient recovery level;
- The existence of a correlation between changes (pre-training versus post-training) in performance indicators and in clinical scores; this needs to be further confirmed through the analysis of a greater number of patients.

However, a correlation analysis between the computed set of performance indicators and the obtained clinical scores cannot be applied in the current status due to the very small number of patients that have completed the experimental protocol. Future developments of this application will be obtained through the enrollment of new patients in the study and through the additional administration of functional scales during the clinical evaluation. This will allow, on the one hand, strengthening the preliminary results on the efficacy of the novel rehabilitation treatment (tDCS+wrist robotic therapy) and fulfilling the statistical analysis mentioned in Chapter 6 - Section 6.3.3, and, on the other hand, carrying out a structured analysis of the correlation between the performance indicators, extracted by the multimodal interface, and the clinical evaluations in order to identify those indicators that can provide a quantitative evaluation of the patient from the motor and/or the functional points of view.
Finally, it is currently under evaluation the idea of extending the training protocol also to the InMotion2 robot.

Eugenia Papaleo

List of Publications

Published

Peer-reviewed International Conferences

Papaleo, E., Zollo, L., Sterzi, S., Guglielmelli, E. (2012, June). An inverse kinematics algorithm for upper-limb joint reconstruction during robot-aided motor therapy. In Biomedical Robotics and Biomechatronics (BioRob), 2012 4th IEEE/RAS-EMBS International Conference on, pp. 1983-1988.

Papaleo, E., Zollo, L., Guglielmelli, E (2012, June). Upper-limb Motion Reconstruction for Robot-aided Therapy Applications. In Terzo Congresso del Gruppo Nazionale di Bioingegneria (GNB), 2012, June 26th-29th, Rome, Italy.

Papaleo, E., Zollo, L., Spedaliere, L., Guglielmelli, E. (2013, May). Patient-tailored adaptive robotic system for upper-limb rehabilitation. In Robotics and Automation (ICRA), 2013 IEEE International Conference on, pp. 3860-3865.

Peer-reviewed International Journals

Badesa, F.J., Morales, R., Garcia-Aracil, N., Sabater, J.M., Zollo, L., Papaleo, E., Guglielmelli, E. (2014). Dynamic Adaptive System for Robot-Assisted Motion Rehabilitation. IEEE SYSTEMS JOURNAL.

Book chapters

Zollo, L., Papaleo, E., Spedaliere, L., Guglielmelli, E., Badesa, F. J., Morales, R., Garcia-Aracil, N. (2014). Multimodal Interfaces to Improve Therapeutic Outcomes in Robot-Assisted Rehabilitation. In Gearing up and accelerating cross-fertilization between academic and industrial robotics research in Europe: pp. 321-343. Springer International Publishing.

Eugenia Papaleo

Accepted

International journals

Badesa, F.J., Morales, R., Garcia-Aracil, N., Perez, C., Sabater, J.M., Papaleo, E., Salerno, A., Zollo, L., Guglielmelli, E. (2014). New concept of Multimodal Assistive Robotic Device. Robotics and Automation Magazine, IEEE. In press.

Papaleo, E., Zollo, L., Garcia-Aracil, N., Badesa, F.J., Morales, R., Sterzi, S., Guglielmelli, E. (2014). Reconstruction of the upper-limb kinematics during robot-aided therapy of stroke patients. Medical and Biology Engineering and Computing, Springer. 2nd revision.

Eugenia Papaleo

Bibliography

[1] Alan S Go, Dariush Mozaffarian, Veronique L Roger, Emelia J Benjamin, Jarett D Berry, William B Borden, Dawn M Bravata, Shifan Dai, Earl S Ford, Caroline S Fox, et al. Heart disease and stroke statistics-2013 update a report from the american heart association. *Circulation*, 127(1):e6–e245, 2013.

[2] Peter Langhorne, Julie Bernhardt, and Gert Kwakkel. Stroke rehabilitation. *The Lancet*, 377(9778):1693–1702, 2011.

[3] Robert M Herndon. *Handbook of neurologic rating scales*. Demos Medical Publishing, 2006.

[4] Rui CV Loureiro, William S Harwin, Kiyoshi Nagai, and Michelle Johnson. Advances in upper limb stroke rehabilitation: a technology push. *Medical & biological engineering & computing*, 49(10):1103–1118, 2011.

[5] Robert Riener and Marko Munih. Guest editorial special section on rehabilitation via bio-cooperative control. *Neural Systems and Rehabilitation Engineering, IEEE Transactions on*, 18(4):337–338, 2010.

[6] Noraxon INC. USA. *The ABC of EMG*, 1.0d edition, april 2005.

[7] John V Basmajian and CJ De Luca. Muscles alive. *PROCEEDINGS OF THE ROYAL SOCIETY OF MEDICINE*, 278:126, 1985.

[8] George Rab, Kyria Petuskey, and Anita Bagley. A method for determination of upper extremity kinematics. *Gait & posture*, 15(2):113–119, 2002.

[9] HF Machiel Van der Loos and Navid Shirzad. Therapy robotics: The power of the interface to motivate.

[10] A.L.I.Ce. Italia onlus, associazione per la lotta all'ictus cerebrale. [Online; accessed December-2013].

Eugenia Papaleo

[11] Margaret Kelly-Hayes, Alexa Beiser, Carlos S Kase, Amy Scaramucci, Ralph B D'Agostino, and Philip A Wolf. The influence of gender and age on disability following ischemic stroke: the framingham study. *Journal of Stroke and Cerebrovascular Diseases*, 12(3):119–126, 2003.

[12] Donald Lloyd-Jones, Robert Adams, Mercedes Carnethon, Giovanni De Simone, T Bruce Ferguson, Katherine Flegal, Earl Ford, Karen Furie, Alan Go, Kurt Greenlund, et al. Heart disease and stroke statistics—2009 update a report from the american heart association statistics committee and stroke statistics subcommittee. *Circulation*, 119(3):480–486, 2009.

[13] Edzard Ernst. A review of stroke rehabilitation and physiotherapy. *Stroke*, 21(7):1081–1085, 1990.

[14] Naoyuki Takeuchi and Shin-Ichi Izumi. Rehabilitation with poststroke motor recovery: A review with a focus on neural plasticity. *Stroke research and treatment*, 2013, 2013.

[15] Michael A Dimyan and Leonardo G Cohen. Neuroplasticity in the context of motor rehabilitation after stroke. *Nature Reviews Neurology*, 7(2):76–85, 2011.

[16] Numa Dancause, Scott Barbay, Shawn B Frost, Erik J Plautz, Daofen Chen, Elena V Zoubina, Ann M Stowe, and Randolph J Nudo. Extensive cortical rewiring after brain injury. *The Journal of neuroscience*, 25(44):10167–10179, 2005.

[17] Erik J Plautz, Garrett W Milliken, and Randolph J Nudo. Effects of repetitive motor training on movement representations in adult squirrel monkeys: role of use versus learning. *Neurobiology of learning and memory*, 74(1):27–55, 2000.

[18] Graeme J Hankey, Konrad Jamrozik, Robyn J Broadhurst, Susanne Forbes, and Craig S Anderson. Long-term disability after first-ever stroke and related prognostic factors in the perth community stroke study, 1989–1990. *Stroke*, 33(4):1034–1040, 2002.

[19] Steven L Wolf, Sarah Blanton, Heather Baer, Jenifer Breshears, and Andrew J Butler. Repetitive task practice: a critical review of constraint-induced movement therapy in stroke. *The neurologist*, 8(6):325, 2002.

[20] RD Zorowitz, E Gross, and DM Polinski. The stroke survivor. *Disability & Rehabilitation*, 24(13):666–679, 2002.

Eugenia Papaleo

[21] Stephen J Page, SueAnn Sisto, Peter Levine, and Robert E McGrath. Efficacy of modified constraint-induced movement therapy in chronic stroke: a single-blinded randomized controlled trial. *Archives of physical medicine and rehabilitation*, 85(1):14–18, 2004.

[22] Marcy L Freed, Leonard Freed, Robert L Chatburn, and Michael Christian. Electrical stimulation for swallowing disorders caused by stroke. *Respiratory Care*, 46(5):466–474, 2001.

[23] J-P Lefaucheur. Stroke recovery can be enhanced by using repetitive transcranial magnetic stimulation (rtms). *Neurophysiologie Clinique/Clinical Neurophysiology*, 36(3):105–115, 2006.

[24] Friedhelm C Hummel and Leonardo G Cohen. Non-invasive brain stimulation: a new strategy to improve neurorehabilitation after stroke? *The Lancet Neurology*, 5(8):708–712, 2006.

[25] Nikhil Sharma, Valerie M Pomeroy, and Jean-Claude Baron. Motor imagery a backdoor to the motor system after stroke? *Stroke*, 37(7):1941–1952, 2006.

[26] Peter Lum, David Reinkensmeyer, Richard Mahoney, William Z Rymer, Charles Burgar, et al. Robotic devices for movement therapy after stroke: current status and challenges to clinical acceptance. *Topics in stroke rehabilitation*, 8(4):40–53, 2002.

[27] John Young and Anne Forster. Review of stroke rehabilitation. *BMJ: British Medical Journal*, 334(7584):86, 2007.

[28] NHS Choices. National stroke strategy. 2011.

[29] Louisa-Jane Burton, Sarah Tyson, and Alison McGovern. Staff perceptions of using outcome measures in stroke rehabilitation. *Disability and Rehabilitation*, 35(10):828–834, 2013.

[30] Gerd Kempermann, Henriette van Praag, and Fred H Gage. Activity-dependent regulation of neuronal plasticity and self repair. *Progress in brain research*, 127:35–48, 2000.

[31] Elaine L Miller, Laura Murray, Lorie Richards, Richard D Zorowitz, Tamilyn Bakas, Patricia Clark, Sandra A Billinger, et al. Comprehensive overview of nursing and interdisciplinary rehabilitation care of the stroke patient a scientific statement from the american heart association. *Stroke*, 41(10):2402–2448, 2010.

Eugenia Papaleo

[32] Albert C Lo, Peter D Guarino, Lorie G Richards, Jodie K Haselkorn, George F Wittenberg, Daniel G Federman, Robert J Ringer, Todd H Wagner, Hermano I Krebs, Bruce T Volpe, et al. Robot-assisted therapy for long-term upper-limb impairment after stroke. *New England Journal of Medicine*, 362(19):1772–1783, 2010.

[33] Gert Kwakkel, Boudewijn J Kollen, and Hermano I Krebs. Effects of robot-assisted therapy on upper limb recovery after stroke: a systematic review. *Neurorehabilitation and neural repair*, 22(2):111–121, 2008.

[34] Bruce T Volpe, Patricio T Huerta, Johanna L Zipse, Avrielle Rykman, Dylan Edwards, Laura Dipietro, Neville Hogan, and Hermano I Krebs. Robotic devices as therapeutic and diagnostic tools for stroke recovery. *Archives of neurology*, 66(9):1086, 2009.

[35] Sivakumar Balasubramanian, Roberto Colombo, Irma Sterpi, Vittorio Sanguineti, and Etienne Burdet. Robotic assessment of upper limb motor function after stroke. *American Journal of Physical Medicine & Rehabilitation*, 91(11):S255–S269, 2012.

[36] Gerdienke B Prange, Michiel JA Jannink, Catharina GM Groothuis-Oudshoorn, Hermie J Hermens, and Maarten J IJzerman. Systematic review of the effect of robot-aided therapy on recovery of the hemiparetic arm after stroke. *Journal of rehabilitation research and development*, 43(2):171, 2006.

[37] Nahid Norouzi-Gheidari, Philippe S Archambault, and Joyce Fung. Effects of robot-assisted therapy on stroke rehabilitation in upper limbs: Systematic review and meta-analysis of the literature. *J. Rehabil. Res. Dev*, 49:479–496, 2012.

[38] William S Harwin, James L Patton, and V Reggie Edgerton. Challenges and opportunities for robot-mediated neurorehabilitation. *Proceedings of the IEEE*, 94(9):1717–1726, 2006.

[39] Eugenio Guglielmelli, Michelle J Johnson, and Takahori Shibata. Guest editorial special issue on rehabilitation robotics. *Robotics, IEEE Transactions on*, 25(3):477–480, 2009.

[40] Neville Hogan, Hermano Igo Krebs, J Charnnarong, P Srikrishna, and Andre Sharon. Mit-manus: a workstation for manual therapy and training. i. In *Robot and Human Communication, 1992. Proceedings., IEEE International Workshop on*, pages 161–165. IEEE, 1992.

Eugenia Papaleo

[41] Maura Casadio, Vittorio Sanguineti, Pietro G Morasso, and Vincenzo Arrichiello. Braccio di ferro: a new haptic workstation for neuromotor rehabilitation. *Technology and Health Care*, 14(3):123–142, 2006.

[42] András Tóth, Gusztáv Arz, Gábor Fazekas, Daniel Bratanov, and Nikolay Zlatov. 25 post stroke shoulder-elbow physiotherapy with industrial robots. In *Advances in Rehabilitation Robotics*, pages 391–411. Springer, 2004.

[43] AE Jackson, RJ Holt, PR Culmer, SG Makower, MC Levesley, RC Richardson, JA Cozens, M Mon Williams, and BB Bhakta. Dual robot system for upper limb rehabilitation after stroke: the design process. *Proceedings of the Institution of Mechanical Engineers, Part C: Journal of Mechanical Engineering Science*, 221(7):845–857, 2007.

[44] Peter S Lum, HFM Van der Loos, Peggy Shor, and Charles G Burgar. A robotic system for upper-limb exercises to promote recovery of motor function following stroke. In *Proceedings Sixth Int. Conf. on Rehab. Robotics*, pages 235–239, 1999.

[45] Stefan Hesse, Gotthard Schulte-Tigges, Matthias Konrad, Anita Bardeleben, and Cordula Werner. Robot-assisted arm trainer for the passive and active practice of bilateral forearm and wrist movements in hemiparetic subjects. *Archives of physical medicine and rehabilitation*, 84(6):915–920, 2003.

[46] Rui Loureiro, Farshid Amirabdollahian, Michael Topping, Bart Driessen, and William Harwin. Upper limb robot mediated stroke therapy—gentle/s approach. *Autonomous Robots*, 15(1):35–51, 2003.

[47] Tobias Nef and Robert Riener. Armin-design of a novel arm rehabilitation robot. In *Rehabilitation Robotics, 2005. ICORR 2005. 9th International Conference on*, pages 57–60. IEEE, 2005.

[48] Alberto Montagner, Antonio Frisoli, Luigi Borelli, Caterina Procopio, Massimo Bergamasco, Maria C Carboncini, and Bruno Rossi. A pilot clinical study on robotic assisted rehabilitation in vr with an arm exoskeleton device. In *Virtual Rehabilitation, 2007*, pages 57–64. IEEE, 2007.

[49] HI Krebs, BT Volpe, M Ferraro, S Fasoli, J Palazzolo, B Rohrer, L Edelstein, N Hogan, et al. Robot-aided neurorehabilitation: from evidence-based to science-based rehabilitation. *Topics in stroke rehabilitation*, 8(4):54–70, 2002.

Eugenia Papaleo

[50] Hermano Igo Krebs, Neville Hogan, Mindy L Aisen, and Bruce T Volpe. Robot-aided neurorehabilitation. *Rehabilitation Engineering, IEEE Transactions on*, 6(1):75–87, 1998.

[51] R Colombo, I Sterpi, A Mazzone, F Pisano, and C Delconte. Modeling upper limb clinical scales by robot-measured performance parameters. In *Rehabilitation Robotics (ICORR), 2011 IEEE International Conference on*, pages 1–5. IEEE, 2011.

[52] L Zollo, E Gallotta, E Guglielmelli, and S Sterzi. Robotic technologies and rehabilitation: new tools for upper-limb therapy and assessment in chronic stroke. *European journal of physical and rehabilitation medicine*, 47(2):223, 2011.

[53] Roberto Colombo, Fabrizio Pisano, Silvestro Micera, Alessandra Mazzone, Carmen Delconte, M Chiara Carrozza, Paolo Dario, and Giuseppe Minuco. Robotic techniques for upper limb evaluation and rehabilitation of stroke patients. *Neural Systems and Rehabilitation Engineering, IEEE Transactions on*, 13(3):311–324, 2005.

[54] Alessandro Panarese, Roberto Colombo, Irma Sterpi, Fabrizio Pisano, and Silvestro Micera. Tracking motor improvement at the subtask level during robot-aided neurorehabilitation of stroke patients. *Neurorehabilitation and Neural Repair*, 26(7):822–833, 2012.

[55] R Colombo, F Pisano, S Micera, A Mazzone, C Delconte, MC Carrozza, P Dario, and G Minuco. Assessing mechanisms of recovery during robot-aided neurorehabilitation of the upper limb. *Neurorehabilitation and neural repair*, 22(1):50–63, 2008.

[56] Sivakumar Balasubramanian, Ruihua Wei, Richard Herman, and Jiping He. Robot-measured performance metrics in stroke rehabilitation. In *Complex Medical Engineering, 2009. CME. ICME International Conference on*, pages 1–6. IEEE, 2009.

[57] Caitlyn Bosecker, Laura Dipietro, Bruce Volpe, and Hermano Igo Krebs. Kinematic robot-based evaluation scales and clinical counterparts to measure upper limb motor performance in patients with chronic stroke. *Neurorehabilitation and neural repair*, 24(1):62–69, 2010.

[58] Angela M Coderre, Amr Abou Zeid, Sean P Dukelow, Melanie J Demmer, Kimberly D Moore, Mary Jo Demers, Helen Bretzke, Troy M Herter, Janice I

Eugenia Papaleo

Glasgow, Kathleen E Norman, et al. Assessment of upper-limb sensorimotor function of subacute stroke patients using visually guided reaching. *Neurorehabilitation and Neural Repair*, 24(6):528–541, 2010.

[59] Brandon Rohrer, Susan Fasoli, Hermano Igo Krebs, Richard Hughes, Bruce Volpe, Walter R Frontera, Joel Stein, and Neville Hogan. Movement smoothness changes during stroke recovery. *The Journal of Neuroscience*, 22(18):8297–8304, 2002.

[60] Ludovic Dovat, Olivier Lambercy, Berna Salman, Vineet Johnson, Theodore Milner, Roger Gassert, Etienne Burdet, and Teo C Leong. A technique to train finger coordination and independence after stroke. *Disability & Rehabilitation: Assistive Technology*, 5(4):279–287, 2010.

[61] Laura Dipietro, Hermano I Krebs, Susan E Fasoli, Bruce T Volpe, Joel Stein, C Bever, and Neville Hogan. Changing motor synergies in chronic stroke. *Journal of neurophysiology*, 98(2):757–768, 2007.

[62] Marco Guidali, Mark Schmiedeskamp, Verena Klamroth, and Robert Riener. Assessment and training of synergies with an arm rehabilitation robot. In *Rehabilitation Robotics, 2009. ICORR 2009. IEEE International Conference on*, pages 772–776. IEEE, 2009.

[63] Peter S Lum, Charles G Burgar, and Peggy C Shor. Evidence for improved muscle activation patterns after retraining of reaching movements with the mime robotic system in subjects with post-stroke hemiparesis. *Neural Systems and Rehabilitation Engineering, IEEE Transactions on*, 12(2):186–194, 2004.

[64] Roberto Colombo, Irma Sterpi, Alessandra Mazzone, Carmen Delconte, Giuseppe Minuco, and Fabrizio Pisano. Measuring changes of movement dynamics during robot-aided neurorehabilitation of stroke patients. *Neural Systems and Rehabilitation Engineering, IEEE Transactions on*, 18(1):75–85, 2010.

[65] M Munih, R Riener, G Colombo, L Lunenburger, F Muller, M Slater, and M Mihelj. Mimics: Multimodal immersive motion rehabilitation of upper and lower extremities by exploiting biocooperation principles. In *Rehabilitation Robotics, 2009. ICORR 2009. IEEE International Conference on*, pages 127–132. IEEE, 2009.

Eugenia Papaleo

[66] Hermano Igo Krebs, Jerome Joseph Palazzolo, Laura Dipietro, Mark Ferraro, Jennifer Krol, Keren Rannekleiv, Bruce T Volpe, and Neville Hogan. Rehabilitation robotics: Performance-based progressive robot-assisted therapy. *Autonomous Robots*, 15(1):7–20, 2003.

[67] Domen Novak, Matjaz Mihelj, Jaka Ziherl, Andrej Olensek, and Marko Munih. Psychophysiological measurements in a biocooperative feedback loop for upper extremity rehabilitation. *Neural Systems and Rehabilitation Engineering, IEEE Transactions on*, 19(4):400–410, 2011.

[68] Alexander Koenig, Domen Novak, Ximena Omlin, Michael Pulfer, Eric Perreault, Lukas Zimmerli, Matjaz Mihelj, and Robert Riener. Real-time closed-loop control of cognitive load in neurological patients during robot-assisted gait training. *Neural Systems and Rehabilitation Engineering, IEEE Transactions on*, 19(4):453–464, 2011.

[69] C Rodriguez Guerrero, J Fraile Marinero, J Perez Turiel, and P Rivera Farina. Bio cooperative robotic platform for motor function recovery of the upper limb after stroke. In *Engineering in Medicine and Biology Society (EMBC), 2010 Annual International Conference of the IEEE*, pages 4472–4475. IEEE, 2010.

[70] Andrea Turolla, Mauro Dam, Laura Ventura, Paolo Tonin, Michela Agostini, Carla Zucconi, Pawel Kiper, Annachiara Cagnin, and Lamberto Piron. Virtual reality for the rehabilitation of the upper limb motor function after stroke: a prospective controlled trial. *Journal of neuroengineering and rehabilitation*, 10(1):85, 2013.

[71] David Jack, Rares Boian, Alma S Merians, Marilyn Tremaine, Grigore C Burdea, Sergei V Adamovich, Michael Recce, and Howard Poizner. Virtual reality-enhanced stroke rehabilitation. *Neural Systems and Rehabilitation Engineering, IEEE Transactions on*, 9(3):308–318, 2001.

[72] Alexander Koenig, Ximena Omlin, Domen Novak, and Robert Riener. A review on bio-cooperative control in gait rehabilitation. In *Rehabilitation Robotics (ICORR), 2011 IEEE International Conference on*, pages 1–6. IEEE, 2011.

[73] Niall Maclean, Pandora Pound, et al. A critical review of the concept of patient motivation in the literature on physical rehabilitation. *Soc Sci Med*, 50(4):495–506, 2000.

Eugenia Papaleo

[74] Matjaz Mihelj, Domen Novak, Jaka Ziherl, A Olensek, and Marko Munih. Challenges in biocooperative rehabilitation robotics. In *Rehabilitation Robotics (ICORR), 2011 IEEE International Conference on*, pages 1–6. IEEE, 2011.

[75] Deborah Falla, A Rainoldi, Roberto Merletti, and G Jull. Myoelectric manifestations of sternocleidomastoid and anterior scalene muscle fatigue in chronic neck pain patients. *Clinical Neurophysiology*, 114(3):488–495, 2003.

[76] Roberto Merletti, Marco Knaflitz, and CARLO J De Luca. Myoelectric manifestations of fatigue in voluntary and electrically elicited contractions. *Journal of Applied Physiology*, 69(5):1810–1820, 1990.

[77] M Bilodeau, S Schindler-Ivens, DM Williams, R Chandran, and SS Sharma. Emg frequency content changes with increasing force and during fatigue in the quadriceps femoris muscle of men and women. *Journal of Electromyography and Kinesiology*, 13(1):83–92, 2003.

[78] Paul Ekman. An argument for basic emotions. *Cognition & Emotion*, 6(3-4):169–200, 1992.

[79] David A Winter. *Biomechanics and motor control of human movement*. Wiley. com, 2009.

[80] R Merletti and H Hermens. Introduction to the special issue on the seniam european concerted action. *Journal of Electromyography and Kinesiology*, 10(5):283–286, 2000.

[81] Tamar Flash and Neville Hogan. The coordination of arm movements: an experimentally confirmed mathematical model. *The journal of Neuroscience*, 5(7):1688–1703, 1985.

[82] Tsuneo Yoshikawa. Manipulability of robotic mechanisms. *The international journal of Robotics Research*, 4(2):3–9, 1985.

[83] F Draicchio, A Silvetti, A Ravanolo, and S Iavicoli. Approcci innovativi per la valutazione del rischio da movimenti ripetuti dell'arto superiore. *Giornale Italiano di Medicina del Lavoro ed Ergonomia*, 30(3):117–119, 2008.

[84] Sukanta K Sabut, Prasanna K Lenka, Ratnesh Kumar, and Manjunatha Mahadevappa. Effect of functional electrical stimulation on the effort and walking speed, surface electromyography activity, and metabolic responses in stroke subjects. *Journal of Electromyography and Kinesiology*, 20(6):1170–1177, 2010.

Eugenia Papaleo

[85] KS Rudolph, MJ Axe, and L Snyder-Mackler. Dynamic stability after acl injury: who can hop? *Knee Surgery, Sports Traumatology, Arthroscopy*, 8(5):262–269, 2000.

[86] Gail Frost, James Dowling, Kerry Dyson, and Oded Bar-Or. Cocontraction in three age groups of children during treadmill locomotion. *Journal of Electromyography and Kinesiology*, 7(3):179–186, 1997.

[87] Anderson de Souza Castelo Oliveira and Mauro Gonçalves. Emg amplitude and frequency parameters of muscular activity: effect of resistance training based on electromyographic fatigue threshold. *Journal of Electromyography and Kinesiology*, 19(2):295–303, 2009.

[88] R Merletti, A Rainoldi, and D Farina. Surface electromyography for non-invasive characterization of muscle. *Exercise and sport sciences reviews*, 29(1):20–25, 2001.

[89] Benno Maurus Nigg, Walter Herzog, and John Wiley. *Biomechanics of the musculo-skeletal system*, volume 2. Wiley New York, 1999.

[90] Roberto Merletti, A Rainoldi, and D Farina. Myoelectric manifestations of muscle fatigue. *Electromyography: physiology, engineering, and noninvasive applications*, pages 233–258, 2004.

[91] S MICERA and F MAYER. Incremento degli indici di accuratezza e fluidità del movimento dell'arto superiore dopo training con il robot planare memos 2 nei soggetti con esiti di ictus. *GIORNALE DI*, 60:160–166, 2012.

[92] F MAYER and A BARONI. Recupero motorio nelle lesioni dell'arto superiore post-ictus: effetti della macchina operativa computer-assistita ultra. *G GERONTOL*, 58:296–302, 2010.

[93] HI Krebs, N Hogan, BT Volpe, ML Aisen, L Edelstein, and C Diels. Overview of clinical trials with mit-manus: a robot-aided neuro-rehabilitation facility. *Technology and Health Care*, 7(6):419–423, 1999.

[94] Laura Marchal-Crespo and David J Reinkensmeyer. Review of control strategies for robotic movement training after neurologic injury. *Journal of neuroengineering and rehabilitation*, 6(1):20, 2009.

[95] Hyunchul Kim, L Miller, Irina Fedulow, Matt Simkins, Gary Abrams, Nancy Byl, and Jacob Rosen. Kinematic data analysis for post stroke patients following bilateral versus unilateral rehabilitation with an upper limb wearable robotic system. 2012.

Eugenia Papaleo

[96] Shyamal Patel, Hyung Park, Paolo Bonato, Leighton Chan, Mary Rodgers, et al. A review of wearable sensors and systems with application in rehabilitation. *Journal of neuroengineering and rehabilitation*, 9(12):1–17, 2012.

[97] Tamar Flash, Yaron Meirovitch, and Avi Barliya. Models of human movement: trajectory planning and inverse kinematics studies. *Robotics and Autonomous Systems*, 2012.

[98] John F Soechting, Christopher A Buneo, Uta Herrmann, and Martha Flanders. Moving effortlessly in three dimensions: does donders' law apply to arm movement? *The Journal of Neuroscience*, 15(9):6271–6280, 1995.

[99] Norman I Badler and Deepak Tolani. Real-time inverse kinematics of the human arm. *Center for Human Modeling and Simulation*, page 73, 1996.

[100] Hyunchul Kim, Levi Makaio Miller, Nancy Byl, Gary Abrams, and Jacob Rosen. Redundancy resolution of the human arm and an upper limb exoskeleton. *Biomedical Engineering, IEEE Transactions on*, 59(6):1770–1779, 2012.

[101] Zhi Li, Hyunchul Kim, Dejan Milutinović, and Jacob Rosen. Synthesizing redundancy resolution criteria of the human arm posture in reaching movements. In *Redundancy in Robot Manipulators and Multi-Robot Systems*, pages 201–240. Springer, 2013.

[102] Jacques Denavit. A kinematic notation for lower-pair mechanisms based on matrices. *Trans. of the ASME. Journal of Applied Mechanics*, 22:215–221, 1955.

[103] K Kreutz-Delgado, M Long, and H Seraji. Challenges in biocooperative rehabilitation robotics. In *Robotics and Automation (ICRA), 1990 IEEE International Conference on*, pages 824–830. IEEE, 1990.

[104] Deepak Tolani, Ambarish Goswami, and Norman I Badler. Real-time inverse kinematics techniques for anthropomorphic limbs. *Graphical models*, 62(5):353–388, 2000.

[105] Matjaz Mihelj. Human arm kinematics for robot based rehabilitation. *Robotica*, 24(3):377–383, 2006.

[106] Eugenia Papaleo, Loredana Zollo, Silvia Sterzi, and Eugenio Guglielmelli. An inverse kinematics algorithm for upper-limb joint reconstruction during robot-aided motor therapy. In *Biomedical Robotics and Biomechatronics*

Eugenia Papaleo

(BioRob), 2012 4th IEEE RAS & EMBS International Conference on, pages 1983–1988. IEEE, 2012.

[107] Bruce T Volpe, Hermano I Krebs, and Neville Hogan. Is robot-aided sensorimotor training in stroke rehabilitation a realistic option? *Current opinion in neurology*, 14(6):745–752, 2001.

[108] Craig D Takahashi, Lucy Der-Yeghiaian, Vu Le, Rehan R Motiwala, and Steven C Cramer. Robot-based hand motor therapy after stroke. *Brain*, 131(2):425–437, 2008.

[109] Patricia Kan, Rajibul Huq, Jesse Hoey, Robby Goetschalckx, and Alex Mihailidis. The development of an adaptive upper-limb stroke rehabilitation robotic system. *Journal of neuroengineering and rehabilitation*, 8(1):33, 2011.

[110] Alexander Duschau-Wicke, Andrea Caprez, and Robert Riener. Patient-cooperative control increases active participation of individuals with sci during robot-aided gait training. *Journal of neuroengineering and rehabilitation*, 7:43–43, 2010.

[111] Mindy F Levin, Ruud W Selles, Martine HG Verheul, and Onno G Meijer. Deficits in the coordination of agonist and antagonist muscles in stroke patients: implications for normal motor control. *Brain research*, 853(2):352–369, 2000.

[112] V Di Lazzaro, F Pilato, M Dileone, P Profice, F Capone, F Ranieri, G Musumeci, A Cianfoni, P Pasqualetti, and PA Tonali. Modulating cortical excitability in acute stroke: a repetitive tms study. *Clinical Neurophysiology*, 119(3):715–723, 2008.

[113] Joachim Liepert, Heike Bauder, Wolfgang HR Miltner, Edward Taub, and Cornelius Weiller. Treatment-induced cortical reorganization after stroke in humans. *Stroke*, 31(6):1210–1216, 2000.

[114] DJ Edwards, HI Krebs, A Rykman, J Zipse, GW Thickbroom, FL Mastaglia, A Pascual-Leone, and BT Volpe. Raised corticomotor excitability of m1 forearm area following anodal tdcs is sustained during robotic wrist therapy in chronic stroke. *Restorative neurology and neuroscience*, 27(3):199–207, 2009.

Eugenia Papaleo

[115] Raimondo Traversa, Paola Cicinelli, Patrizio Pasqualetti, Maria Filippi, and Paolo Maria Rossini. Follow-up of interhemispheric differences of motor evoked potentials from theaffected'andunaffected'hemispheres in human stroke. *Brain research*, 803(1):1–8, 1998.

[116] Marcel Ed Kinsbourne and W Smith. Hemispheric disconnection and cerebral function. 1974.

[117] Bradley Vines, Carlo Cerruti, and Gottfried Schlaug. Dual-hemisphere tdcs facilitates greater improvements for healthy subjects' non-dominant hand compared to uni-hemisphere stimulation. *BMC neuroscience*, 9(1):103, 2008.

[118] Hooman Mahmoudi, Afshin Borhani Haghighi, Peyman Petramfar, Sepehr Jahanshahi, Zahra Salehi, and Felipe Fregni. Transcranial direct current stimulation: electrode montage in stroke. *Disability & Rehabilitation*, 33(15-16):1383–1388, 2011.

[119] Florinda Ferreri, Patrizio Pasqualetti, Sara Määttä, David Ponzo, Fabio Ferrarelli, Giulio Tononi, Esa Mervaala, Carlo Miniussi, and Paolo Maria Rossini. Human brain connectivity during single and paired pulse transcranial magnetic stimulation. *Neuroimage*, 54(1):90–102, 2011.